

Studies of Bacterial Homeostasis in *Sinorhizobium meliloti* and *Escherichia coli*

by

Bryan William Davies

B. Sc. in Biochemistry
McMaster University, 2001

Submitted to the Department of Biology in Partial Fulfillment of the Requirements for
the Degree of

Doctor of Philosophy

at the

Massachusetts Institute of Technology

February, 2008

[June 2008]

© 2008 Massachusetts Institute of Technology
All rights reserved.

Signature of Author: _____

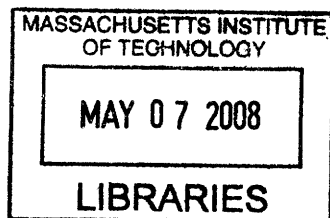
Department of Biology
February, 2008

Certified by: _____

Graham C. Walker
Thesis Supervisor

Accepted by: _____

Stephen P. Bell
Chairman, Graduate Committee



ARCHIVES

Table of Contents

Abstract	3
Acknowledgments	4
Chapter 1: Introduction	5
Chapter 2: Identification of Novel <i>Sinorhizobium meliloti</i> Mutants Compromised for Oxidative Stress Protection and Symbiosis	17
Chapter 3: Disruption of <i>sitA</i> Compromises <i>Sinorhizobium meliloti</i> for Manganese Uptake and Required for Protection against Oxidative Stress	31
Chapter 4: A Highly Conserved Protein of Unknown Function Plays an Essential Role for <i>Sinorhizobium meliloti</i> in Symbiosis and Environmental Stress Protection	65
Chapter 5: Identification of a universally conserved bacterial protein required for ribosome maturation	93
Chapter 6: Damage-Independent Replication Fork Arrest in <i>Escherichia coli</i> reveals a Molecular Switch Between Cell Survival and Cell Death	141
Chapter 7: Investigations into the Mechanism of Hydroxyurea Resistance Conferred by Loss of YbeY Activity	181
Chapter 8: Perspectives and Future Direction	211
References	215

Abstract

The symbiosis between *Sinorhizobium meliloti* and its plant host *Medicago sativa*, offers a tractable model to explore the bacterial requirements for endocytic survival in a eukaryotic host. It has been shown that during development of this symbiosis, *M. sativa* releases an oxidative burst that *S. meliloti* must be able to overcome in order for symbiotic development to continue. Employing a novel two-part screen, I identified *Sinorhizobium meliloti* mutants that were both sensitive to oxidative stress and symbiotically defective on the host plant *Medicago sativa*. The mutants affect a wide variety of cellular processes and represent both novel and previously identified genes important in symbiosis.

One mutant I identified was disrupted in *sitA*, which encodes the periplasmic binding protein of the putative iron/manganese ABC transporter SitABCD. Disruption of *sitA* causes elevated sensitivity to the reactive oxygen species hydrogen peroxide and superoxide. Disruption of *sitA* leads to elevated catalase activity and a severe decrease in superoxide dismutase B (SodB) activity and protein level. The decrease in SodB level strongly correlates with the superoxide sensitivity of the *sitA* mutant. I demonstrate that all free-living phenotypes of the *sitA* mutant can be rescued by the addition of exogenous manganese but not iron, a result that strongly implies SitABCD plays an important role in manganese uptake in *S. meliloti*.

A second mutant I identified in my screen was disrupted in a previously unexplored orf, *SMc01113*. *SMc01113* produces an 18 kD protein that is a member of a highly conserved family, universal among bacteria. In addition to being required for *S. meliloti* symbiosis with alfalfa, *SMc01113* is also required to protect the bacterium from a wide range of environmental stresses. Our findings support a role for this novel protein in RNA and/or phospholipid metabolism.

The striking pleiotropy of the *SMc01113* mutant led me to further investigate the molecular function of *SMc01113*. I show that the *SMc01113* protein is part of a large Cluster of Orthologous Group (COG), COG0319 and that homologs of this protein are functionally equivalent. Using the model system of *Escherichia coli*, I demonstrate that the *E. coli* homolog, YbeY, is required for ribosome maturation. Loss of YbeY activity affects maturation of both 16S and 23S rRNA and causes a severe loss of polysomes. 70S ribosomes formed in a $\Delta ybeY$ mutant show reduced translational activity and fidelity. I further demonstrate the human homolog, C21orf57, may play a similar role in human mitochondria.

While investigating the $\Delta ybeY$ mutant, I found that, in contrast to the wide range of stresses it was sensitive to, the $\Delta ybeY$ mutant was very resistant to the DNA replication inhibitor hydroxyurea. Using a systems-level analysis of the genomic transcriptional response to hydroxyurea, I show that hydroxyurea triggers pathways involved in both cell survival and cell death, and suggest a model where, for any given bacterium in a population, hydroxyurea can induce a molecular switch from a survival mode to a programmed cell death mode. I use this model to explore possible mechanisms for the increased resistance of the $\Delta ybeY$ mutant to hydroxyurea.

Acknowledgments

I would like to thank my advisor, Graham Walker, for his encouragement, support, and scientific advice, and the members of my thesis committee for their helpful suggestions. Thanks are also due to all members of the Walker lab, both past and present, for their scientific and technical advice. Special mention is due to members of the RajBhandary lab for their patience and scientific teaching. Thanks also to the Bell lab for all their technical support. I would like to thank my friends and family for their support over the past years and encouragement as I step forward.

Chapter 1

Introduction

My thesis covers several areas of bacterial research. I began by studying the symbiosis between the soil bacterium *Sinorhizobium meliloti* and its host plant *Medicago sativa* (alfalfa). This led me to explore role of manganese in oxidative stress protection, and also a novel protein of unknown function that is part of a highly conserved protein family, universally conserved among bacteria. My investigation of this protein family led me into several fields including protein translation and DNA replication. Each of these fields covers a wide breadth of research. In the following introduction I will confine my discussion to the material most applicable to my work.

***Sinorhizobium meliloti* Symbiosis and the Role of Oxidative Stress.**

Under conditions of poor nitrogen availability, the α -proteobacterium *Sinorhizobium meliloti* can invade and establish a chronic symbiotic infection within the host plant *Medicago sativa* (alfalfa) (1, 2). The development of the symbiosis is complex. It begins by an intricate chemical conversation with each organism secreting, and responding to, small molecule signals. These chemical exchanges induce physiological changes in the plant host including cortical cell division in the roots to produce nodules, and root hair curling that traps nearby bacteria, creating an entry point for *S. meliloti* (1-4). Through a plant-derived structure called an infection thread, *S. meliloti* cells traverse the root hair cell until they are finally endocytosed into the cells within the developing plant nodule (4, 5). In the nodule, *S. meliloti* differentiates into a nitrogen-fixing bacteroid capable of converting atmospheric nitrogen into a usable form for plant consumption (1, 2).

While in the infection thread, *S. meliloti* is exposed to an oxidative burst released by the host plant that is composed of at least hydrogen peroxide (H₂O₂) and superoxide (6). *S. meliloti* encodes a set of enzymes to defend against these reactive oxygen species (ROS) including superoxide dismutases, catalases and alkylhydroperoxidases (7). It has become evident that *S. meliloti* must be able to manage oxidative stress while in the host plant as loss of certain oxidative stress defense mechanisms cause symbiotic defects. For example, *S. meliloti* strains deficient in both catalase B and catalase C (*katB/C*) or both catalase A and catalase C (*katA/C*), enzymes that detoxify H₂O₂, are symbiotically defective (8, 9). However, exactly which rhizobial defenses are required to combat oxidative stress is a complex question. Several genes known to be required for defense against ROS in the free living state are dispensable for symbiosis. For example, disruption of the global regulator of H₂O₂ protection, *oxyR*, makes the free-living strain extremely sensitive to H₂O₂, but does not affect symbiosis (10).

I was interested in identifying novel genes involved in *S. meliloti* oxidative stress protection and determining if these genes also played a role in the development of symbiosis. To explore this question I undertook a two-part screen to identify transposon mutants of *S. meliloti* that were both sensitive to H₂O₂ and symbiotically defective (see Chapter 2). Through this screen I identified several genes that have not previously been recognized as being important either in symbiosis or in oxidative stress protection for *S. meliloti*. One mutant identified in the screen has a transposon insertion in the *sitA* gene. *sitA* is the first gene in the four gene operon *sitABCD* that had been annotated as coding for a putative iron/manganese ABC transporter (7).

The Role of Manganese in Oxidative Stress Protection

Iron and manganese are important metals for oxidative stress protection. Iron is used as a cofactor in defense enzymes such as catalase (11). Although in this context iron is helpful in protection against ROS, free iron in the Fe^{2+} state, can serve to exacerbate oxidative stress by producing hydroxyl radicals from peroxides through Fenton chemistry (12). In contrast to iron, manganese ions can help defend against ROS by scavenging both H_2O_2 and superoxide, as part of low molecular weight complexes with cellular ligands such as phosphate, lactate or bicarbonate. Although the exact chemistry of the scavenging has not been determined, the mechanism is thought to involve manganese ions cycling between the Mn^{2+} and Mn^{3+} states (13-16). In its enzymatic capacity, manganese also aids in oxidative stress defense by acting as the essential cofactor in dedicated ROS scavenging enzymes such as manganese-containing superoxide dismutases and catalases (17, 18). In addition to safe guarding bacteria against ROS, manganese has also been shown to play an important role in virulence. Disruption of manganese uptake in pathogens *Salmonella enterica* serovar Typhimurium and *Streptococcus pyogenes* attenuates their virulence (19, 20).

Considering the known roles for manganese in oxidative stress protection and the requirement of manganese uptake in pathogen/host interactions, the *sitA* mutant I identified was an intriguing candidate for further exploration. To define the role of SitA in *S. meliloti* free-living and symbiotic physiology, I first determined the deficiency responsible for the *sitA* mutant free-living phenotypes and subsequently explored the downstream effectors that contribute to the oxidative stress sensitivity and symbiotic defect (Chapter 3).

Investigation of a Highly Conserved Protein of Unknown Function Required for *S. meliloti* Symbiosis and Environmental Stress Protection.

The genome of *S. meliloti* strain Rm1021 was recently sequenced and revealed 6204 predicted protein-coding regions. Of these 6204 genes, a putative function could be postulated for only 59.7% of Rm1021 genes on the basis of bioinformatics analysis. An even smaller percentage of genes have actually been biochemical validated (7). These facts highlight a major stumbling block in all current omic level efforts. At best, we understand the function of only 54% of genes in any organism we are examining (21, 22). For *E. coli*, arguably the most highly studied organism, we currently understand the actual biological function of only 53.1% percent of the genes (21). This numbers drops for the majority of the other sequenced prokaryotes and dips precipitously for most eukaryotic and archaeal organisms (22, 23). This lack of knowledge of the fundamental functions of the majority of genes in the every genome is a serious stumbling block in all omic efforts (22). With advances into areas of network modeling and systems biology a more complete knowledge of the genome is becoming increasingly important in order to build and interpret accurate models.

Continuation of the screening strategy I developed to identify oxidative stress sensitive and symbiotically deficient *S. meliloti* mutants (Chapter 2) led to the discovery that orf *SMc01113*, which encodes a protein of unknown function, is essential for symbiosis (Chapter 4). The *SMc01113* protein is part of a highly conserved protein family (24), present in all bacteria. The family is also one of 206 that comprise the predicted minimal genome required to be a bacteria (25). In *S. meliloti*, I found that the

function of SMC01113 is not only critically required to establish the chronic intracellular infection necessary for symbiosis, but also for defense against a wide range of environmental stresses (Chapter 4). The universal conservation of this protein among bacteria and extremely pleiotropic nature of the *S. meliloti* SMC01113 mutant drove me to continue my studies of this highly conserved and very important protein family, not only to learn more about *S. meliloti* requirements for symbiosis, but also to deepen our knowledge of all bacteria.

I show that homologs of this protein are functionally equivalent (Chapter 5). As we describe in this thesis, deletion of the *Escherichia coli* homolog, *ybeY*, resulted in highly pleiotropic strain, similar to that observed by the disruption of SMC01113 in *S. meliloti*. Due to the greater utility of biochemical and genetic techniques, I continued my investigation of this protein family in *E. coli* where I identified a role for the *E. coli* homolog, YbeY, in ribosome maturation (Chapter 5).

Ribosome Maturation and Protein Translation

Protein translation is a complicated process performed by the ribosome and its associated factors (27-30). In bacteria, a large 50S subunit and smaller 30S subunit associate to form an active 70S ribosome, competent for translation. The 50S subunit is composed of a 23S and 5S rRNA along with 33 ribosomal proteins while the 30S subunits is composed of a 16S rRNA and 21 ribosomal proteins (28, 30, 31). While reconstitution of active 30S and 50S subunits has been performed *in vitro* using only their respective rRNA and ribosomal proteins (32, 33), it is well recognized that many additional accessory factors are required for 50S and 30S formation *in vivo* (29, 34).

Proper assembly of the ribosome is crucial to its function. Several mutants have been identified that disrupt processing of rRNA or assembly of subunits that have detrimental effects on ribosome synthesis and cell viability (29, 34).

Ribosome maturation occurs in a cooperative and ordered fashion (29, 34). Before transcription is even complete, ribosomal proteins associate with rRNA forming ribonucleoprotein particles that are acted on by RNase III. RNase III begins rRNA maturation cleaving it into precursors that will go on to become mature 16S, 23S and 5S rRNA. RNases capable of the final maturation of the 23S (35, 36) and the 5' end of 16S rRNA (37) have been identified, however the enzyme responsible for the 3' maturation of 16S rRNA has remained elusive (37). Immature 23S rRNA can form functional ribosomes (38), but immature 16S rRNA cannot (39). While final maturation of some rRNA termini can be performed *in vitro* using 70S ribosomes (37), it appears that the final maturation steps for both 16S and 23S rRNA *in vivo* may actually require formation of polysome structures (38, 39).

Protein translation proceeds through 4 stages; initiation, elongation, termination and ribosome recycling. Initiation of protein synthesis is a complex process (40). While it cannot be entirely separated from the preceding ribosome recycling phase of translation, I will outline the general steps of initiation following 70S dissociation. Initiation begins with the 30S subunit bound by initiation factors (IF) 1 and 3. IF1 binds specifically to the base of the tRNA binding aminoacyl (A) site of the 30S ribosomal subunit and is thought to direct the initiator tRNA (fMet-tRNA^{fMet}) to the ribosomal peptidyl (P) tRNA binding site (41, 42). IF2, initiator tRNA and mRNA then associate with the 30S subunit in an as of yet unknown order (34). IF2 is a GTP/GDP-binding

protein whose main function is to specifically interact with fMet-tRNA_f^{Met} and to position it correctly in the ribosomal P-site, thereby increasing the fidelity and rate of translation initiation (43, 44). IF2 also promotes 30S/50S subunit association (45). The Shine-Dalgarno (SD) sequence of canonical mRNAs interact with the anti-SD sequence of the 16S rRNA (46), and the initiation codon is adjusted to the P-site of the ribosome (47). fMet-tRNA_f^{Met} is then positioned in the P-site and, after a conformational change in the 30S subunit promoting fMet-tRNA_f^{Met} codon-anticodon interactions, the 30S initiation complex is formed (48, 49). IF1 and IF3 are ejected from the complex, while IF2 promotes association with the 50S subunit (50). fMet-tRNA_f^{Met} is adjusted to the correct position in the P-site, and IF2 is released from the complex. The resulting complex is then competent to enter elongation phase of translation.

Error rates of translation *in vivo* have been estimated to be on the order of 10^{-3} to 10^{-4} (51). Translational errors can arise from improper tRNA aminoacylation, incorrect tRNA selection by the ribosome, or frameshifting during translation. tRNA aminoacylation is very accurate. For example Ile-tRNA^{Ile}-synthetase will exclude Val with an efficiency of 2.5×10^{-5} (52, 53). This suggests that the errors in decoding by the ribosome are responsible the cause of most translation errors.

Translational frameshifting occurs by slipping of the ribosome to an alternate reading frame. Frameshifting is generally detrimental as it changes the reading frame of the message being translated producing a truncated protein (54). The exact mechanism of frameshifting has not been established (55), however factors known to potentiate the event have been discovered. These factors include certain mutations in 23S and 16S rRNA (56, 57), mutations in ribosomal proteins (58, 59) and elongation factor 2 (60) as

well as loss of certain tRNA modifications (61). Interestingly however, expression of certain genes actually require frameshifting for expression such as the Gag-Pol-Pro protein in retroviruses (62) that require -1 frameshifting or the *E. coli prfB* gene that requires +1 frameshifting (63).

I present data that supports a role for YbeY in ribosome maturation. Specifically YbeY may act in the, as yet undetermined, process of 16S 3' maturation. Not only does loss of YbeY activity affect ribosome maturation but the ribosomes that are formed show decreased translational activity and increased frameshifting. I further demonstrate that the human homolog, C21orf57, may perform a similar task as YbeY in human mitochondria.

Hydroxyurea and Damage-Independent DNA Replication Fork Inhibition

While investigating the *E. coli ΔybeY* mutant I constructed, I made another intriguing observation. Although this mutant exhibited extreme sensitivity to several environmental stresses, it was very resistant to hydroxyurea. Hydroxyurea (HU) is commonly used in both prokaryotes and eukaryotes to study DNA damage-independent replication fork arrest (64-66). HU is potent inhibitors of class I ribonucleotide reductase (RNR), the enzyme responsible for the synthesis of dNTPs under aerobic conditions in many organisms. Depletion of dNTP pools through HU treatment leads to replication fork arrest, most likely through substrate starvation (66-68).

DNA damage, induced by mutagens such as UV, interferes with DNA replication through a mechanism different from that caused by HU (67, 69). When a replication fork encounters DNA damage caused by UV, replication proceeds discontinuously, leaving

gaps juxtaposed to the lesion (70). The excess ssDNA generated results in formation of the RecA/ssDNA nucleoprotein filaments that facilitate auto-cleavage of the transcriptional repressor LexA and derepression of the SOS-regulon. The SOS response, involves the upregulation of more than 40 genes involved in numerous aspects of DNA repair and other cellular functions (71). The genomic response to UV damage has been investigated and described in two independent studies using microarray analysis (72, 73). The majority of genes identified in these experiments belong to the SOS-regulon. The authors identified only a small subset of genes that varied independently of the major SOS transcriptional repressor, LexA, or that were downregulated in response to UV. HU treatment had been shown to upregulate two genes of the SOS-regulon, *recA* and *sulA* (74) however the extent of SOS induction as well as other cellular responses brought about by HU-dependent fork arrest had not been investigated in detail.

Before investigating the $\Delta ybeY$ mutant's resistance to HU, I needed to understand the full spectrum of cellular effects incurred by HU treatment. Work by several groups has shown that HU is exquisitely specific for inhibiting DNA synthesis through RNR inhibition (75, 76). However, a complete picture of the subsequent effects of dNTP pool depletion and replication fork arrest on cell physiology had been lacking. In addition, it was not known how *Escherichia coli* responds differently to replication interference resulting from DNA damage compared to a damage-independent mechanism.

In collaboration with Jim Collin's group at Boston University, I combined microarray technology with systems level analysis to determine the genome-wide transcriptional response to HU in the model organism *Escherichia coli* (Chapter 6). Using my collaborators analysis of the transcriptional response to HU in *E. coli* to guide

my investigation, I demonstrate that HU induces global molecular changes that encompass not only DNA repair but importantly pathways that extend into envelope stress, iron transport and toxin-antitoxin regulation. These data support a model that *E. coli* induces a distinctive transcriptional profile in response to damage-independent fork arrest that permits individual cells in the population to switch from a survival mode to a programmed cell death mode.

A Role for YbeY in DNA Replication?

Recently a body of work has emerged suggesting an intricate coupling of protein translation and DNA replication (67, 77, 78). The highly conserved GTPase, ObgE/CtgA, exemplifies this association. ObgE/CtgA has been shown to bind the ribosome (79, 80) and is required for ribosome assembly (78, 81). ObgE/CtgA has also been shown to regulate chromosome partitioning and subsequent cell events (67, 82, 83). In Chapter 7, I explored the possibility that, like ObgE/CtgA, YbeY may act as a mediator between translation and replication and how this role may lead to the increased resistance to HU observed in the $\Delta ybeY$ mutant.

With my model of the cellular response of *E. coli* to HU, I began studying the resistance of the $\Delta ybeY$ mutant to HU. I used a systems-level analysis of genome-wide transcriptional response of the $\Delta ybeY$ mutant to HU treatment and compared this to the response of the parental strain MC4100. The results showed a striking deviation in response. The $\Delta ybeY$ mutant initiated the major DNA repair response like the parental strain MC4100, but was much less sensitive to activation of cell death programs (Chapter

7). In addition I show that YbeY expression is responsive to HU treatment and YbeY directly associates with ribonucleotide reductase *in vivo*.

Chapter 2

Identification of Novel *Sinorhizobium meliloti* Mutants Compromised for Oxidative
Stress Protection and Symbiosis.*

* **Davies, B. W., and G. C. Walker**, 2007. Identification of Novel *Sinorhizobium meliloti* Mutants Compromised for Oxidative Stress Protection and Symbiosis. *J. Bacteriol.* **189**: 2110-2113.

**Identification of Novel *Sinorhizobium meliloti* Mutants Compromised for Oxidative
Stress Protection and Symbiosis.**

Running title:

S. meliloti mutants defective in oxidative stress protection and symbiosis.

Bryan W. Davies and Graham C. Walker*.

Department of Biology, Massachusetts Institute of Technology, Cambridge, MA 02139.

*Corresponding author. Mailing address: Department of Biology, Massachusetts Institute of Technology, Cambridge, MA 02139. Phone (617) 253 6711. Fax: (617) 253 2643.

Email: gwalker@mit.edu.

Abstract

Employing a novel two-part screen, we identified *Sinorhizobium meliloti* mutants that were both sensitive to hydrogen peroxide and symbiotically defective on the host plant *Medicago sativa*. The mutants affect a wide variety of cellular processes and represent both novel and previously identified genes important in symbiosis.

Introduction

During symbiotic development with the host plant *Medicago sativa*, *Sinorhizobium meliloti* is subjected to a prolonged oxidative burst released by its host (6). The burst is composed of at least superoxide and hydrogen peroxide (H_2O_2), both of which are deleterious to cell survival. The prolonged burst is a chronic stress for *S. meliloti* with both superoxide and H_2O_2 readily detected in nodules several weeks after infection (6). It has become apparent that *S. meliloti* must be able to manage oxidative stress while in its host, but the issue is complex. For example, *S. meliloti* single mutants that lack either catalase A (*katA*) or catalase C (*katC*), which detoxify H_2O_2 , are symbiotically proficient, whereas the *katA/katC* double mutant is symbiotically defective. Furthermore, novel regulatory mechanisms may control the *S. meliloti* response to oxidative stress *in planta* as disruption of the major regulator of H_2O_2 defense in the free-living bacterium, *oxyR*, does not adversely affect symbiosis (8, 9). Given the obvious necessity of managing oxidative stress in the plant, and the apparent complexity of the defense network required to meet this stress, we hypothesized there might be additional oxidative stress defense mechanisms outside the spectrum of classic defense enzymes required for symbiosis. To explore this hypothesis, we undertook a novel two-part screen to identify *S. meliloti* mutants that are both sensitive to oxidative stress in the free-living state and symbiotically defective. Through this screen we identified several genes that have not previously been recognized as being important either in symbiosis or in oxidative stress protection for *S. meliloti*.

Identification of H₂O₂-sensitive and symbiotically defective *S. meliloti*

mutants. *S. meliloti* is exposed to a chronic H₂O₂ stress in the infection thread and nodule (6). Previous work has shown that certain *S. meliloti* strains compromised for H₂O₂ detoxification are symbiotically defective (8, 9). Considering this work, we choose to use H₂O₂ as the oxidative stress agent with which to screen *S. meliloti* mutants. We obtain a random pool of *S. meliloti* mutants by mutagenizing the wild type strain, Rm1021, with mTn5-GusNm (mTn5) (84, 85). The mTn5 was introduced into Rm1021 on a plasmid by triparental mating (85, 86). mTn5 mutants were selected on Luria-Bertani (LB) agar plates containing 200 µg/ml neomycin at 30 °C. We measured the endogenous peroxide level of LB using the Amplex Red Hydrogen Peroxide/Peroxidase Assay Kit (Molecular Probes) and found it to be 1.8 µM. Since a sublethal dose of H₂O₂ for wild type *S. meliloti* is 1 mM we felt confident the endogenous peroxide levels of the LB would not perturb our study (10). Matings were diluted so as to obtain approximately 100 colonies per plate and H₂O₂-sensitive mutants were subsequently identified by replica plating onto LB plates containing 0.7 mM H₂O₂ and 10 mM HEPES pH 7.0. After 3 days, we identified colonies unable to grow on plates containing H₂O₂. H₂O₂ sensitivity was confirmed by zone of inhibition assays (87). The mTn5 mutants showing sensitivity to H₂O₂ were tested for symbiotic proficiency with the plant host *Medicago sativa* (88). After 4 weeks, plant height was measured and compared to Rm1021-inoculated plants. Mutant-inoculated plants that were statistically shorter than Rm1021-inoculated plants were initially considered symbiotically defective. To confirm that the mTn5 was linked to both the H₂O₂ sensitivity and symbiotic deficiency, each mutant allele was transduced back into the parental strain Rm1021 (89). Three

independent transductants for each mutant allele were tested for both H₂O₂ sensitivity and symbiotic proficiency. To more precisely analyze the symbiotic phenotype, nitrogenase activity was then determined using acetylene reduction (90).

Santos, R., *et al.*, showed that *S. meliloti* is exposed to chronic oxidative stress while in the plant (6). Furthermore, Herouart D., *et al.* (91) demonstrated that *S. meliloti* defective in *katA* are sensitive to acute oxidative stress but do not show a symbiotic defect. These results suggest that chronic resistance to oxidative stress may be an important factor for *S. meliloti* to establish a functional symbiosis. Because of these observations, we employed assays such as zone of inhibition that measure *S. meliloti* sensitivity to chronic oxidative stress. In total, we screened 1.5x10⁴ mTn5 mutants. After transduction, we isolated 112 H₂O₂-sensitive mutants. Of these, 9 mutants were also symbiotically defective. To more broadly characterize the oxidative stress sensitivity of these mutants, we tested them for chronic sensitivity to superoxide by zone of inhibition assay using the superoxide generator menadione.

We used random primer PCR to identify the insertion point of the mTn5 in each mutant (Table 1) (85). The mTn5 has not been tested to determine if it contains the outward reading promoter present in the parental Tn5 (92, 93). As such, insertion of the mTn5 may cause polar effects on downstream genes, however work from our lab shows expression of downstream genes can occur in at least some of these contexts (94).

The *exoP*::mTn5, *glgA1*::mTn5 and *sitA*::mTn5 mutants all show small increases in sensitivity to H₂O₂ by zone of inhibition assay (Table 1). To better quantify the H₂O₂ sensitivity of these mutants, cultures of each mutant strains and Rm1021 were serially diluted and spread on LB plates and LB plates containing 0.3 mM H₂O₂ to determine

their relative plating efficiencies. After 3 days of growth, visible colonies were counted. Using this chronic stress method we determined that *exoP::mTn5*, *glgA1::mTn5* and *sitA::mTn5* show plating efficiencies of $2.1 \% \pm 0.2 \%$, $11.3 \% \pm 2.3 \%$, and $4.6 \% \pm 2.1 \%$, respectively, relative to Rm1021 on LB plates containing 0.3 mM H₂O₂.

Defects in genes associated with succinoglycan production cause H₂O₂ sensitivity. Rm1021 produces an acidic exopolysaccharide, succinoglycan that is required for proper symbiotic development (88-73). Succinoglycan is produced in both high and low molecular weight forms and carries succinyl, acetyl and pyruvyl modifications (95, 96). The low molecular weight fraction of succinoglycan is of particular interest because past studies have reported that the low molecular weight succinoglycan, rather than the high molecular weight succinoglycan, is able to restore the ability of invasion-deficient mutants to invade nodules (97-99). Our screen identified three genes previously shown to be required for succinoglycan production and symbiosis (Table 1) (100).

ExoP is required for polymerization of the succinoglycan monomer. It is thought to work in conjunction with ExoQ, to produce high molecular weight succinoglycan or with ExoT to produce the low molecular weight form (100, 101). A role for succinoglycan in protection against oxidative stress has not previously been reported for *S. meliloti*. One possibility is that succinoglycan can act as a diffusion barrier against H₂O₂ thereby protecting cells against exogenous H₂O₂. Consistent with this hypothesis, we find that an *exoY* mutant, which completely lacks succinoglycan, shows increased sensitivity towards H₂O₂ (zone of inhibition = 5.9 ± 0.1 cm) (101). This hypothesis is

supported by studies on the nodulation of *Sesbania rostrata* by *Azorhizobium caulinodans*. The early stages of this symbiosis are characterized by a massive production of H₂O₂ by the plant host. *In situ* H₂O₂ localization demonstrated that increased exopolysaccharide production by *A. caulinodans* prevented the incorporation of H₂O₂ inside the bacterium, suggesting a role for exopolysaccharide in protecting *A. caulinodans* against H₂O₂ (102). Additionally, the extensive pyruvyl modifications on Rm1021 succinoglycan may also play a role in protection against H₂O₂ as pyruvate has been shown to scavenge H₂O₂ non-enzymatically (103). The sensitivity of these exopolysaccharide mutants appears specific to H₂O₂ as none of the exopolysaccharide mutants showed increased sensitivity to menadione relative to Rm1021 (Table 1).

We also identified *exoD* in our screen. Although mutations in *exoD* lead to altered succinoglycan production, no biosynthetic role in succinoglycan synthesis has been attributed to *exoD*. Furthermore, genetic evidence has shown that altered production of succinoglycan is not the cause of the symbiotic defect in an *exoD* mutant (104). Although efforts have been made to define a physiological function for ExoD, further research will be required to explain why loss of this gene causes increased H₂O₂ sensitivity.

Metabolic defects cause H₂O₂ sensitivity and symbiotic defects. Our screen identified mutants in several different metabolic pathways, including nucleoside biosynthesis and sugar storage and metabolism (Table 1). We identified *tkt2*, which encodes one of two paralogs of transketolase found in the Rm1021 genome. This mutant is sensitive to both H₂O₂ and menadione. Transketolase functions at two stages in the

non-oxidative steps of the pentose phosphate pathway (105). Enhanced flux of sugars through the pentose phosphate pathway has been linked to oxidative stress resistance, possibly by increasing the production of reducing power in the form of NADPH (106-108).

Another mutant which is both sensitive to H₂O₂ and symbiotically defective has a mTn5 insertion in *glgA1*, which is a putative glycogen synthase that adds glucose to growing starch chains. In *S. meliloti*, *glgA1* lies directly upstream of the gene for phosphoglucomutase (*pgm*). *pgm* is also an *exo* gene (*exoC*) which catalyzes the reversible conversion of glucose-1-phosphate to glucose-6-phosphate for entry into carbon metabolism. *S. meliloti* *exoC* mutants induce empty, ineffective nodules on alfalfa and are dim on calcofluor due to a deficiency in succinoglycan synthesis (88). Calcofluor is a dye that fluoresces under UV light when bound to certain α -linked polysaccharides, such as succinoglycan (88). In contrast to *exoC* mutants, our *glgA1* mutant is bright on calcofluor (data not shown) and indistinguishable from Rm1021 indicating that the mTn5 insertion in our *glgA1* mutant is not polar on *exoC*. A role for glucose storage in oxidative stress protection has not previously been reported in *S. meliloti* and will require further investigation to elucidate its role. Interestingly, a glycogen synthase mutant identified in *Rhizobium tropici* shows enhanced symbiotic performance on the plant host *Phaseolus vulgaris*. This contrasting result highlights how different symbiotic associations can have significantly different host/symbiont requirements (109).

Our screen also identified *purL*, which encodes phosphoribosylformylglycinamide (FGAM) synthetase, the fourth enzyme in the

pathway for purine biosynthesis (110). Purine auxotrophs of most rhizobial species, including *S. meliloti*, have previously been shown to be symbiotically defective, however they have not been reported as sensitive to oxidative stress (111-113). It was recently shown that a *Sinorhizobium fredii purL* mutant has an altered lipopolysaccharide (LPS) layer though the reasons for this remain unclear (111). We considered the possibility that an altered LPS layer might allow easier diffusion of H₂O₂ into the cell, thus explaining an increased sensitivity. However, we found that, unlike *S. fredii*, disruption of *purL* in *S. meliloti* does not cause an observable change in the LPS layer by SDS-PAGE analysis (data not shown).

Defects in metal transport, protein biosynthesis and cytochrome C biogenesis cause H₂O₂ sensitivity and symbiotic defects. SitA is the periplasmic binding protein of a putative Mn/Fe ABC transporter. Our investigation of the *sitA::mTn5* mutant is discussed in the accompanying manuscript (114).

We were very surprised to identify peptidyl-tRNA hydrolase (*pth*) in our screen since Rm1021 has only one copy of *pth* in its genome (7). Pth scavenges peptidyl-tRNA molecules that arise normally during protein biosynthesis, is ubiquitous among bacteria and, in most cases, is an essential enzyme (115). Our *pth::mTn5* mutant also shows considerable sensitivity to menadione suggesting that Pth may have a general role in oxidative stress protection. One possibility is that translation increases in response to oxidative stress that in turn increases the demand on tRNA recycling.

The final gene we identified was *cycK*. *cycK* is part of the *cycHJKL* operon involved in cytochrome C-type biosynthesis. *cyc* mutants have been identified previously

in *S. meliloti* and other *rhizobial* species as required for symbiosis, but not for oxidative stress protection (116-118). The *cycK::mTn5* mutant exhibits the greatest increase in sensitivity to H₂O₂ and menadione (Table 1). In *S. meliloti*, C-type cytochromes are required for nitrate reduction *ex planta* and nitrogen fixation in root nodules (117). The role of *cycK* and cytochrome-C in oxidative stress defense will require further investigation.

Of the 112 mTn5 mutants we identified that were H₂O₂-sensitive but symbiotically proficient, we identified the mTn5 insertion point for the 3 mutants that displayed the most severe H₂O₂ sensitivity (Table 2). The mutant exhibiting the greatest sensitivity was disrupted in the global regulator of H₂O₂ protection, *oxyR*, which has previously been shown not to be required for symbiosis (10). *actR* was originally identified in *S. meliloti* as part of a two component system required for growth at low pH (119). Recent work in *E. coli* has shown that pH changes and oxidative stress affect the regulation of a large and overlapping set of genes suggesting a strong relationship between acid stress and oxidative stress (120). Interestingly, the *actR::mTn5* mutant is also very sensitive to menadione suggesting a general role in oxidative stress protection. We also identified a putative orf (SMc01853) coding for a protein with a DnaJ-domain. As oxidative stress causes protein damage, SMc01853 may act as a chaperon to manage oxidized proteins.

Comparison of Table 1 and Table 2 shows that the sensitivity of a mutant strain to H₂O₂ or menadione *ex planta* does not correlate with its ability to effectively nodulate alfalfa. This suggests that, of the several oxidative stress defense systems available to *S. meliloti*, only a specific subset may be required to combat the oxidative stress

encountered *in planta*. This may be due to the specific composition of the oxidative burst *S. meliloti* experiences *in planta*, which has not been fully characterized (6). Further study of Table 1 also shows a lack of correlation between the sensitivity of a strain to H₂O₂ or menadione *ex planta* and its capacity to fix nitrogen *in planta*. This may be because the oxidative stress sensitivity of some of the mutants is not the cause of their symbiotic deficiency. Alternatively, the different oxidative stress defense systems may be required at different developmental stages, allowing some mutants to proceed further in symbiosis than others. Our screen has identified several genes previously not associated with oxidative stress protection in *S. meliloti*. The results of this screen suggest that oxidative stress protection encompasses a much broader range of cellular functions than traditionally recognized.

Acknowledgements

We would like to thank members of the Walker lab for careful review of this manuscript. This work was supported by National Institutes of Health grant GM31010 to G.C.W. and a National Sciences and Engineering Research Council of Canada graduate scholarship to B.W.D. G.C.W. is an American Cancer Society Research Professor.

Table 1. Rm1021 mTn5 mutants identified as both H₂O₂ sensitive and symbiotically defective.

Mutant	H ₂ O ₂ Zone of Inhibition (cm)	Menadione Zone of Inhibition (cm)	Plant Height (cm)	Acetylene Reduction (pmol/nod/h)
Rm1021 (WT)	4.6±0.1	2.6±0.1	7.8±1.8	48.5±5.3
<i>exoP</i>	4.9±0.1	2.6±0.1	1.8±0.4	0.0±0
<i>exoD</i>	5.5±0.1	2.6±0.1	2.1±0.8	0.0±0
<i>exoQ</i>	5.2±0.1	2.6±0.1	1.8±0.1	3.1±1.4
<i>glgA1</i>	4.9±0.1	2.7±0.1	1.6±1.0	11.8±15.8
<i>tkt2</i>	5.6±0.1	3.0±0.1	2.2±0.5	5.9±5.2
<i>purL</i>	5.0±0.1	2.7±0.1	1.7±0.4	3.5±2.5
<i>sitA</i>	4.9±0.1	3.5±0.1	3.8±2.1	15.9±18.4
<i>cycK</i>	7.0±0.1	>8.0	1.7±0.4	0.3±0.3
<i>pth</i>	5.3±0.1	3.7±0.1	2.0±0.6	0.2±0.3
Blank control	---	---	2.1±0.1	0.0±0

Table 2. Rm1021 mTn5 mutants that were symbiotically proficient but displayed high sensitivity to H₂O₂.

Mutant	H ₂ O ₂ Zone of Inhibition (cm)	Menadione Zone of Inhibition (cm)
Rm1021 (WT)	4.6±0.1	2.6±0.1
<i>actR</i>	5.3±0.2	6.0±0.1
<i>oxyR</i>	7.4±0.1	4.2±0.1
SMc01853 (contains DnaJ domain)	5.6±0.1	2.7±0.1

Chapter 3

Disruption of *sitA* Compromises *Sinorhizobium meliloti* for Manganese Uptake Required
for Protection Against Oxidative Stress*

* **Davies, B. W., and G. C. Walker.** 2007. Disruption of *sitA* Compromises *Sinorhizobium meliloti* for Manganese Uptake Required for Protection Against Oxidative Stress. *J. Bacteriol.* **189**: 2101-2109.

**Disruption of *sitA* Compromises *Sinorhizobium meliloti* for Manganese Uptake
Required for Protection Against Oxidative Stress**

Bryan W. Davies and Graham C. Walker*

Department of Biology, Massachusetts Institute of Technology, Cambridge, MA 02139.

*Corresponding author. Mailing address: Department of Biology, Massachusetts Institute of Technology, Cambridge, MA 02139. Phone (617) 253 6711. Fax: (617) 253 2643.

Email: gwalker@mit.edu.

Running title:

S. meliloti sitA is required for oxidative stress protection

Abstract

During the initial stages of symbiosis with the host plant *Medicago sativa*, *Sinorhizobium meliloti* must overcome an oxidative burst produced by the plant in order for proper symbiotic development to continue. While identifying mutants defective in symbiosis and oxidative stress defense, we isolated a transposon-insertion mutant of *sitA*, which encodes the periplasmic binding protein of the putative iron/manganese ABC transporter SitABCD. Disruption of *sitA* causes elevated sensitivity to the reactive oxygen species hydrogen peroxide and superoxide. Disruption of *sitA* leads to elevated catalase activity and a severe decrease in superoxide dismutase B (SodB) activity and protein level. The decrease in SodB level strongly correlates with the superoxide sensitivity of the *sitA* mutant. We demonstrate that all free-living phenotypes of the *sitA* mutant can be rescued by the addition of exogenous manganese but not iron, a result that strongly implies SitABCD plays an important role in manganese uptake in *S. meliloti*.

Introduction

Symbiosis with the gram-negative α -proteobacterium *Sinorhizobium meliloti* allows the host plant, *Medicago sativa* (alfalfa), to utilize atmospheric nitrogen fixed by the microsymbiont. Through a complex exchange of chemical signals, *S. meliloti* induces root hair curling and nodule formation on alfalfa. *S. meliloti* trapped in the curled root hairs invade *M. sativa* through a tube-like structure called an infection thread and are eventually released into the cells of the developing nodule where they differentiate into nitrogen-fixing bacteroids (1, 2).

While in the infection thread, *S. meliloti* is exposed to an oxidative burst released by the host plant that is composed of at least hydrogen peroxide (H_2O_2) and superoxide (6). *S. meliloti* encodes a set of enzymes to defend against these reactive oxygen species (ROS) including superoxide dismutases, catalases and alkylhydroperoxidases(7). It has become evident that *S. meliloti* must be able to manage oxidative stress while in the host plant as loss of certain oxidative stress defense mechanisms cause symbiotic defects. For example, *S. meliloti* strains deficient in both catalase B and catalase C (*katB/C*) or both catalase A and catalase C (*katA/C*), enzymes that detoxify H_2O_2 , are symbiotically deficient (8, 9). However, exactly which rhizobial defenses are required to combat oxidative stress is a complex question. Several genes known to be required for defense against ROS in the free living state are dispensable for symbiosis. For example, disruption of the global regulator of H_2O_2 protection, *oxyR*, makes the free-living strain extremely sensitive to H_2O_2 , but does not affect symbiosis (10).

We were interested in identifying novel genes involved in *S. meliloti* oxidative stress protection and determining if these genes also played a role in the development of

symbiosis. To explore this question we undertook a two-part screen to identify transposon mutants of *S. meliloti* that were sensitive to H₂O₂, and that were also defective in symbiosis (114). One mutant identified in the screen has a transposon insertion in the *sitA* gene. *sitA* is the first gene in the four gene operon *sitABCD* that has been annotated as coding for a putative iron/manganese ABC transporter (7).

Iron and manganese are important metals for oxidative stress protection. Iron is used as a cofactor in defense enzymes such as catalase (11). Although in this context iron is helpful in protection against ROS, free iron in the Fe²⁺ state, can serve to exacerbate oxidative stress by producing hydroxyl radicals from peroxides through Fenton chemistry (12). In contrast to iron, manganese ions can help defend against ROS by scavenging both H₂O₂ and superoxide, as part of low molecular weight complexes with cellular ligands such as phosphate, lactate or bicarbonate. Although the exact chemistry of the scavenging has not been determined, the mechanism is thought to involve manganese ions cycling between the Mn²⁺ and Mn³⁺ states (13-16). In its enzymatic capacity, manganese also aids in oxidative stress defense by acting as the essential cofactor in dedicated ROS scavenging enzymes such as manganese-containing superoxide dismutases and catalases (17, 18).

In addition to safe guarding bacteria against ROS, manganese has also been shown to play an important role in virulence. Disruption of manganese uptake in pathogens *Salmonella enterica* serovar Typhimurium and *Streptococcus pyogenes* attenuates their virulence (19, 20). Furthermore, in *S. pyogenes* disruption of manganese uptake has also been linked to oxidative stress sensitivity (20). The use of manganese in virulence is most pointedly observed in the extreme case of the Lyme disease pathogen

Borrelia burgdorferi. *B. burgdorferi* has dispensed with a requirement for iron and has evolved survival strategies that are fully accommodated by manganese (121).

Considering the known roles for manganese in oxidative stress protection and the requirement of manganese uptake in pathogen/host interactions, the *sitA* mutant we identified was an intriguing candidate for further exploration. To define the role of SitA in *S. meliloti* free-living and symbiotic physiology, we first determined the deficiency responsible for the *sitA* mutant free-living phenotypes and subsequently explored the downstream effectors that contribute to the oxidative stress sensitivity and symbiotic defect.

Materials and Methods

Bacterial strains, phage, plasmids and growth conditions. Bacterial strains, generalized transducing phage and plasmids are listed in Table 1. *E. coli* strains were cultured at 37 °C in LB. *S. meliloti* strains were cultured at 30 °C in either LB supplemented with 2.5 mM MgSO₄ and 2.5 mM CaCl₂ (LB/MC) or M9 minimal media with 15 mM succinate (M9) (122). M9 was prepared without iron or manganese sources in plastic containers and filter sterilized. Manganese (Mn²⁺) was added as MnSO₄ (Sigma) and iron (Fe²⁺) as FeSO₄ (Sigma). Plastic tubes were used for growth and sensitivity assays. Unless otherwise stated, strains were initially grown on LB/MC before dilution into M9. The following antibiotics were used: streptomycin (500 µg/ml), neomycin (200 µg/ml), chloramphenicol (20 µg/ml), and tetracycline (10 µg/ml).

Genetic techniques and DNA manipulations. Transductions with fM12 were performed as described (89). Random mini-Tn5-GusNm (mTn5) mutagenesis and tri-parental matings were performed as described (85, 86). The protocols of Sambrook (123) were used for routine manipulations of plasmid and chromosomal DNA. To construct strains GWBD2, GWBD8, GWBD9 and GWBD10 a 300-500bp internal fragment of *sodB*, *pphA*, *degP1* or *relA* was cloned into pKNOCK-Tc respectively. To construct strains GWBD4, and GWBD11, a 300-500bp internal fragment of *sitB* or *degP2* was cloned into pJH104 respectively. The resulting plasmids were conjugated into Rm1021 via triparental mating to introduce a disruption by single-crossover homologous recombination. Single-crossover disruptions were transduced into Rm1021 and verified by PCR. To construct plasmid pGW1, full length *sitA* was PCR amplified and cloned into pMSO4. pGW1 was introduced into GWBD1 by triparental mating.

Hydrogen peroxide and plumbagin sensitivity assays. For H₂O₂ sensitivity assays, *S. meliloti* cultures were diluted into M9 medium and grown 3 days to OD₆₀₀ 1.0-1.2. These cultures were diluted to OD₆₀₀ 0.1 into M9 with or without 10 μM MnSO₄ or 30 μM FeSO₄ and grown 2 h at 30 °C before the addition of H₂O₂ to a final concentration of 8 mM. At the indicated times, samples were taken, serially diluted, and spotted onto LB agar. After 4 days of growth at 30 °C, the number of colony forming units was determined. For plumbagin sensitivity assays *S. meliloti* cultures were diluted into M9 medium with or without 10 μM MnSO₄ or 30 μM FeSO₄ and grown overnight to OD₆₀₀ 1.0-1.2. These cultures were diluted to OD₆₀₀ 0.1 into M9 with or without 10 μM MnSO₄ or 30 μM FeSO₄ before the addition of plumbagin to a final concentration of 0.75 mM.

At the indicated times, samples were taken, serially diluted, and spotted onto LB agar. After 4 days of growth at 30⁰C, the number of colony forming units was determined. H₂O₂ concentrations in solution were determined using Amplex Red Hydrogen Peroxide/Peroxidase Assay Kit (Molecular Probes).

Bacterial lysates, enzyme activity assays and immunoblots. *S. meliloti* lysates were obtained from cultures grown in M9 with or without 10 μM MnSO₄ or 30 μM FeSO₄. Cells were disrupted by sonication and protein concentration was determined by Bradford assay. In-gel catalase and superoxide dismutase assays were performed as previously described (124, 125). Immunoblotting was performed as previously described (126) with polyclonal Mn superoxide dismutase antibody (QED Biosciences).

RNA isolation and RT-PCR. Total RNA was isolated from *S. meliloti* cultures grown in M9 using Qiagen RNeasy Mini Kit and quantified by OD₂₆₀. DNA contamination was tested for by PCR amplification of 23S rRNA genomic sequence in the absence of RT. RT-PCR was performed using SuperScript One Step RT-PCR Kit (Invitrogen) using increasing amounts of RNA for 15 or 35 PCR cycles to determine the linear range for each target transcript. Primers were designed to amplify 300-500bp internal sequences for the indicated genes. RT-PCR reactions with primers specific to 23S rRNA were used as a control to ensure equal amounts of RNA template between reactions.

Plant assays. Alfalfa seedlings were nodulated on Petri dishes of Jensen agar as previously described (88). Three-day-old seedlings were inoculated with approximately 10^7 bacteria. Plant height, nodule number and nitrogen fixation were determined after 4 weeks of growth. Nitrogen fixation was quantified via the acetylene reduction assay (90). Ethylene-acetylene separation and quantitation were carried out on a Shimadzu GC-8A gas chromatograph. The amount of ethylene produced was calculated by peak integration and conversion to picomoles of ethylene formed per nodule by comparison to a standard curve developed from injected standard amounts of ethylene. 4 week old nodules were examined by electron microscopy using standard techniques (127, 128).

Bacteria were isolated as previously described (129). Briefly, nodules were surface sterilized with 70% ethanol for 30 s, followed by three water washes, and treatment with 10% bleach for 30 s, followed by three water washes. The nodules were then crushed with a sterile pestle in 100 μ l of LB/MC medium containing 0.3 M glucose. The nodule suspension was serially diluted (10^0 to 10^{-6}) and plated onto LB/MC medium containing 0.3 M glucose.

Results

The *sitA::mTn5* mutant is symbiotically defective on *Medicago sativa*. The *sitA* mutant we identified is disrupted by a mTn5 transposon at base 162 of the 903 bp *sitA* open reading frame. After determining the H₂O₂ sensitivity and symbiotic defect of the original isolate, we transduced the *sitA::mTn5* allele into the parental wild type strain, Rm1021. We tested several transductants and confirmed that both the H₂O₂ sensitivity

and symbiotic defect are linked to the mTn5 insertion in *sitA*. We selected one transductant, GWBD1, for further study. For clarity, we refer to strain GWBD1 as *sitA::mTn5*.

We inoculated *sitA::mTn5* and Rm1021 onto *Medicago sativa* seedlings. After 4 weeks, we assayed nodule number, plant height and ability to fix nitrogen as measured by acetylene reduction (Table 2). Both *sitA::mTn5* and Rm1021-inoculated plants began producing nodules after 1 week. After 4 weeks, *sitA::mTn5*-inoculated plants showed approximately 20% more nodules than Rm1021-inoculated plants. Nodules from Rm1021-inoculated plants were mostly pink (Fig. 1A) due to leghemoglobin which is a marker of a healthy symbiosis (130).

In contrast, all *sitA::mTn5*-inoculated plants produced mainly small white nodules indicative of a defective symbiosis (Fig. 1B). In addition to the small white nodules, *sitA::mTn5*-inoculated plants produced another type of nodule that was intermediate in size between healthy pink nodules and defective white nodules (Fig. 1C). This type of nodule has a slight pink zone at the base proximal to the root. We did observe an occasional pink nodule on a *sitA::mTn5*-inoculated plant but at a very low frequency.

sitA::mTn5-inoculated plants were significantly shorter and had a substantial reduction in acetylene reduction activity compared with Rm1021-inoculated plants (Table 2). These characterizations were consistent with the decrease in healthy pink nodules observed on *sitA::mTn5*-inoculated plants. While we were characterizing *sitA::mTn5*, a report describing a *sitA* deletion was published (131). In agreement with our observations, that report showed acetylene reduction was decreased for alfalfa

inoculated with the *sitA* deletion strain but did not further characterize the physiology of the symbiotic defect.

sitA::mTn5-inoculated plants showed reduced but measurable levels of acetylene reduction, suggesting that the strain is able to colonize the nodules. However, the majority of nodules produced by *sitA::mTn5* were small and white, indicative of a failed symbiosis. This suggests that if *sitA::mTn5* is able to colonize nodules it does so with a greatly reduced efficiency. To gain a better understanding of the effect of the *sitA* transposon disruption on symbiotic development of *S. meliloti*, we examined the ultrastructure of each type of nodule induced by *sitA::mTn5* by electron microscopy (Fig. 1E). Each nodule type from *sitA::mTn5*-inoculated plants had a similar ultrastructure that differs markedly from nodules induced by the parental strain Rm1021 (Fig. 1D). The most striking difference was the presence of large starch granules in *sitA::mTn5*-induced nodules. These large deposits found lining the wall of the plant cell in *sitA::mTn5*-induced nodules were completely absent from Rm1021-induced nodules. Deposits of large starch granules have also been observed in several other symbiotically defective strains of *S. meliloti*, though the reason for their presence is still not understood (132-134). We also observed that the plant vacuoles in *sitA::mTn5*-induced nodules were much smaller and displayed more irregular shapes than vacuoles in Rm1021-induced nodules.

We found it intriguing that, although *sitA::mTn5* clearly produces three morphologically distinct types of nodules, the ultrastructure of each type was very similar. This observation led us to hypothesis that, although *sitA::mTn5* were found in each type of nodule, perhaps their intracellular survival varies. To determine the number

of bacteria in the nodules, we crushed each type of nodule from *sitA::mTn5*-inoculated plants as well as nodules induced by Rm1021 to recover any bacteria present and plated for colony forming units. Interestingly, although the micrographs show comparable number of bacteria in each type of *sitA::mTn5*-induced nodule, we were only able to recover bacteria from the pink nodules. However, these nodules contained approximately 1000-fold fewer bacteria than pink nodules from Rm1021-inoculated plants (data not shown).

It was possible that the bacteria recovered from *sitA::mTn5*-induced nodules had acquired a suppressor mutation allowing for their survival. To determine if a suppressor had accumulated, we confirmed the presence of the mTn5 insertion in *sitA* in bacteria isolated from pink *sitA::mTn5*-induced nodules, and used these isolates to re-inoculate *M. sativa*. After 4 weeks, we found the same plant phenotypes and spectrum of nodules as were found when inoculating with the original *sitA::mTn5* strain (data not shown). This result indicates that the pink nodules formed by *sitA::mTn5* are not due to the acquisition of a suppressing mutation. As *M. sativa* is an outbred tetraploid, we hypothesize that the formation of pink nodules with *sitA::mTn5* is most likely due to the genetic variability of the plant host (135).

Genetic characterization of *sitA::mTn5*. *sitA* is the first transcribed gene of the *sitABCD* operon (7). We therefore felt it essential to determine the effect of the mTn5 disruption on expression of the downstream genes in the operon, *sitBCD*. We performed RT-PCR on genes *sitB*, *sitC* and *sitD*. In *sitA::mTn5*, *sitB*, *sitC* and *sitD* are all expressed but at reduced levels compared to that in Rm1021 (Fig. 2). Although there is decreased

expression from *sitBCD*, we nevertheless found that expression of *sitA* alone from a plasmid was sufficient to rescue the *sitA::mTn5* symbiotic defect (data not shown). However, *sitBCD* expression is still important for symbiotic development since a strain carrying a polar disruption of *sitB* (GWBD4) shows a symbiotic defect equivalent to that of *sitA::mTn5* (data not shown).

Growth of *sitA::mTn5* is limited for manganese. When we first isolated the *sitA* transposon mutant we observed that it formed colonies more slowly than Rm1021 on LB plates. *sitA* is part of the *sitABCD* operon which is designated as a putative iron/manganese ABC transporter in the *S. meliloti* genome (7). It seemed likely that the decreased growth rate of *sitA::mTn5* is due to insufficient uptake of one or both of these metals. We subsequently found that *sitA::mTn5* has a decreased growth rate compared to Rm1021 in LB liquid media and the growth defect is even more severe in M9 medium. Rm1021 was able to grow in M9 alone, however *sitA::mTn5* showed no appreciable growth (Fig. 3A). To determine if either iron or manganese limitation was responsible for the growth defect, we supplemented the growth medium with either MnSO_4 or FeSO_4 . Addition of 10^{-5} M MnSO_4 completely restored the growth rate of *sitA::mTn5* to that of Rm1021 (Fig. 3B). Addition of FeSO_4 caused an increase in the growth rate of Rm1021 but did not affect the growth of *sitA::mTn5* even when included at $30 \mu\text{M}$ (Fig. 3C). Taken together, these data indicate that the growth defect of *sitA::mTn5* is due to a defect in manganese uptake and not a defect in iron uptake.

***sitA::mTn5* sensitivity to H₂O₂ is specifically rescued by manganese.**

sitA::mTn5 was identified as H₂O₂-sensitive in our initial screen (114). In that study, we assayed H₂O₂ sensitivity using zone of inhibition assays on LB plates. Under those conditions *sitA::mTn5* appeared only slightly more sensitive than Rm1021 to H₂O₂. Similar to the growth defect, we postulated that the sensitivity would be more apparent in minimal medium. As *sitA::mTn5* does not grow in M9, we first grew the strain in M9 supplemented with 10 μ M MnSO₄. We then diluted the culture in M9 without supplement and allowed the cultures to grow for 3 days to starve the cells for Mn²⁺ before assaying H₂O₂ sensitivity. Indeed, the *sitA::mTn5* cultures starved for Mn²⁺ showed a substantial increase in sensitivity to H₂O₂ relative to Rm1021 (Fig. 4A). Furthermore, we found that if manganese-starved *sitA::mTn5* cultures were then supplemented with 10 μ M MnSO₄ for 2 hours, the increased sensitivity to H₂O₂ was greatly diminished (Fig. 4B). We did not observe increased rescue with longer incubation times or increased MnSO₄ concentrations up to 100 μ M (data not shown). Also in agreement with the growth phenotypes, supplementing the medium with FeSO₄ does not rescue the H₂O₂ sensitivity (Fig. 4C).

As discussed previously, Mn²⁺ ions in low molecular weight complexes are able to detoxify H₂O₂. We were concerned that the rescue of H₂O₂ sensitivity by MnSO₄ might be a general detoxification of the medium by free Mn²⁺. To test this, we monitored the decomposition of H₂O₂ in M9 with and without 10 μ M MnSO₄ over time using the Amplex Red Detection system. We found that addition of 10 μ M MnSO₄ does not affect H₂O₂ concentration in solution (data not shown).

Catalases are the major component of an adaptive response to H₂O₂ and have been shown to be upregulated in bacteria compromised for other oxidative stress defenses (91, 136, 137). *S. meliloti* contains three catalases, KatA, KatB and KatC, none of which are manganese-dependent (8, 9, 91). We speculated that since *sitA::mTn5* exhibits increased sensitivity to H₂O₂, catalase activity may be altered in this strain. We assayed total cell lysates of *sitA::mTn5* and Rm1021 grown in M9, with and without MnSO₄, for catalase activity and observed an altered catalase activity profile in *sitA::mTn5* (Fig. 5). Most notably, KatA activity is upregulated in *sitA::mTn5*. KatA is controlled by the global sensor of H₂O₂ stress, OxyR (10). Upregulation of KatA suggests that even during normal growth, *sitA::mTn5* experiences an increased intracellular stress from reactive oxygen species. Furthermore, we found that *sitA::mTn5* grown in M9 supplemented with MnSO₄ showed a catalase profile that appeared identical to Rm1021, indicating that manganese starvation is responsible for the increase in oxidative stress (Fig. 5).

When comparing the catalase profile of *sitA::mTn5* to its sensitivity to H₂O₂ we noted two intriguing phenomenon. First, although KatA activity is strongly up regulated in *sitA::mTn5* the strain is still quite sensitive to H₂O₂. Second, although addition of 10 μM MnSO₄ restores the *sitA::mTn5* catalase activity profile to that of Rm1021 (Fig. 5), *sitA::mTn5* still remains slightly sensitive to H₂O₂ (Fig. 4B). These results suggest that there is an additional mechanism employed by *S. meliloti* to manage H₂O₂ stress that is dependent on SitA and possibly on full SitBCD activity as well.

***sitA::mTn5* shows increased sensitivity to superoxide that is specifically rescued by manganese.** Our initial characterization of *sitA::mTn5* indicated an

increased sensitivity to superoxide (114). This phenotype was more apparent in M9, where *sitA::mTn5* showed very strong sensitivity to plumbagin (Fig. 6A), a redox cycling quinone that generates superoxide (138). *sitA::mTn5* sensitivity to plumbagin appears much more pronounced than its sensitivity to H₂O₂ as *sitA::mTn5* requires only overnight starvation of Mn²⁺ before sensitivity to plumbagin is observed. As with the sensitivity to H₂O₂, growing *sitA::mTn5* in M9 supplemented with MnSO₄ prior to assaying with plumbagin decreased its sensitivity (Fig. 6B). Also like H₂O₂ sensitivity, supplementation with FeSO₄ did not rescue *sitA::mTn5* plumbagin sensitivity (Fig. 6C). The addition of MnSO₄ had an even greater effect on *sitA::mTn5* plumbagin sensitivity than on its H₂O₂ sensitivity as addition of MnSO₄ to the assay completely abolished *sitA::mTn5* sensitivity to plumbagin.

SodB activity is decreased in the *sitA::mTn5* mutant and correlates with a decrease in intracellular SodB level. Having established the ability of MnSO₄ to alleviate *sitA::mTn5* sensitivity to both H₂O₂ and plumbagin, we sought to determine the mechanism(s) manganese was acting through to provide oxidative stress protection. There is an increasing list of enzymes that require Mn²⁺ for activity (12). *S. meliloti* encodes a superoxide dismutase (SodB) that can use either Fe²⁺ or Mn²⁺ as a cofactor, but shows a much higher activity when utilizing Mn²⁺ (18). In gel activity assays using total cell lysates from M9 cultures showed that SodB activity is greatly reduced in *sitA::mTn5* (Fig. 7A). The decrease in activity parallels a similar decrease in SodB protein level from the same lysate (Fig. 7B). Addition of MnSO₄ to the cell lysate does not rescue SOD activity (data not shown). However, if cell lysates were made from

sitA::mTn5 cultures grown in M9 supplemented with 10 μ M MnSO₄, both SodB activity and protein levels were restored nearly to wild type levels (Fig. 7A,B). This rescue is specific as addition of FeSO₄, even at 30 μ M, to *sitA::mTn5* cultures did not restore SodB activity (data not shown).

To understand at which level of expression Mn²⁺ affects SodB, we performed RT-PCR using mRNA extracted from Rm1021 and *sitA::mTn5* cultures grown in M9. Using primers specific to a 300 bp internal fragment of the *sodB* gene we found that transcription of *sodB* is unaffected in *sitA::mTn5* under these conditions (Fig. 7C). In conjunction with the western blot showing a substantial decrease in SodB levels this implies that the Mn²⁺ is affecting the production of SodB by either enhancing translation of *sodB* mRNA and/or stabilizing SodB once translated.

Our biochemical data implicates SodB in the oxidative stress sensitivity of *sitA::mTn5*. We constructed a *sodB* mutant (GWBD2) and *sitA::mTn5 sodB* double mutant (GWBD3) to test for epistasis of oxidative stress sensitivity. Unfortunately we were unable to find conditions under which we could accurately compare the plumbagin sensitivity of *sitA::mTn5* and the *sodB* mutant due to the >10⁶-fold increase in plumbagin sensitivity of the *sodB* mutant relative to *sitA::mTn5*. However we did find that the decrease in SodB was not responsible for *sitA::mTn5* H₂O₂ sensitivity as the *sodB* mutant did not show increased sensitivity to H₂O₂ compared to Rm1021 (data not shown).

The decrease in SodB activity is not the cause of the *sitA::mTn5* symbiotic defect. The genetic and biochemical data offered strong evidence that the plumbagin sensitivity of *sitA::mTn5* is due to a decrease in SodB. To determine if a loss of SodB

activity could also be responsible for the symbiotic defect, we inoculated alfalfa with our *sodB* mutant. After 4 weeks the plant height and acetylene reduction activity were measured (Table 2). We found the *sodB* mutant inoculated plants to be indistinguishable from Rm1021 inoculated plants discounting the decrease in SodB activity as the cause of the *sitA::mTn5* symbiotic defect. In agreement with this result, we also found that plants inoculated with our *sitA::mTn5 sodB* double mutant exhibited the same degree of symbiotic deficiency as *sitA::mTn5*-inoculated plants alone (Table 2).

Discussion

The recognized roles of manganese in bacterial physiology are steadily growing (139). Proper uptake of manganese through SitABCD transporter homologs of *S. enterica* serovar Typhimurium and *S. pyogenes* have been shown to be required for full virulence of these pathogens (19, 20). We have shown that in *S. meliloti*, *sitA* is involved in Mn²⁺ uptake and a disruption of SitA results in a symbiotic defect thus extending the requirement of manganese to bacterial/plant symbiosis as well.

We found that a polar disruption of *sitB* causes a symbiotic defect similar to that of *sitA::mTn5* thereby implicating *sitB*, and potentially *sitCD* as well, as being required for proper symbiotic development. A previous study that isolated a *sitB* transposon mutant found that disruption of *sitB* did not affect symbiosis (140). That study used both a different strain of *S. meliloti* (strain 242) and different cultivar of *Medicago sativa* (Creola), which may explain the discrepancy between their results and ours. However, in agreement with this previous study, we found that our *sitB* mutant (GWBD4) had a

severe growth defect in media lacking manganese. As with *sitA::mTn5*, our *sitB* mutant did not grow in M9 and this defect was fully complemented by the addition of 10 μ M MnSO_4 (data not shown). As our *sitA::mTn5* and *sitB* mutants share very similar phenotypes both *in planta* and in free-living states, we feel that phenotypes we observe in *sitA::mTn5* represent a defect in the entire SitABCD transporter which requires all of its components to function efficiently.

Our work demonstrates that SitABCD plays a very important role in Mn^{2+} transport in *S. meliloti* and that it is a deficiency in Mn^{2+} that is responsible for the oxidative stress sensitivity and growth defect observed from disrupting *sitA* in Rm1021. Our findings are consistent with studies of SitABCD homologs in *S. enterica* serovar Typhimurium which showed that SitABCD can transport both Fe^{2+} and Mn^{2+} , however transport of Mn^{2+} is favored 100 times over Fe^{2+} (141). Previous work suggested that Mn^{2+} alone could not rescue the growth defect of a *sitA* deletion (131). The authors of that work graciously sent us their *sitA* deletion strain for comparison with our *sitA::mTn5* strain. We found the discrepancy in results is due to the concentration of MnSO_4 added to the medium. The previous authors reported that 1 μ M MnSO_4 was not sufficient to rescue the *sitA* deletion strain growth defect. We also found that 1 μ M MnSO_4 was not sufficient to rescue our *sitA::mTn5* strain growth defect but that adding 10 μ M MnSO_4 rescues the growth phenotype of both our and their *sitA* mutant strains when tested under our conditions (data not shown).

Our work has established the important role for manganese in oxidative stress protection in *S. meliloti*. The requirement for manganese in this capacity is most likely much greater than what we have observed. Since manganese is needed for growth, we

were required to provide a low level of manganese to serve this function. As such, we are unable to observe the actual severity of oxidative stress sensitivity in a truly manganese-free *S. meliloti* culture.

Our biochemical analysis strongly suggests that superoxide sensitivity of *sitA::mTn5* is due to a decrease in SodB activity and abundance. *S. meliloti* SodB has previously been shown to be able to utilize either iron or manganese but has stronger activity in the presence of manganese (18). Given the dual metal utilization of SodB, we found it interesting that disruption of manganese uptake specifically causes a decrease in SodB activity and protein level. Our results suggest a strong role for manganese, but not iron, for SodB to carry out its physiological role.

Our work has shown that the transcription of *sodB* is not affected in the *sitA::mTn5* background. This indicates that Mn^{2+} regulates SodB at the translational or post-translational level. One possibility is that Mn^{2+} is required for translation of *sodB* transcript, possibly by binding to the transcript and altering its secondary structure in a riboswitch-type manner (142). Alternatively, Mn^{2+} insertion in SodB may be required for enzyme stability so that in the absence of Mn^{2+} SodB is rapidly degraded.

Superoxide is dismutated by superoxide dismutase into O_2 and H_2O_2 , the latter of which is decomposed by catalase to O_2 and water (138). Given the decrease in SodB activity observed in *sitA::mTn5*, the 10 000- fold increase in sensitivity to plumbagin is understandable (Fig. 6A). We found that a *sodB* mutant does not show increased sensitivity to H_2O_2 , ruling out SodB deficiency as the cause of the H_2O_2 sensitivity of *sitA::mTn5*. Since SodB functions upstream of hydrogen peroxide detoxification, it is not unexpected that the *sodB* mutant was not sensitive to hydrogen peroxide.

Rm1021 does not appear to encode a Mn^{2+} -dependent catalase or any other obvious Mn^{2+} -dependent enzyme that could detoxify H_2O_2 (7). So what is the SitA-dependent mechanism responsible for the H_2O_2 sensitivity observed in *sitA::mTn5*? One explanation is that intracellular manganese alone acts as an oxidative stress defense mechanism. In non-protein low molecular weight complexes, Mn^{2+} has been shown to decompose H_2O_2 (15, 16). Supporting this idea are the results that the sensitivity to H_2O_2 of *sitA::mTn5* could be alleviated by growing the *sitA::mTn5* with $MnSO_4$ for only 2 h after starvation while protection against plumbagin required a much longer growth period in the presence of $MnSO_4$. This may be because time is required for *de novo* synthesis of SodB after addition of Mn^{2+} , whereas once uptaken, Mn^{2+} ions alone are able to attenuate the toxicity of H_2O_2 , decreasing the time required for rescue. Complicating this however, is the observation that the addition of exogenous Mn^{2+} does not fully restore *sitA::mTn5* resistance to H_2O_2 (Fig. 4B). This may be because once depleted of manganese, *sitA::mTn5* uptake of Mn^{2+} is not adequate to fully restore sufficient intracellular levels required for H_2O_2 resistance.

sitA::mTn5 is symbiotically defective. Although a *sodB* mutant in Rm5000 has previously been reported as symbiotically deficient we find that a *sodB* mutant in the Rm1021 background does not exhibit a detectable symbiotic defect (143). This discrepancy may be due to differences in strain background. Our findings eliminate the decrease in SodB level in *sitA::mTn5* as the cause of the symbiotic defect. Thus the question still remains, what causes the symbiotic defect in the *sitA::mTn5* mutant? From homology searches, potential Mn^{2+} -dependent enzymes encoded in the *S. meliloti* genome include DegP1, DegP2, PphA, RelA/SpoT, and SodB. We have created

disruptions of each of these genes using single cross-over suicide plasmids and have found that only the *relA/spoT* mutant shows a symbiotic defect, a result that was shown previously (144). The *relA/spoT* mutant and *sitA::mTn5* do share some free-living phenotypes, such as an inability to grow in M9, however *sitA::mTn5* does not possess other characteristics of the *relA/spoT* mutant such as overproduction of succinoglycan (data not shown). We are continuing to investigate this relationship. Although we postulate that the *sitA::mTn5* symbiotic defect is due to loss of a Mn^{2+} -dependent enzymatic activity it may be that *S. meliloti* is part of an increasing list of bacteria that utilize the activities of Mn^{2+} alone and that it is simply a decrease in intracellular Mn^{2+} that is the cause of the symbiotic defect in *sitA::mTn5*.

Acknowledgements

We would like to thank members of the Walker lab for careful review of this manuscript. This work was supported by National Institutes of Health grant GM31010 to G.C.W. and a National Sciences and Engineering Research Council of Canada graduate scholarship to B.W.D. G.C.W. is an American Cancer Society Research Professor.

Table 1. Bacterial strains, phages and plasmids

Strain/Phage/ Plasmid	Relevant Characteristics	Source/Reference
<u>Strain</u>		
MT616	<i>E. coli</i> MM294 pRK600, Cm ^R	T. Finan
DH5_	<i>E. coli endA1 hsdR17 supE44 thi-1 recA1 gyrA relA1 D(lacZYA-argG) U169 deoR</i>	BRL corp.
DH5__pir	<i>E. coli endA1 hsdR17 supE44 thi-1 recA1 gyrA relA1 D(lacZYA-argG) U169 deoR R6K ori</i>	BRL corp.
Rm1021	SU47 Sm ^R	F. Ausubel
<i>sitA</i>	Rm1021 <i>sitA</i> ::mTn5 original isolate	This study
GWBD1	Rm1021 <i>sitA</i> ::mTn5 transduced	This study
GWBD2	Rm1021 <i>sodB</i> ::pKNOCK-Tc	This study
GWBD3	GWBD1 <i>sodB</i> ::pKNOCK-Tc	This study
GWBD4	Rm1021 <i>sitB</i> ::pJH104	This study
GWBD5	GWBD1 pGW1	This study
GWBD6	GWBD1 pMSO4	This study
GWBD7	Rm1021 pMSO4	This study

GWBD8	Rm1021 <i>pphA</i> ::pKNOCK-Tc	This study
GWBD9	Rm1021 <i>degP1</i> ::pKNOCK-Tc	This study
GWBD10	Rm1021 <i>relA</i> ::pKNOCK-Tc	This study
GWBD11	Rm1021 <i>degP2</i> ::pJH104	This study
<i>ΔsitA</i>	Rm1021 derivative, <i>ΔsitA</i> , 025009-01	T. Chao
<u>Phage</u>		
fM12	Generalized transducing phage	T. Finan
<u>Plasmid</u>		
pKNOCK-Tc	<i>R6K ori</i> Tc ^R	M. Alexeyev
pCRS487	pUT::mTn5-GNm; Ap ^R Km ⁵	W. Reeve
pJH104	Nm ^R	This study
pMSO4	Sp ^R	This study
pGW1	<i>sitA</i> complementation plasmid	This study

Table 2. Plant height and nitrogenase activity of *M. sativa* plants inoculated with Rm1021 and indicated derivative strains after 4 weeks of growth.

Strain	Plant Height (cm)	Acetylene Reduction (pmol/nodule/h)
Rm1021	11.1 ± 1.8	46.2 ± 13.5
<i>sitA</i> ::mTn5 (GWBD1)	5.5 ± 1.6	12.3 ± 8.0
<i>sodB</i> (GWBD2)	9.5 ± 0.8	35.3 ± 11.3
<i>sitA</i> ::mTn5 <i>sodB</i> (GWBD3)	4.9 ± 2.1	9.9 ± 6.3

Fig. 1. Morphology and ultrastructure of *M. sativa* nodules induced by Rm1021 and *sitA*::mTn5. (A) Pink nodule induced by Rm1021. (B) Small white nodule induced by *sitA*::mTn5. (C) Intermediate nodule induced by *sitA*::mTn5. (D) Ultrastructure of pink nodule induced by Rm1021 (Bar = 1.2 µM). (E) All nodules induced by *sitA*::mTn5 had a similar ultrastructure. The ultrastructure of a small white nodule induced by *sitA*::mTn5 is shown (Bar = 1.5 µM). Starch granules (S) and plant vacuoles (V) are indicated.

Fig. 2. Transcript levels of *sitB*, *sitC* and *sitD* were analyzed by RT-PCR from total RNA extracted from Rm1021 and *sitA*::mTn5 strains grown in M9 medium. Transcript level of 23S rRNA was determined as a loading control.

Fig. 3. Growth of Rm1021 and *sitA*::mTn5 in M9 minimal medium. Strains grown on LB medium were diluted to OD₆₀₀ = 0.001 in M9 and growth was monitored by OD₆₀₀.

Due to detection limitations of the spectrophotometer, we could only determine measurements above $OD_{600} = 0.01$. (A) Rm1021 (□) and *sitA::mTn5* (□) growth in M9. (B) Rm1021 (□) and *sitA::mTn5* (□) growth in M9 supplemented with 10 μ M $MnSO_4$. (C) Rm1021 (□) and *sitA::mTn5* (□) growth in M9 supplemented with 30 μ M $FeSO_4$.

Fig. 4. Sensitivity of Rm1021 and *sitA::mTn5* to H_2O_2 . Strains grown in M9 minimal medium were diluted to $OD_{600} = 0.1$ in M9 alone or M9 supplemented with 10 μ M $MnSO_4$ or 30 μ M $FeSO_4$. After 2 h, the strains were challenged with 8 mM H_2O_2 . Samples were taken at the indicated times post challenge and plated for cfu. The data is represented as % survival relative to $t = 0$ h. (A) Rm1021 (□) and *sitA::mTn5* (□) in M9. (B) Rm1021 (□) and *sitA::mTn5* (□) in M9 supplemented with 10 μ M $MnSO_4$. (C) Rm1021 (□) and *sitA::mTn5* (□) in M9 supplemented with 30 μ M $FeSO_4$.

Fig. 5. Catalase activity pattern of Rm1021 and *sitA::mTn5* in M9 minimal medium. Total protein lysates were isolated from saturated cultures grown in M9 supplemented with or without 10 μ M $MnSO_4$. 35 μ g from each lysate were submitted to electrophoresis through a native 7.5% polyacrylamide gel and assayed for catalase activity. The positions of KatA, KatB and KatC are noted according to Siguid *et. al.* (1999).

Fig. 6. Sensitivity of Rm1021 and *sitA::mTn5* to plumbagin. Strains grown overnight in M9 supplemented with or without 10 μ M $MnSO_4$ or 30 μ M $FeSO_4$ were diluted to $OD_{600} = 0.1$ in the same respective medium and challenged with 0.75 mM plumbagin. Samples

were taken at the indicated times post challenge and plated for cfu. The data is represented as % survival relative to $t = 0$ h. (A) Rm1021 (□) and *sitA::mTn5* (○) in M9. (B) Rm1021 (□) and *sitA::mTn5* (○) in M9 supplemented with 10 μ M MnSO₄. (C) Rm1021 (□) and *sitA::mTn5* (○) in M9 supplemented with 30 μ M FeSO₄.

Fig. 7. Superoxide dismutase activity pattern and protein profile of Rm1021 and *sitA::mTn5* in M9 minimal medium. Total protein lysates were isolated from saturated cultures grown in M9 supplemented with or without 10 μ M MnSO₄. 35 μ g of each lysate were submitted to electrophoresis and (A) stained for superoxide dismutase activity or, (B) blotted for SodB protein. A *sodB* mutant strain (GWBD2) is shown as a negative control for the absence of SodB. (C) Transcript level of *sodB* was analyzed by RT-PCR from total RNA extracted from Rm1021 and *sitA::mTn5* strains grown in M9 medium. Transcript level of 23S rRNA was determined as a loading control.

Fig 1.

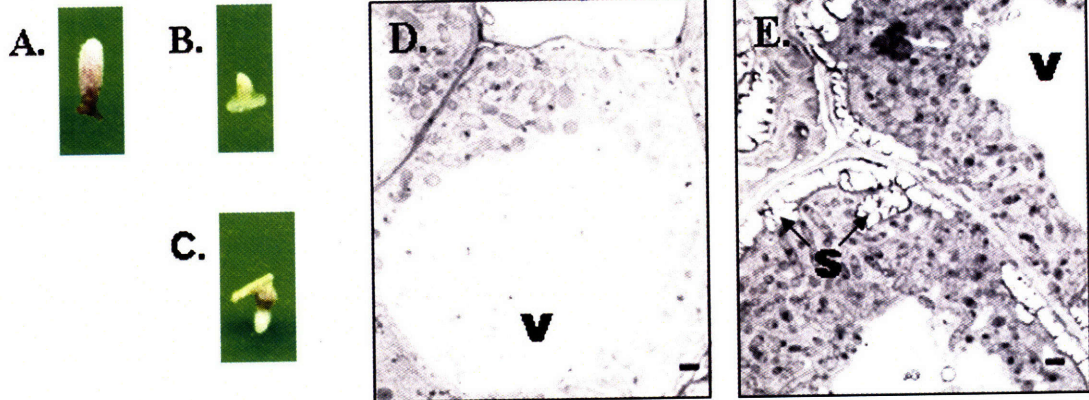


Fig. 2

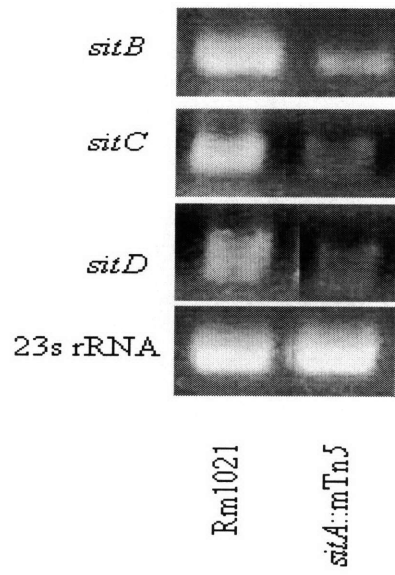


Fig. 3

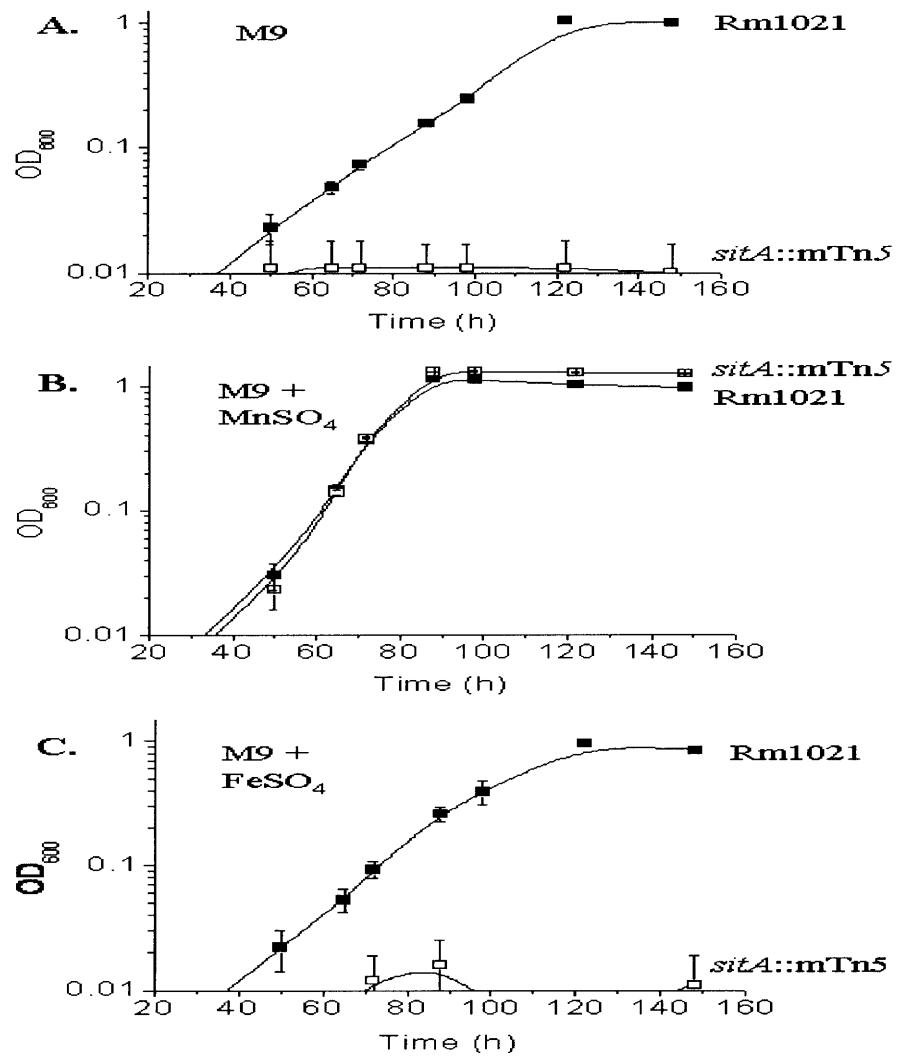


Fig. 4

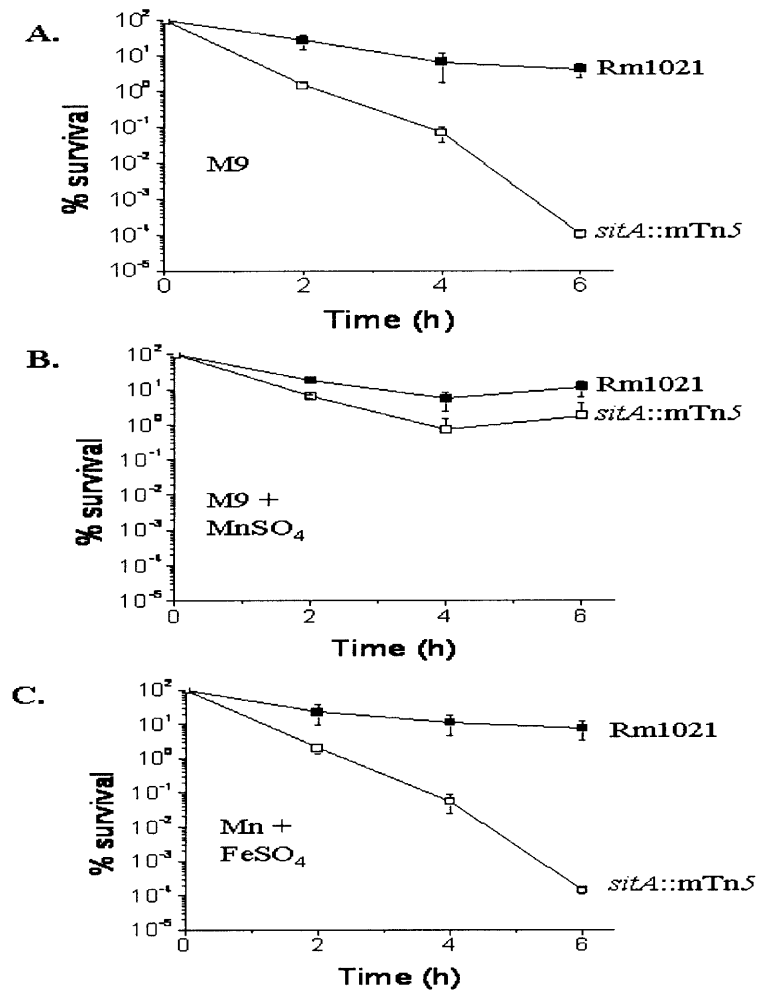


Fig. 5

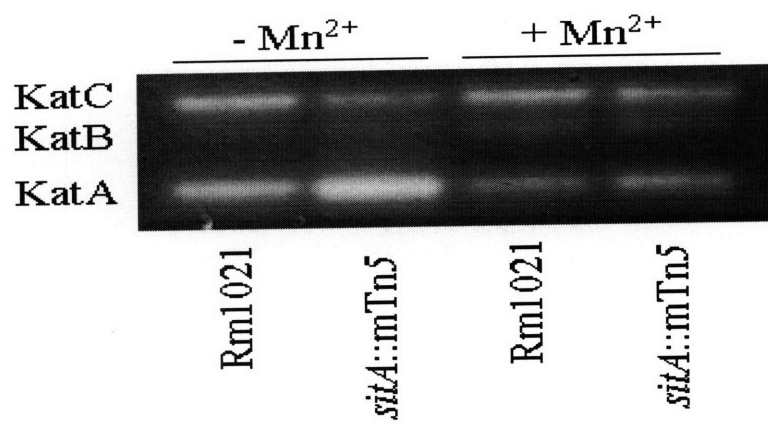


Fig. 6

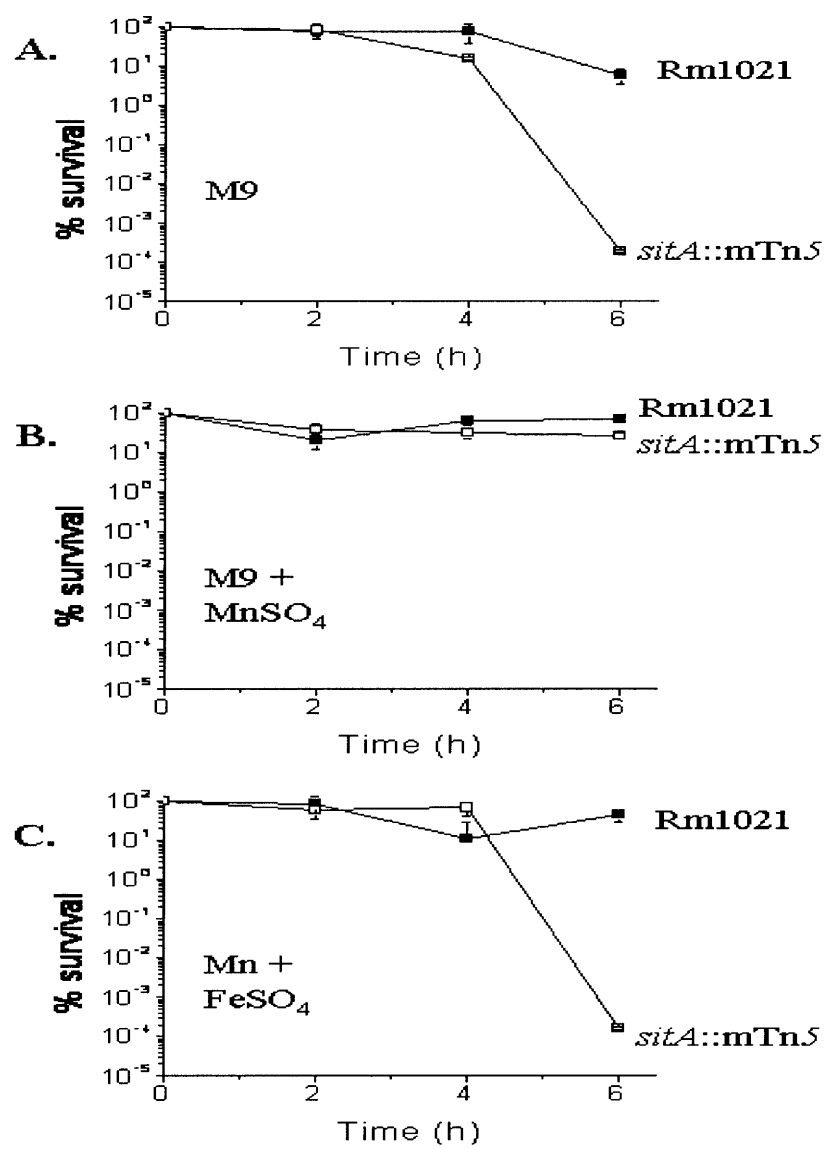
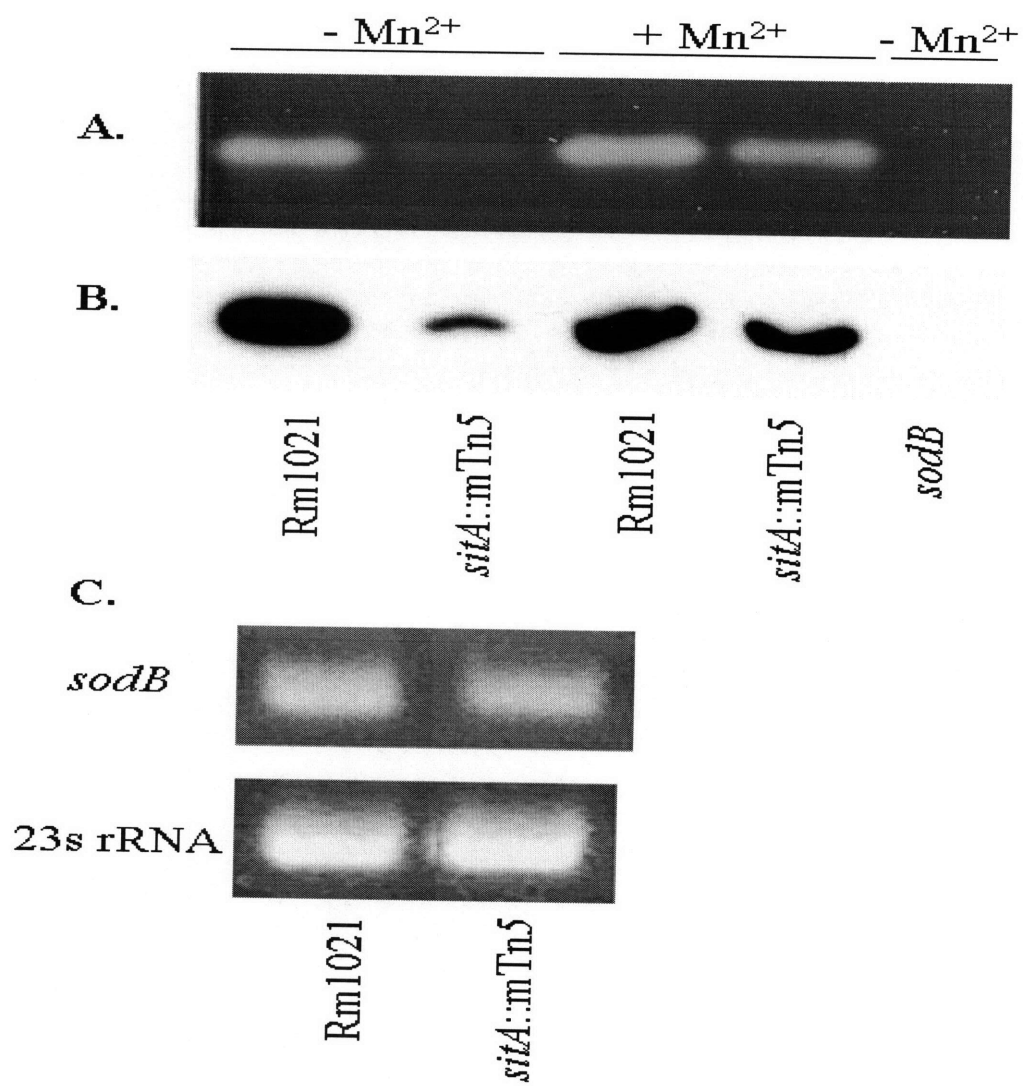


Fig. 7



Chapter 4

A Highly Conserved Protein of Unknown Function Plays an Essential Role for
Sinorhizobium meliloti in Symbiosis and Environmental Stress Protection*

Davies, B. W., and G. C. Walker. 2007. A Highly Conserved Protein of Unknown Function Plays an Essential Role for *Sinorhizobium meliloti* in Symbiosis and Environmental Stress Protection. *J. Bacteriol.* In revision.

**A Highly Conserved Protein of Unknown Function Plays an Essential Role for
Sinorhizobium meliloti in Symbiosis and Environmental Stress Protection.**

Bryan W. Davies and Graham C. Walker *

Department of Biology, Massachusetts Institute of Technology, Cambridge, MA 02139.

*Corresponding author. Mailing address: Department of Biology, Massachusetts Institute of Technology, Cambridge, MA 02139. Phone: (617) 253 6711. Fax: (617) 253 2643.

Email: gwalker@mit.edu.

Running title:

Characterization of a *S. meliloti* *SMc01113::mTn5* mutant

Absract

The composite genome of the soil bacterium *Sinorhizobium meliloti* encodes 6204 predicted protein-coding regions. Decades of research have helped to elucidate the function of a small percentage of these genes, but complete biochemical annotation is still far from complete. Detailed knowledge of the functional genome is crucial not only for understanding the basic biology of *S. meliloti* but also how it develops in symbiosis. We report here the first characterization of the symbiotically essential orf *SMc01113*. *SMc01113* produces an 18 kD protein that is a member of a highly conserved protein family, universal among bacteria. In addition to being required for *S. meliloti* symbiosis with alfalfa, *SMc01113* is also required to protect the bacterium from a wide range of environmental stresses. Our findings support a role for this novel protein in RNA and/or phospholipid metabolism.

Introduction

Under conditions of poor nitrogen availability, the α -proteobacterium *Sinorhizobium meliloti* can invade and establish a chronic symbiotic infection within the host plant *Medicago sativa* (alfalfa) (1, 2). The development of the symbiosis is complex. It begins by an intricate chemical conversation with each organism secreting, and responding to, small molecule signals. These chemical exchanges induce physiological changes in the plant host including cortical cell division in the roots to produce nodules, and root hair curling that traps nearby bacteria, creating an entry point for *S. meliloti* (1-4). Through a plant-derived structure called an infection thread, *S. meliloti* cells traverse the root hair cell until they are finally endocytosed into the cells within the developing plant nodule (4, 5). In the nodule, *S. meliloti* differentiates into a nitrogen-fixing bacteroid capable of converting atmospheric nitrogen into a usable form for plant consumption (1, 2).

Numerous symbiotically deficient mutants of *S. meliloti* have been identified that are affected in a wide array of biochemical pathways, from intermediary metabolism to cell envelope synthesis (4, 145). Characterization of these mutants has provided insights into bacterial functions necessary for each developmental stage of symbiosis. For example, mutations that disrupt exopolysaccharide production by *S. meliloti* strain Rm1021 result in early developmental defects characterized by aborted infection threads and the absence of bacteria in plant nodules (4, 100, 146). Other mutations, including some that alter lipopolysaccharide synthesis, do not affect early development of symbiosis but instead result in severe defects in later stages (4, 147). However, despite

the many genetic studies that have been carried out, we still do not have a clear picture of the full genomic complement required by *S. meliloti* to successfully complete each developmental stage of symbiosis.

The genome of *S. meliloti* strain Rm1021 was recently sequenced and revealed 6204 predicted protein-coding regions. Of these 6204 genes, a putative function could be postulated for only 59.7% of Rm1021 genes on the basis of bioinformatics analysis. An even smaller percentage of genes have actually been biochemical validated (7). This fact highlights a major stumbling block in all current omic level efforts. At best, we understand the function of only 50% of genes in any organism we are examining (21, 22). A screening strategy we developed for identifying symbiotically deficient mutants (148) led to the discovery that *SMc01113*, which encodes a protein of unknown function, is essential for symbiosis. The *SMc01113* protein is highly conserved, being present in all bacteria, and its function is critically required both to establish the chronic intracellular infection necessary for symbiosis and for defense against a wide range of environmental stresses.

Materials and Methods

Bacterial strains, phage, plasmids and growth conditions. Bacterial strains, generalized transducing phage and plasmids are listed in Table 1. *E. coli* strains were cultured at 37°C in LB. *S. meliloti* strains were cultured at 30°C in LB supplemented

with 2.5 mM MgSO₄ and 5.0 mM CaCl₂ (LB/MC) (122). The following antibiotics were used: streptomycin (500 µg/ml), neomycin (200 µg/ml) and spectinomycin (100 µg/ml).

Genetic techniques, DNA manipulations and protein purification.

Transductions with ΦM12 were performed as described (89). Random mini-Tn5-GusNm (mTn5) mutagenesis and tri-parental matings were performed as described (148). The protocols of Sambrook (123) were used for routine manipulations of plasmid and chromosomal DNA. To construct plasmid pGW2, full length *SMc01113* was PCR amplified and cloned into pMSO4. pGW2 was introduced into GWBD12 by triparental mating to produce strain GWBD14. His-tagged *SMc01113* was purified using Qiagen Ni-NTA agarose according to manufactures protocol.

Stress assays and enzyme activity assays. Zone of inhibition assays were performed as previously described (149). 10µl of each stress agent was used at the following concentration, methyl methane sulfonate (99% pure), naladixic acid (2 M), tetracycline (10 mg/ml), chloramphenicol (20 mg/ml), crystal violet (4 mg/ml), ampicillin (100 mg/ml), cefotaxime (10 mg/ml), menadione (1 M), hydrochloric acid (16 M). Efficiency of plating (EOP) assays were performed as described (150). For UV sensitivity assays, cultures were serially diluted and plated on LB agar. Plates were irradiated at 25 J/m² for the indicated times and cfu determined. Phage resistance assays were performed as described (87). In-gel catalase assays were performed as previously described by (150).

Plant assays. Alfalfa seedlings were nodulated on Petri dishes of Jensen agar as previously described (88). Three-day-old seedlings were inoculated with approximately 10⁷ bacteria. Plant height, nodule number and nitrogen fixation were determined after 4

weeks of growth. Nitrogen fixation was quantified via the acetylene reduction assay (90). Ethylene-acetylene separation and quantitation were carried out on a Shimadzu GC-8A gas chromatograph. The amount of ethylene produced was calculated by peak integration and conversion to picomoles of ethylene formed per nodule by comparison to a standard curve developed from injected standard amounts of ethylene. 4 week old nodules were examined by electron microscopy using standard techniques (128).

Results

A *SMc01113*::mTn5 mutant is severely defective for symbiosis with alfalfa.

We previously described a two-part screening strategy we used to identify a number of mTn5 mutants of *S. meliloti* strain Rm1021 that were both sensitive to H₂O₂ and defective in symbiosis with alfalfa (148). Continuation of that screen identified an additional mutant disrupted in the hypothetical orf *SMc01113*.

The *SMc01113* mutant we identified is disrupted by a mTn5 transposon inserted at base 284 of the 507 bp *SMc01113* open reading frame. After determining the H₂O₂ sensitivity and symbiotic defect of the original isolate, we transduced the *SMc01113*::mTn5 allele into the parental strain, Rm1021. We tested several transductants and confirmed that both the H₂O₂ sensitivity and symbiotic defect are linked to the mTn5 insertion in *SMc01113*. We selected one transductant, GWBD12 for further investigation. We will refer to strain GWBD12 as the *SMc01113*::mTn5 mutant.

The *SMc01113::mTn5* mutant had a striking symbiotic defect with the plant host alfalfa. To quantify the symbiotic defect of the *SMc01113::mTn5* mutant, we inoculated the *SMc01113::mTn5* mutant and its Rm1021 parent onto alfalfa seedlings. After 4 weeks, we assayed plant height, nodule type, and ability to fix nitrogen as measured by acetylene reduction (Table 2). After 4 weeks, Rm1021 inoculated plants were on average 80% taller than the *SMc01113::mTn5* mutant inoculated plants, and were a healthy green color compared the unhealthy yellow color of plants inoculated with the *SMc01113::mTn5* mutant (Fig. 1A, Table 2). Nodules from Rm1021 inoculated plants were mostly pink (Table 2, Fig. 1B), a color due to leghemoglobin, which is a marker of a successful symbiosis (130). In contrast, *SMc01113::mTn5* mutant inoculated plants produced only small white nodules (Table 2, Fig. 1C) indicative of a failed symbiosis. Consistent with both of these observations, Rm1021 inoculated plants showed much higher levels of nitrogen fixation than those inoculated with the *SMc01113::mTn5* mutant (Table 2). The symbiotic defect of the *SMc01113::mTn5* mutant was fully complemented by ectopic expression of *SMc01113* from a plasmid (Table 2).

To gain a better understanding of the nature of the symbiotic deficiency, we examined the ultrastructure of the white nodules produced by plants inoculated with the *SMc01113::mTn5* mutant. Nodule cells from plants inoculated with Rm1021 were full of bacteroids (Fig. 1D). In striking contrast, nodule cells from plants inoculated with the *SMc01113::mTn5* were completely devoid of bacteroids (Fig. 1E). The absence of bacteroids explains the extremely low acetylene reduction capacity of *SMc01113::mTn5* mutant inoculated plants (Table 2). In addition, plant cells of *SMc01113::mTn5* mutant

induced nodules were misshapen and lacked observable vacuoles when compared to those from Rm1021 induced nodules (Fig. 1D vs. 1E).

The small white nodules produced by plants inoculated with the *SMc01113::mTn5* mutant were very similar to nodules induced by Rm1021 strains defective in exopolysaccharide production, both in gross morphology and in ultrastructure (88, 151). This similarity led us to test the *SMc01113::mTn5* mutant for an alteration in exopolysaccharide production, however we found no change in exopolysaccharide (succinoglycan) production by the *SMc01113::mTn5* mutant as measured by calcofluor binding assays (data not shown) (151). Nonetheless, the absence of bacteroids in nodules from plants inoculated with the *SMc01113::mTn5* mutant or exopolysaccharide mutants contrasts strikingly with nodules induced by Rm1021 lipopolysaccharide (LPS) mutants, which are also proficient for exopolysaccharide synthesis. While defective for symbiosis, nodules from plants inoculated with LPS mutants are still filled with bacteroids (147). This suggests that the symbiotic defect of the *SMc01113::mTn5* mutant resembles that of exopolysaccharide deficient mutants in that the nodule invasion process is aborted before release of invading bacteria in the cells of the developing nodule.

SMc01113 is a member of a highly conserved protein family. *SMc01113* codes for a hypothetical, highly conserved protein of unknown function (7). The protein family that includes *SMc01113* is designated as COG0319 (24, 152). We cloned orf *SMc01113* into a protein expression vector and found that it did produce an 18kD protein as predicted (Fig. 2A).

Homologs of SMc01113 are found in all sequenced bacteria and are predicted to be putative metal-dependent hydrolases (24, 152). The predicted function is based on a conserved motif H(X)₃H(X)₄DH (Fig. 2B) that bears a resemblance to certain eukaryotic metal-dependent proteases (153). Homologs are strongly conserved throughout the alphaproteobacteria (Fig. 2B). The crystal structure of the homolog from *Aquifex aecolius* was recently solved and revealed that the spatial arrangement of three conserved histidines could allow them bind a metal ion (154). The same authors tested the purified protein for more than 15 different general biochemical activities but obtained only negative results in all assays (154). This suggests that the SMc01113 protein may have a unique or unusual substrate rather than having a generalized hydrolytic function active against a variety of substrates. This study is the first to offer insight into the biological role(s) of this universally conserved bacterial gene.

The *SMc01113::mTn5* mutant is sensitive to agents targeting key biological processes. Previous computational and biochemical analyses failed to elucidate a function for the SMc01113 protein family (152, 154). However, as described below, when we tested the *SMc01113::mTn5* mutant for altered sensitivity to several different stresses we found that the strain was sensitive to a remarkably wide spectrum of environmental stresses targeting several key cellular processes and structures. These included oxidative stress protection, DNA repair, cell wall synthesis, protein synthesis and cell envelope stability (Table 3, Fig. 3 and 4). All *SMc01113::mTn5* mutant sensitivities were fully complemented by ectopic expression of *SMc01113* from a plasmid (data not shown).

(i) Oxidative Stress. We originally identified the *SMc01113::mTn5* mutant based on its increased sensitivity to H₂O₂ (148). We initially measured the sensitivity of the *SMc01113::mTn5* mutant to H₂O₂ by a plating assay, where we observed a 16% increase of its zone of inhibition (ZI) relative to the parental strain Rm1021 (Table 3). To better quantify the difference in H₂O₂ sensitivity, we determined the efficiency of plating (EOP) of each strain. Cultures of Rm1021 and the *SMc01113::mTn5* mutant were serially diluted, plated on LB agar containing increasing concentrations of H₂O₂ and cfu were counted after 4 days growth. We found the *SMc01113::mTn5* mutant was substantially more sensitive than Rm1021 over a range of H₂O₂ concentrations (Fig. 3A). Bacteria deficient in catalase activity also show increased sensitivity to H₂O₂ (8, 9, 136). We assayed total cell lysates of Rm1021 and the *SMc01113::mTn5* mutant for catalase activity and found no observable differences in catalase activity between the two strains (Fig. 1B). This suggests that an alteration in catalase activity is not responsible for the increased sensitivity of the *SMc01113::mTn5* mutant to H₂O₂. We also tested the *SMc01113::mTn5* mutant for sensitivity against the superoxide generator menadione (138) by ZI assay. The *SMc01113::mTn5* mutant did not show altered sensitivity to menadione (Table 3). This suggests that oxidative stress deficiency defect of the mutant is specific to H₂O₂-induced stress.

(ii) DNA Metabolism. Since H₂O₂ causes DNA damage (136), we tested the sensitivity of the *SMc01113::mTn5* mutant to other agents that damage DNA; methyl methane sulfonate (MMS), ultraviolet radiation (UV) and nalidixic acid. MMS produces a variety of DNA lesions including N³-methyladenine, lethal lesions that inhibit DNA synthesis and need to be actively repaired (155-157). UV induces a variety of

photoproducts that interfere with DNA replication (70). Nalidixic acid targets DNA gyrase, whose role is to overcome topological problems encountered during DNA replication (158). Strikingly, we found that the *SMc01113::mTn5* mutant displayed an increased sensitivity to all of these agents (Table 3, Fig. 4A). These results indicate that the *SMc01113::mTn5* mutant has a general problem dealing with DNA damage or DNA replication problems rather than a defect in a specific DNA repair process.

(iii) Protein Synthesis. Our recognition that the *SMc01113::mTn5* had a pleiotropic phenotype then led us to test the sensitivity of the strain to agents that inhibit protein synthesis. We found that the *SMc01113::mTn5* mutant exhibited increased sensitivity to both tetracycline and chloramphenicol (Table 3). Both antibiotics inhibit translation, however tetracycline does so by blocking the binding of the incoming aminoacylated tRNA to the A site (159, 160) while chloramphenicol inhibits peptide bond formation (161).

In addition, we used the Phenotype MicroArrays (PMs) system to simultaneously test the mutant strain for further phenotypes (162). Using this technology we found that the *SMc01113::mTn5* mutant was also sensitive to the aminocyclitol spectinomycin, the aminoglycoside hygromycin B and macrolides spiramycin and tylosin (Table 4). As each of these antibiotics affects ribosome activity in a different way, these results suggest a possible defect in ribosome structure or general impairment of translation that increases its sensitive to all types of ribosome directed antibiotics.

(iv) Cell Envelope Integrity. Maintenance of cell envelope integrity has been shown to be crucial for Rm1021 to develop a normal symbiosis (87, 147, 149). We tested the integrity of the *SMc01113::mTn5* mutant cell envelope with crystal violet and

the detergent deoxycholate (DOC). An altered sensitivity to detergents is usually an indicator of a change in the bacterial cell envelope and the hydrophobic dye, crystal violet, is frequently used as an indicator of alterations in the cell envelope such as those caused by changes in the LPS (149). The *SMc01113::mTn5* mutant showed increased sensitivity to crystal violet when assayed by zone of inhibition assay (Table 3). The *SMc01113::mTn5* mutant was also very sensitive to DOC by EOP assay (Fig. 4B). The increased sensitivity to both these agents strongly suggests that the *SMc01113::mTn5* mutant has a cell envelope defect in addition to the other defects described above.

Lipopolysaccharide (LPS) comprises the outer leaflet of the outer membrane of Gram-negative bacteria. *S. meliloti* mutants with alterations in their LPS layer not only exhibit sensitivity to detergents but also show alteration in phage sensitivity, and often have symbiotic defects (87). The striking sensitivity of the *SMc01113::mTn5* mutant to DOC and crystal violet, along with its severe symbiotic defect, had us question whether the LPS layer was drastically altered in the mutant. We tested the mutant and parental strain against a panel of phage but found both strains showed the same pattern of sensitivity and resistance (Table 5). We also found that the *SMc01113::mTn5* strain was not sensitive to low pH (Table 3), another indicator of LPS alterations (149). This suggests that a gross LPS alteration is not the cause of the cell envelope instability of the *SMc01113::mTn5* mutant.

(v) Peptidoglycan Synthesis. The severe sensitivity of the *SMc01113::mTn5* mutant to agents that affect outer cell envelope integrity led us to question whether additional components of the cell envelope may also be compromised. We tested *SMc01113::mTn5* mutant against two inhibitors of peptidoglycan synthesis; ampicillin

and cefotaxime. Both ampicillin and cefotaxime inhibit the transpeptidase reaction required to crosslink glycan-linked peptide chains to form the mature peptidoglycan layer (163). The *SMc01113::mTn5* mutant was severely sensitive to both cell wall inhibitors (Table 3). To better quantify this sensitivity, we performed an EOP assay to measure cefotaxime sensitivity and found a 10^5 -fold increase in sensitivity at high doses (Fig. 4C). Since the peptidoglycan layer connects the inner and outer membrane, a weakened cell wall may perturb the outer membrane leading to increased sensitivity to other cell envelope destabilizing agents such as DOC and crystal violet.

Discussion

S. meliloti SMc01113 is a member of a highly conserved family that is found in every bacterium whose genome has been sequenced and is said to be part of the 206 genes that are required to be a bacterium (25). This genetic study offers the first insights into the biological function of this gene family in any bacterium. We were struck by the wide spectrum of stresses to which the *SMc01113::mTn5* mutant is sensitive. These results would seem to imply that the SMc01113 protein either plays numerous independent biological roles or that it instead perturbs a fundamental cellular function that affects a wide range of processes. Considering the striking diversity of the chemical structures and modes of action of agents to which the *SMc01113::mTn5* mutant is sensitive, we consider it more likely that the SMc01113 protein affects one central biological function rather than playing an active role in many different stress responses.

In addition to identifying phenotypes of the *SMc01113::mTn5* mutant, we used computational analysis to identify gene neighbors of *SMc01113* and its homologs throughout the bacterial domain (164, 165). The repeated occurrence of genes in each other's neighborhood in genomes has been shown to indicate a functional association between the proteins they encode (164). Our analyses showed that *SMc01113* and its homologs were always present near genes that function in RNA and phospholipid metabolism. These include genes for tRNA processing and ribosome maturation such as *trmB* and *era*, as well as those responsible for phospholipid turnover and modification including *lnt* and *dgkA*. A recent paper describing a similar analysis of the *SMc01113* genomic locus arrived at a similar conclusion (166).

A defect in either RNA or phospholipid metabolism could explain why the *SMc01113::mTn5* mutant is sensitive to so many agents or treatments. Sensitivity to DOC, crystal violet, ampicillin and cefotaxime all suggest a weakened cell envelope in the *SMc01113::mTn5* mutant. Altered phospholipid metabolism could result in a destabilized cell membrane that in turn could disrupt synthesis of new cell wall. This combination could lead to sensitivity of the observed agents. However, exactly how altered phospholipid metabolism would affect DNA metabolism or ribosome function is unclear.

A defect in RNA metabolism could occur at many levels. The large spectrum of ribosome inhibitors to which the *SMc01113::mTn5* mutant is sensitive raises the possibility the mutant may have a defect in ribosome assembly or function. Stress conditions often activate bacteria to synthesis defense proteins (136). Decreased translation efficiency could hinder this response and leave a bacterium vulnerable to a

wide array of stresses. Recent reports have also shown that ribosome maturation and DNA replication are intimately linked, which could explain the additional sensitivities of the *SMc01113::mTn5* mutant to UV, MMS and nalidixic acid (67, 81). In addition, we found that the *SMc01113::mTn5* mutant had a modest growth defect in LB (doubling time $Rm1021 = 3.0 \pm 0.1$ h vs. *SMc01113::mTn5* = 4.4 ± 0.3 h). Since growth rate is intimately coupled to protein synthesis (167) a defect in ribosome maturation could also account for the difference in growth rate.

Our previous report of our two part screening strategy for symbiotic mutants identified a mutant defective in translation (148). This mutant had a mTn5 insertion in the gene coding for peptidyl-tRNA hydrolase and also exhibited a severe symbiotic phenotype and increased sensitivity to H₂O₂ (148). If SMc01113 is involved in protein translation, these results suggest that symbiotic development is very sensitive to any perturbation to translation.

While its biochemical function remains elusive, our results clearly show that SMc01113 is absolutely required for Rm1021 to establish an intracellular infection with alfalfa (Fig. 1). Since homologs of SMc01113 are found in every sequenced bacteria, this gene cannot have evolved for solely for function in *Rhizobial* symbiosis. Nevertheless, in the many nodulation assays we have carried out with the *SMc01113::mTn5* mutant, we have never observed the formation of a pink nodule (data not shown). This suggests that the function of *SMc01113* cannot be compensated for by any other gene or pathway in *S. meliloti* during symbiosis. Serious effort will be required to identify the functional defect of such a pleiotropic mutant. Future work to identify the specific pathway the SMc01113 protein functions in will not only increase our

understanding of symbiosis but will also expand our knowledge of the role this novel protein plays in all bacteria.

Acknowledgments

This work was supported by National Institutes of Health grant GM31010 to G.C.W. and a National Sciences and Engineering Research Council of Canada graduate scholarship to B.W.D. G.C.W. is an American Cancer Society Research Professor.

Table 1. Bacterial strains, phages and plasmids

Strain/Phage/ Plasmid	Relevant Characteristics	Source/Reference
<u>Strain</u>		
MT616	<i>E. coli</i> MM294 pRK600, Cm ^R	T. Finan
DH5_	<i>E. coli</i> <i>endA1 hsdR17 supE44 thi-1 recA1</i> <i>gyrA relA1 D(lacZYA-argG) U169 deoR</i>	BRL corp.
DH5_ _pir	<i>E. coli</i> <i>endA1 hsdR17 supE44 thi-1 recA1</i> <i>gyrA relA1 D(lacZYA-argG) U169 deoR</i> <i>R6K ori</i>	BRL corp.
Rm1021	SU47 Sm ^R	F. Ausubel
SMc01113	Rm1021 <i>SMc01113::mTn5</i> original isolate	This study
GWBD12	Rm1021 <i>SMc01113::mTn5</i> transduced	This study
GWBD5	Rm1021 (pMSO4)	B. Davies
GWBD13	<i>SMc01113::mTn5</i> (pMSO4)	This study
GWBD14	<i>SMc01113::mTn5</i> (pGW2)	This study
<u>Phage (Φ)</u>		
M1		G. Campbell

M5		G. Campbell
M6		G. Campbell
M7		G. Campbell
M9		G. Campbell
M10		G. Campbell
M11		G. Campbell
M12	Generalized transducing phage	T. Finan
 <u>Plasmids</u>		
pCRS487	pUT::mTn5-GNm; Ap ^R Km ⁵	W. Reeve
pMSO4	Sp ^R	M. Barnett
pGW2	<i>SMc01113</i> complementation plasmid	This study
pET11a	T7 promoter, Ap ^R	Novagen
pGW3	<i>SMc01113</i> in pET11a	This study

Table 2. Plant heights, nodule types and nitrogenase activities of alfalfa inoculated with Rm1021 and derivative strains after 4 weeks of growth.

Strain	Plant Height (cm)	Pink nodules (%/plant)	White nodules (%/plant)	Acetylene Reduction (nmol/nodule/h)
Rm1021	10.2±1.0	93.6±8.3	6.4±8.3	19.5±0.4
<i>SMc01113::mTn5</i>	2.2±1.0	0	100	1.1±1.1
Rm1021(pMSO4)	10.8±2.0	93.4±8.2	6.6±7.5	N/A
<i>SMc01113::mTn5</i> (pMSO4)	2.6±0.6	0	100	N/A
<i>SMc01113::mTn5</i> (pGW2)	11.1±2.2	91.1±9.9	8.9±10.0	N/A

N/A: not available

Table 3. Zone of inhibition (ZI) results for Rm1021 and *SMc0113::mTn5* mutant strains screened against several environmental stresses.

Stress	Zone of Inhibition (cm)	
	Rm1021	<i>SMc0113::mTn5</i>
H ₂ O ₂	3.7±0.1	4.3±0.1
Menadione	3.2±0.1	3.2±0.1
Methyl methane sulfonate (MMS)	4.4±0.1	5.0±0.1
Nalidixic Acid (NA)	5.4±0.1	6.3±0.1
Tetracycline (Tc)	6.0±0.1	6.6±0.1
Chloramphenicol (Cm)	5.5±0.1	6.1±0.1
Crystal Violet	3.6±0.1	4.2±0.1
Conc. Hydrochloric Acid	4.2±0.1	4.2±0.2
Ampicillin (Ap)	5.1±0.1	7.7±0.1
Cefotaxime (Cf)	4.1±0.1	6.8±0.1

Table 4. Mutant Phenotypes of the *SMc01113::mTn5* mutant by Phenotype Microarray analysis.

Test ^a	Difference ^b
Spectinomycin	-105
Hygromycin B	-101
Spiramycin	-103
Tylosin	-125

^a Chemicals were tested in 96-well PMs

^b The OmniLog-Pm software generates time course curves for respiration (tetrazolium color formation) and calculates differences in the areas for mutant and control cells. The units are arbitrary. Negative values indicate that the control showed greater rates of respiration than the mutant. The differences are averages of values reported for two or more mutants of each type compared with the corresponding control strains.

Table 5. Phage sensitivity of Rm1021 and *SMc01113::mTn5* mutant strains.

Strain	Phage Sensitivity							
	_M1	_M5	_M6	_M7	_M9	_M10	_M11	_M12
Rm1021	S	S	S	S	S	R	R	S
<i>SMc01113::mTn5</i>	S	S	S	S	S	R	R	S

R: resistant, S: sensitive.

Fig. 1. Nodule morphology and ultrastructure of alfalfa inoculated by Rm1021 and *SMc01113::mTn5*. A. Plants inoculated with either Rm1021 or the *SMc01113::mTn5* mutant after 4 weeks growth. Plants were inoculated as indicated. B. Pink nodule induced by Rm1021. C. Small white nodule induced by *SMc01113::mTn5*. D. Ultrastructure of pink nodule induced by Rm1021 (Bar = 1.0 μ M). E. The ultrastructure of a small white nodule induced by the *SMc01113::mTn5* mutant is shown (Bar = 1.0 μ M). Plant vacuoles (V) are indicated.

Fig. 2. Protein expression and sequence alignment of SMc01113. A. Purified His-tagged SMc01113 run by SDS PAGE. B. SMc01113 homologs were aligned using T-coffee (168). The red bar underlines the conserved motif used to classify this protein family.

Fig. 3. Sensitivity of Rm1021 and the *SMc01113::mTn5* mutant to H₂O₂. A. Strains grown in LB/MC were diluted to OD₆₀₀ 0.1 in LB/MC, serially diluted and spotted on LB agar containing increasing amounts of H₂O₂. Cfu were counted after 4 days growth at 30°C. Rm1021 (□) and *SMc01113::mTn5* (□). B. Catalase activity pattern of Rm1021 and *SMc01113::mTn5*. Total protein lysates were isolated from saturated cultures grown in LB/MC. 35 μ g from each lysate were submitted to electrophoresis through a native 7.5% polyacrylamide gel and assayed for catalase activity.

Fig. 4. Sensitivity of Rm1021 and the *SMc01113::mTn5* mutant to UV, deoxycholate and cefotaxime (Cf). Strains grown in LB/MC were diluted to OD₆₀₀ 0.1 in LB/MC, serially diluted and spotted on LB agar. A. Plates were irradiated for increasing periods of time at 25 J/m². B. Plates contained increasing amounts of deoxycholate. C. Plates contained increasing amounts of cefotaxime (Cf). Cfu were counted after 4 days growth at 30°C. Rm1021 (□) and *SMc01113::mTn5* (○).

Fig. 1

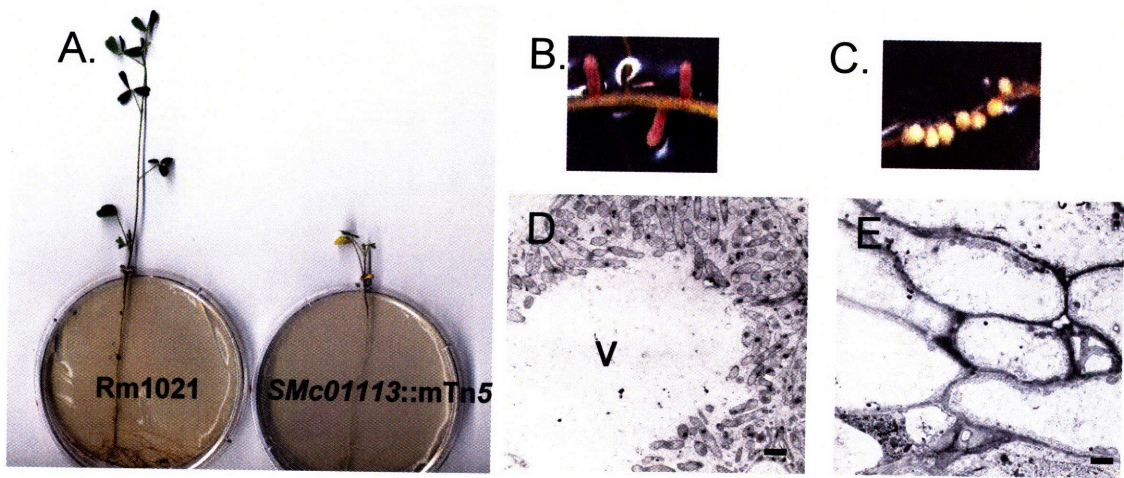
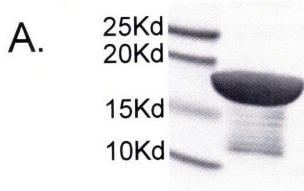


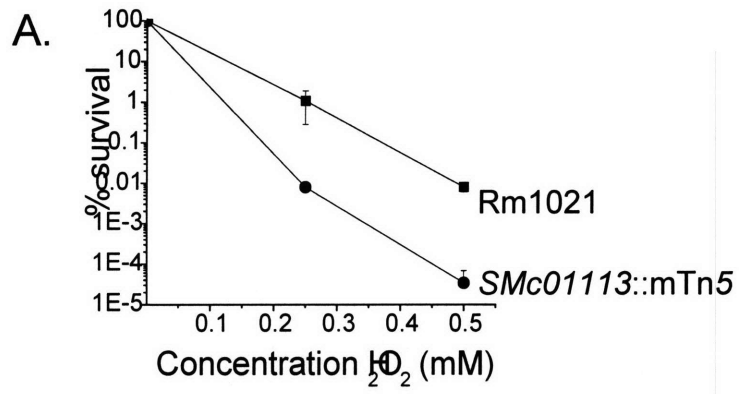
Fig. 2



B.

Atumefaciens	----MRAFRATDVKT--	MAALDIQISVEAEGWSSE	NLAAFATV	VLNA	VDF	LKREEE																																												
Smeliloti	-----	MTALDIQISVEAGDWPPE	ELQSF	CERVLE	AADEL	LAREEN																																												
Babortus	-----	MS--DNALHIDIMLEAGN	WPEAS	LES	LVSN	VAANNL																																												
Retli	-----	MAELDIQISIEDIGWPEE	TLLV	FCERVL	GAAI	VLRDNEK																																												
Rleguminosarum	-----	MAELDIQISVEDIGWPEE	TLLS	FCERVL	GAAV	VLRDSEK																																												
Bjaponicum	MGADASAFSFRKTMSEN--	LPMTENLVVADCFQRE	PDSEAV	IQRAV	AAAE	SVDDE--																																												
Mloti	-----	MPEDNLSGGGPP	VDID	ISVEAGD	FEDE	AGLARLVDRANDAAFAETGV---																																												
Aaeolicus	-----	MSSTK--	RQKNRV	LKLRK	KVRK	KIEKWAELLSALGLNN-																																												
consensus	-----	ms-----	l	d	q	i	s	v	e	a	---	w	p	---	e	e	l	---	f	v	e	r	v	l	a	a	a	---	f	l	---	e																		
Atumefaciens	QPEEKMPV	LSLV	ETDD	EM	TR	EA	EW	DK	KA	NV	LS	FP	AP	FP	EP	GG	MP	GP	---	ML	GI																													
Smeliloti	QPLEAQA	ALS	LV	ETDD	Q	S	RA	IA	EA	EW	GQ	KA	NV	LS	FP	AP	FP	VP	TP	GR	MP	GP	---	ML	GI																									
Babortus	-GLKSAT	S	EL	S	V	ETDD	A	S	I	Q	L	L	G	E	W	G	K	D	K	F	N	V	LS	FP	AP	FP	V	K	A	G	S	Q	P	GP	---	ML	GI													
Retli	QPEEKMP	V	LS	V	ETDD	A	S	I	Q	L	L	G	E	W	G	K	D	K	F	N	V	LS	FP	AP	FP	V	Q	R	G	K	V	P	GP	---	ML	GI														
Rleguminosarum	QPEETMA	P	V	LS	V	ETDD	A	S	I	Q	L	L	G	E	W	G	K	D	K	F	N	V	LS	FP	AP	FP	V	Q	P	G	K	M	P	GP	---	ML	GI													
Bjaponicum	----VAEA	V	V	M	L	T	D	A	G	A	R	T	L	S	N	W	G	I	D	K	F	N	V	LS	FP	AP	Q	E	G	E	G	K	E	G	D	A	R	M	L	GI										
Mloti	----TGR	S	LS	V	ETDD	A	S	I	Q	L	L	G	E	W	G	K	D	K	F	N	V	LS	FP	AP	FP	A	E	F	A	Q	G	G	L	P	E	---	ML	GI												
Aaeolicus	----V	LS	V	Y	T	D	A	S	I	Q	L	L	G	E	W	G	K	D	K	F	N	V	LS	FP	AP	FP	M	G	E	F	F	G	G	Y	---	K	---	ML	GI											
consensus	qp-p---	E	l	s	v	f	t	d	d	a	s	i	r	e	i	n	a	e	w	r	g	k	d	k	p	t	n	v	l	s	f	p	a	f	p	v	---	g	---	m	l	g	i							
Atumefaciens	VIARETV	EA	EA	LE	L	D	K	S	F	E	D	H	L	T	H	L	V	H	G	F	L	H	L	F	G	Y	D	H	M	D	E	E	E	A	E	---	E	M	E	S	L	E	T	R	I	L	A	V	G	
Smeliloti	VVAHET	TR	E	A	E	L	E	K	P	F	D	A	H	L	T	H	L	V	H	G	F	L	H	L	F	G	Y	D	H	I	E	D	E	A	E	---	R	M	E	G	L	E	T	R	I	L	A	V	G	
Babortus	VIARETV	EA	E	A	E	K	E	G	K	P	I	E	N	E	L	S	H	L	V	H	G	F	L	H	L	F	G	Y	D	H	E	T	D	E	A	E	---	V	M	E	A	R	R	E	I	L	H	A	L	
Retli	VIARETV	EA	Q	E	L	E	K	S	F	D	H	L	T	H	L	V	H	G	F	L	H	L	F	G	Y	D	H	M	N	N	A	E	A	E	---	T	M	E	G	L	E	T	R	I	L	A	V	G		
Rleguminosarum	VIARETV	EA	E	A	E	L	E	K	S	F	D	H	L	T	H	L	V	H	G	F	L	H	L	F	G	Y	D	H	M	N	S	A	E	A	E	---	I	M	E	G	L	E	T	R	I	L	A	V	G	
Bjaponicum	AIAYET	M	R	E	N	D	E	K	K	P	D	H	L	T	H	L	V	H	G	F	L	H	L	F	G	Y	D	H	E	M	D	D	A	E	---	E	M	E	A	L	E	T	Q	I	L	A	V	G		
Mloti	VIARETV	EA	E	A	L	E	K	K	P	V	Q	N	H	T	H	L	V	H	G	F	L	H	L	F	G	Y	D	H	E	T	D	A	E	A	---	A	M	E	A	L	E	T	Q	I	L	A	V	G		
Aaeolicus	VISQD	T	A	E	S	Q	A	R	E	L	G	H	S	L	E	E	V	K	R	L	V	H	G	F	L	H	L	F	G	Y	D	H	E	K	G	E	E	E	K	K	F	R	E	L	E	N	Y	L	S	K
consensus	viareTveReA-	e	l	d	k	-	f	d	d	h	t	h	l	v	h	g	f	l	h	l	f	g	y	d	h	e	-	d	e	e	-	-	m	e	g	l	e	t	r	i	l	a	-	l	g					
Atumefaciens	LSDEYAGQ	EP	----	L																																														
Smeliloti	LSDEYGD	QPP	----	H																																														
Babortus	LPDPYAVS	Q	EDINND																																															
Retli	LSDEYEGQ	L	KME-F																																															
Rleguminosarum	LSDEYEGQ	L	KME-F																																															
Bjaponicum	LPDPYADR	P	GT---	H																																														
Mloti	LPDPYA	-----																																																
Aaeolicus	KAL	-----																																																
consensus	lsdpya-qe	-----																																																

Fig. 3



B.

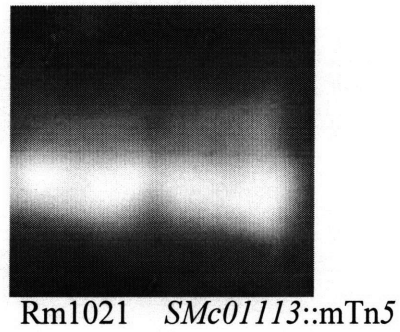
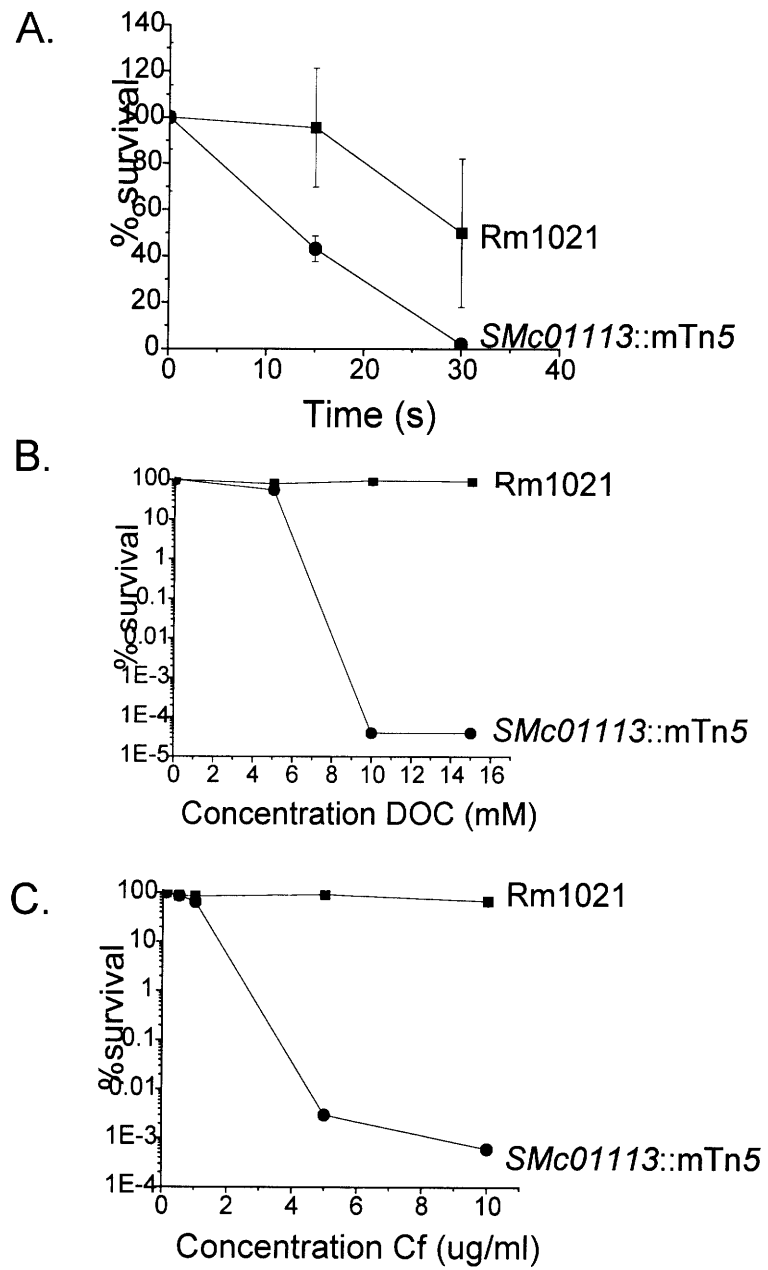


Fig. 4



Chapter 5

**Identification of a universally conserved bacterial protein required for ribosome
maturation**

Abstract

In Chapter 3, I introduced the symbiotically essential orf in *S. meliloti*, *SMc01113*. The striking pleiotropy of the *SMc01113* mutant lead me to further investigate the molecular function of *SMc01113*. I show here that the *SMc01113* protein is part of a large Cluster of Orthologous Group (COG), COG0319 and that homologs of this protein are functionally equivalent. Using the model system of *Escherichia coli*, I demonstrate that the *E. coli* homolog, YbeY, is required for maturation of the ribosomes. Loss of YbeY activity affects maturation of both 16S and 23S rRNA and causes a severe loss of polysomes. 70S ribosomes formed in a $\Delta ybeY$ mutant show reduced translational activity and fidelity. I further demonstrate the human homolog, C21orf57, may play a similar role in human mitochondria.

Introduction

Protein translation is a complicated process performed by the ribosome and its associated factors (27-30). In bacteria the ribosome is divided into two main units; a large 50S subunit and smaller 30S subunit. The 50S subunit is composed of a 23S and 5S rRNA along with 33 ribosomal proteins while the 30S subunit is composed of a 16S rRNA and 21 ribosomal proteins (28, 30, 31). These two subunits come together to form an active 70S ribosome that is competent for translation. Although reconstitution of active 30S and 50S subunits has been performed *in vitro* using only their respective rRNA and proteins (32, 33), it is recognized that many accessory factors are required for 50S and 30S formation *in vivo* (29, 34). Proper assembly of the ribosome is crucial to its function. Several mutants have been identified that disrupt processing of rRNA or assembly of subunits that have detrimental effects on ribosome synthesis, translation fidelity and cell viability (29, 34).

The maturation of a ribosome occurs in a cooperative and ordered fashion (29, 34). 16S, 23S and 5S rRNA are cotranscribed as part of a large precursor. Before transcription is even complete ribosomal proteins associate with rRNA forming ribonucleoprotein complexes that are acted on by RNase III. RNase III begins rRNA maturation, cleaving it into precursors that will go on to become mature 16S, 23S and 5S rRNA. RNases capable of the final maturation of the 23S (35, 36) and the 5' end of 16S rRNA (37) have been identified, however the identity of the enzyme responsible for the 3' maturation of 16S rRNA has remained elusive (37). While final maturation of certain rRNA termini can be performed using only 70S ribosomes *in vitro* (37), it appears that

the final rRNA maturation steps *in vivo* may actually require formation of polysome structures (38, 39).

Protein translation proceeds through 4 stages; initiation, elongation, termination and ribosome recycling. Initiation of protein synthesis is a complex process (40). While it cannot be entirely separated from the preceding ribosome recycling phase of translation, I will outline the general steps of initiation following 70S dissociation.

Initiation begins with the 30S subunit bound by initiation factors (IFs) 1 and 3. IF1 binds specifically to the base of the tRNA binding aminocyl (A) site of the 30S ribosomal subunit and is thought to direct the initiator tRNA (fMet-tRNA_f^{Met}) to the ribosomal peptidyl (P) tRNA binding site (41, 42). IF2, initiator tRNA and mRNA then associate with the 30S subunit in an as of yet unknown order (34). IF2 is a GTP/GDP-binding protein whose main function is to specifically interact with fMet-tRNA_f^{Met} and to position it correctly in the ribosomal P-site, thereby increasing the fidelity and rate of translation initiation (43, 44). IF2 also promotes 30S/50S subunit association (45). The Shine-Dalgarno (SD) sequence of canonical mRNAs interact with the anti-SD sequence of the 16S rRNA (46), and the initiation codon is adjusted to the P-site of the ribosome(47). fMet-tRNA_f^{Met} is then positioned in the P-site and, after a conformational change in the 30S subunit promoting fMet-tRNA_f^{Met} codon-anticodon interactions, the 30S initiation complex is formed (48, 49). IF1 and IF3 are ejected from the complex, while IF2 promotes association with the 50S subunit to the 30S complex(50). fMet-tRNA_f^{Met} is adjusted to the correct position in the P-site, and IF2 is released from the complex. The resulting complex is then competent to enter elongation phase of translation.

Error rates of translation *in vivo* have been estimated to be on the order of 10^{-3} to 10^{-4} (51). Translational errors can arise from improper tRNA aminoacylation, incorrect tRNA selection by the ribosome, or frameshifting during translation. tRNA aminoacylation is very accurate. For example Ile-tRNA^{Ile}-synthetase will exclude Val with an efficiency of 2.5×10^{-5} (52, 53). This suggests that the errors in decoding by the ribosome are responsible the cause of translation errors.

Translational frameshifting occurs by slipping of the ribosome to an alternate reading frame. Frameshifting is generally detrimental as it changes the reading frame of the message being translated producing a truncated protein (54). The exact mechanism of frameshifting has not been established (55), however factors known to potentiate the event have been discovered. These factors include certain mutations in 23S and 16S rRNA (56, 57), mutations in ribosomal proteins (58, 59) and elongation factor 2 (60), as well as loss of certain tRNA modifications (61). Interestingly however, expression of certain genes actually require frameshifting for expression such as the Gag-Pol-Pro protein in retroviruses (62) that require -1 frameshifting or the *E. coli prfB* gene that requires +1 frameshifting (63).

In Chapter 4, I discussed the identification of a universally conserved bacterial protein of unknown function, required for symbiosis of *Sinorhizobium meliloti* with the plant host *Medicago sativa*. I show here that homologs of this protein are functionally equivalent, and that the *E. coli* homolog, YbeY, is required for maturation of the ribosomes. Loss of YbeY activity affects maturation of both 16S and 23S rRNA and causes a severe loss of polysomes. 70S ribosomes formed in a $\Delta ybeY$ mutant show reduced translational activity and fidelity.

Materials and Methods

Strains, plasmids, growth conditions and DNA manipulations. Strains and plasmids are shown in Table S1. Strains were grown aerobically in Luria-Berani (LB) at 37 °C. Ampicillin was used at 100 µg/ml. Allele deletion was performed using the methods of Warner (169). Allele transfers were done by P1 transduction. DNA manipulations were done according to the methods of Sambrook (123).

Phenotypic analysis. Stress and plant assays were performed as previously described (150). Methionine and uridine incorporation assays were performed essential as described (170).

Protein purification. *ybeY* was cloned into pET28A with a C-terminal FLAG-TEV-MBP-His tag. YbeY expression was induced with 1mM IPTG. Protein lysates were bound to amylose resin (NEB), loaded into a column and washed with 10 column volumes of buffer. Protein was eluted in 10 ml buffer with 10mM maltose. The eluted proteins were digested with TEV protease for 48 h at 4°C. The digested sample was passed over a sizing column. YbeY fractions were collected and concentrated in a final buffer of 20mM Tris pH 7.5, 200mM NaCl, 5mM CaCl₂, 5mM ZnSO₄, 2 mM BME and 10% glycerol. Final protein concentration was determined by Bradford.

Polysome and rRNA analysis. Polysome profiles were obtained essentially as described (171). rRNA was extracted from logarithmically growing cultures in LB at 37°C using

Qiagen RNasey Mini Kit. Synergel/Agarose gel electrophoresis and northern analysis was performed as described (123, 172).

Ribonuclease protection assay were performed using RPA III assay from Ambion as per manufactures instructions. Primer extension assays were performed using AMV reverse transcriptase primer extension system from Promega as per manufactures instructions.

Protein lysates and immunoblots. Strains were grown in and lysed by two passages through a bead beater with glass beads. Immunoblotting was performed as previously described (126), loading equal amounts of protein for each sample.

***In vitro* translation and *lacZ* assays.** *In vitro* translation assays were performed essentially as described (173). *LacZ* assays were performed as described (122).

Results

Members of COG0319 show functional equivalency across bacterial genuses.

In Chapter 4, I reported on the characterization of a mutant of the plant symbiont *Sinorhizobium meliloti* that was extremely defective in symbiosis and also showed increased sensitivity to a wide spectrum of environmental stresses. This mutant was disrupted in an orf of unknown function, *SMc01113*. The *SMc01113* protein is part of a large Cluster of Orthologous Group (COG), COG0319. A Cluster of Orthologous Group (COG) consists of individual homologous genes or homologous groups of paralogs from

several completely sequenced genomes, which will ultimately correspond to an ancestral domain (152). Members of COG0319 are predicted metal-dependent hydrolases based on a conserved motif HXXXHXXXDH (Fig. 1). This protein family is ubiquitous among bacteria and is part of the predicted 206 genes comprising the minimal bacterial genome (25). My computational analysis showed that homologs are also present in eukaryotes including humans (Fig. 1). My analysis also revealed another highly conserved motif NXXXRXXXTXVVSF (Fig. 1).

The universal conservation of this protein among bacteria and extreme pleiotropic nature of the *S. meliloti* *SMc01113* mutant drove me to continue my studies of this highly conserved and very important protein family not only to learn more about its role in *S. meliloti* symbiosis, but also to more broadly understand its function in all bacteria. Due to its experimental tractability and vast information resources, I choose to use *E. coli* to further study the function of this family of protein. In *E. coli*, the COG0319 homolog is designated *ybeY*. I constructed an unmarked, non-polar deletion of *ybeY* in *E. coli* strain MC4100 by the methods of Warner (169), which I refer to as the $\Delta ybeY$ mutant. Like the *S. meliloti* *SMc01113* mutant I described in Chapter 3, the *E. coli* $\Delta ybeY$ mutant exhibited a decreased growth rate in rich media compared to the parental strain MC4100 (40 ± 2 min vs. 28 ± 3 min) (Fig. 2A), and significant sensitivity to DOC, β -lactams, H₂O₂ and temperature (Fig. 2B, C, D and Fig. 3). All phenotypes are rescued by ectopic expression of *ybeY* in the $\Delta ybeY$ mutant background (Fig. 3 and Supporting Figure (S) Fig. S1).

The similar spectrum of phenotypes shared by the *E. coli* and *S. meliloti* COG0319 mutants strongly suggested that these homologs play a similar role in their

respective bacterium. To test for functional complementation between COG0319 members I expressed the *S. meliloti* homolog *SMc01113*, as well as the *B. subtilis* homolog, *yqfG*, in the *E. coli* $\Delta ybeY$ mutant background. Expression of either homolog rescued the $\Delta ybeY$ mutant phenotypes as effectively as *ybeY* itself (Fig. 3 and Fig. S1, S2). I also expressed *ybeY* in the *S. meliloti* background and found it was able to rescue all free-living and symbiotic phenotypes (Fig. S3 and Table S2). These results strongly support a universally conserved role for COG0319 members in bacteria.

$\Delta ybeY$ is defective in 70S formation. My bioinformatics analysis on the genomic location of *ybeY* homologs in similar gene clusters in non-closely related bacteria proposed that *ybeY* homologs were functionally linked to the modification of the translation machinery in different classes of bacteria (164, 165). This information, in combination with the pleiotropic nature of $\Delta ybeY$ mutant led me to hypothesis that YbeY may function in protein translation.

Since the ribosome is the fundamental unit of translation (30), I began my molecular analysis of the defect in the $\Delta ybeY$ mutant by analyzing the polysome profile of MC4100 and $\Delta ybeY$ mutant strains. Cell extracts from logarithmically growing cultures were separated over a sucrose gradient to evaluate the cellular content of 30S, 50S, 70S and polysome particles. In comparison to MC4100, the $\Delta ybeY$ profile showed a dramatic decrease in polysomes and a striking increase in both free 50S and free 30S subunits (Fig. 4A vs. B). Integration of the area under these curves showed that the polysome decrease is equal to the 30S and 50S subunit increase in the $\Delta ybeY$ mutant (data not shown). Exotic expression of *ybeY* restored the $\Delta ybeY$ mutant polysome

profile to that of the MC4100 strain demonstrating that the defect was due to the absence of *ybeY* (Fig. S4).

YbeY is required for 16S and 23S rRNA maturation. Ribosomes are composed of 3 rRNA molecules and their associated ribosomal proteins (30). To explore the cause of the $\Delta ybeY$ mutant abnormal polysome profile, I first looked at protein content of the 70S, 50S and 30S peaks from MC4100 and $\Delta ybeY$ mutant strains. However, I did not observe any gross differences in ribosomal protein content between MC4100 and $\Delta ybeY$ mutant 70S, 50S or 30S particles (Fig. S5).

Next I examined the rRNA. *E. coli* ribosomes contain 3 different rRNAs; a 16S in the 30S subunit and a 23S and 5S both in the 50S subunit. These three rRNA are originally transcribed as part of a large precursor RNA that is then processed through a series of cleavage events, to give the individual mature species (174). I found that in the $\Delta ybeY$ mutant, there was an increased amount of a 16S precursor (p16S) (Fig. 5A). This precursor was also found in MC4100 rRNA but at a much lower level suggesting it is a natural precursor on its way to forming mature 16S (m16S). Ectopic expression of *ybeY* relieved this maturation defect in $\Delta ybeY$ (Fig. 6A). The increase in immature 16S accumulation was not due to the slower growth rate of the $\Delta ybeY$ mutant, as I observed the same elevated level of p16S rRNA in the $\Delta ybeY$ mutant when grown at the same rate as MC4100 (data not shown).

I wanted to determine how this precursor 16S rRNA species was distributed among the 70S and 30S particles. In the WT strain both m16S and p16S rRNA were found in the 30S fraction however, only the mature form was found in the 70S ribosome

(Fig. 5B). In the $\Delta ybeY$ mutant, p16S rRNA was the dominate form of rRNA found in the 30S fraction (Fig. 5B). m16S was present in the $\Delta ybeY$ mutant 30S particles along with another faster migrating band not seen in MC4100 30S rRNA I refer to it as 16S*. Interestingly, there was a substantial amount of p16S rRNA in the $\Delta ybeY$ mutant 70S ribosomes (Fig. 5B). Immature 16S rRNA is not competent for translation (175) suggesting that a large fraction of the 70S ribosomes in $\Delta ybeY$ mutant are not functional. The absence of the 16S* from 70S ribosomes (Fig. 6B) suggest that it results from improper processing of p16S in the $\Delta ybeY$ mutant that prevents its 30S subunit from being incorporated into mature ribosomes.

After being cotranscribed, RNase III cleaves 16S rRNA away from the remaining transcript as a 17S precursor species (174). 17S rRNA is acted on at both 5' and 3' ends to yield m16S. Two enzymes, CafA and RNase E act to remove 155 bp from the 5' end of the 17S rRNA (37). The enzyme responsible for removing 33 bp from the 3' end of 17S is not known (37). To determine if the p16S from the $\Delta ybeY$ mutant was 17S rRNA, I began by using Northern analysis with probes that annealed the ends of the 17S precursor (Fig. 6A). I found that both 5' and 3' immature ends of 17S rRNA were present in the $\Delta ybeY$ mutant and at much higher levels than in MC4100 (Fig. 6B, C). To further support this finding I compared the mobility of the $\Delta ybeY$ mutant p16S rRNA to that of a $\Delta cafA$ mutant which is known to be defective mainly in 5' processing (37) (Fig. 6D). Side by side comparison showed that 16S from the $\Delta cafA$ strains runs slower than WT 16S but faster than the p16S in the $\Delta ybeY$ mutant, supporting that the $\Delta ybeY$ mutant is defective in both 5' and 3' processing and is 17S rRNA.

The $\Delta cafA$ strain shows altered 5' 16S maturation but grows normally (37). This suggests that the phenotypes of the $\Delta ybeY$ mutant may arise from difficulty in processing the 3' end of 17S rRNA. I finely mapped the 3' and 5' termini of MC4100 and the $\Delta ybeY$ mutant 16S rRNA to determine if there were aberrant species found in the $\Delta ybeY$ mutant (Fig. 7A, B). The $\Delta ybeY$ mutant had more precursor 5' end than MC4100 but the length of the 5' end of the precursor was identical in both strains (Fig. 7B). The $\Delta ybeY$ mutant also contained more precursor 3' end, than MC4100 (Fig. 7A) and shows several bands between the immature and mature bands. All of these bands are also found in the MC4100 sample but to a far lesser extent. This suggests that the intermediary bands between mature and immature species represent real intermediates in 3' 16S processing. Fig. 7A shows several distinct bands between the mature and immature 3' 16S rRNA species but also at least one smear that may represent single base pair losses. These data are consistent with both endo and exoribonucleases activities being involved in maturation of the 16S rRNA 3' end.

Precursor 23S rRNA contains only 3 or 7 extra bases on the 5' end and 7-9 extra bases on the 3' end (176, 177). These additional bases would not cause a significant shift on my agarose/synergels. Final processing of 23S is thought to occur in polysomes (38). Since the $\Delta ybeY$ mutant had a severe decrease in polysomes (Fig. 4) I questioned if 23 S rRNA may also be affected in the mutant. I mapped the 5' and 3' ends of 23S rRNA as I had done for 16S and found an increase in immature state for both 5' and 3' 23S rRNA ends in the $ybeY$ mutant (Fig. 7).

YbeY associates with 50S subunits and 70S ribosomes *in vivo*. My

bioinformatics analysis of COG0319 family members in the context of their genomic location showed that *SMc01113* and its homologs were always present near genes that function in RNA metabolism (164, 165). These include genes for tRNA processing and ribosome maturation such as *miaB* and *era* respectively (178, 179). Era has been shown to bind the 30S subunit *in vitro* (180) and depletion of Era leads to accumulation of 17S rRNA (181). I considered that YbeY may act directly as a ribosome maturation factor. If so I thought it should be possible to localize YbeY to 30S or 50S subunits. I added an epitope to the C-terminus of the genomic copy of *ybeY* in MC4100. This strain behaved like the parental strain, MC4100, in all assays tested (data not shown) suggesting the epitope does not interfere with YbeY function. I was able to detect the tagged protein in whole cell lysates and determined that YbeY is present at approximately 1000 molecules per cell growing logarithmically in rich media at 37° C (data not shown). I made polysome profiles as above (Fig. 4), isolated the peak fractions of the 30S, 50S, 70s and first polysome fractions and blotted for YbeY. However, I was unable to detect YbeY in any of these fractions and only found it in the non-ribosomal part of the gradient (data not shown).

I postulated that the association of YbeY with the ribosome may be very transient especially since levels were so much lower than the number of ribosomes in a cell (1000 YbeY/cell vs. 20 000 ribosomes/cell in logarithmic growth (30)). I thought that if YbeY did act in ribosome maturation then I may be able to trap it on the ribosome if I slowed down the ribosome maturation process. To do this I deleted *rnc*, that codes for RNase III. RNase III is responsible for the initial cleavage events that separate 16S, 23S and 5S

precursors immediately after transcription (174). Disruption of RNAse III greatly slows the maturation of these RNA species (174). Interestingly, disruption of *rnc* caused an increase in the levels of YbeY protein (Fig. 8A). In the Δrnc mutant I was able to localize YbeY in the polysome profile and found it associated with 50S, 70S and 2X polysomes (Fig. 8B). I also blotted 3X polysomes but did not find YbeY present (data not shown). I used equivalent A_{260} values when analyzing each fraction. This result suggests that equal YbeY binds equally well to 50S subunits and 70S ribosomes.

$\Delta ybeY$ mutant shows altered initiation factor association with 30S subunit.

The $\Delta ybeY$ mutant shows a drastic relative increase in 30S and 50S particles to 70S (Fig. 4). Immature 23S in 50S particles can be efficiently associated into polysomes suggesting the processing defect of the 23S would not account for the decrease in polysomes. Immature 16S is not found in great abundance in 70S ribosomes of WT cells (Fig. 5B) and 30S particles with immature 16S are not functional for translation (175). I postulated the immature 16S rRNA in the $\Delta ybeY$ mutant 30S particles slowed them from forming initiation complexes that could associate to form active 70S ribosomes. This would in turn decrease the abundance of polysomes. To explore this hypothesis, I examined initiation factor association with MC4100 and $\Delta ybeY$ mutant ribosomes, 30S and 50S particles. Initiation factor 1 (IF1) guides the initiator tRNA to the A site as well as stimulates IF3 anti-association activity, while initiation factor 2 (IF2) is required for 30S and 50S association to form the active 70S initiation complexes (40). In total cell extracts, I found an increase in both IF1 and IF3, and a decrease in IF2 in $\Delta ybeY$ mutant levels relative to MC4100 (Fig. 10A). Examining 30S particles, I found modest decrease

in IF1 binding and increase in IF3 binding the $\Delta ybeY$ mutant relative to MC4100 (Fig. 9B). However I observed a striking 30 fold decrease in IF2 bound to 30S subunits of the $\Delta ybeY$ mutant (Fig. 9B). Interestingly I also observed an increase in IF3 binding in 70S ribosomes for the $\Delta ybeY$ mutant (Fig. 9B). This was a very intriguing finding as IF3 has only been reported as binding the 30S subunit after ribosome disassembly to help release deacylated tRNA during ribosome recycling (182). These results indicate that, not only is 70S formation perturbed in the $\Delta ybeY$ mutant, but 70S disassociation may also be promoted.

$\Delta ybeY$ mutant 70S ribosomes show decreased activity *in vitro*. The $\Delta ybeY$ mutant contained an equal number of 70S ribosomes as MC4100 but far fewer polysomes (Fig. 4). 70S ribosomes from the $\Delta ybeY$ mutant also showed increased content of 17S rRNA (Fig. 5B) and IF1 and IF3 (Fig. 9B). This suggested that 70S ribosomes from the $\Delta ybeY$ mutant were not as active as those from MC4100. To test this directly, I reconstituted translation *in vitro* using 70S ribosomes from the $\Delta ybeY$ mutant and MC4100 (Fig. 10) and found a significant reduction in translation efficiency in ribosome isolated from the $\Delta ybeY$ mutant. As 30S particles containing 17S precursor are inactive in translation (175), the increased abundance of 17S in the $\Delta ybeY$ mutant ribosomes could account for the decreased activity I observe *in vitro* (Fig. 10).

The $\Delta ybeY$ mutant has reduced translational fidelity. 70S ribosomes from the $\Delta ybeY$ mutant contained a significant proportion of 17S precursor (Fig. 5B) and showed significantly lower translation activity (Fig. 10). While the increased content in 17S

could account for the decreased activity, I questioned if the ribosomes that were formed in the $\Delta ybeY$ mutant had any additional functional defects. I tested the translation fidelity of the $\Delta ybeY$ mutant using *lacZ* constructs that contained either nonsense codons or frameshifts early in *lacZ*. Read through would be required to bypass the nonsense codons, while frameshifting would be necessary to restore the reading frame distorted by addition or subtraction of a base pair. I found a small increase in read through in the $\Delta ybeY$ mutant (Fig. 11B) but a substantial increase in frameshifting (Fig. 11A). This suggests that the decoding center in the $\Delta ybeY$ mutant is perturbed.

Characterization of the human homolog of YbeY. By computational analyses found a human homolog of YbeY (Fig.1). This human homolog, designated *C21orf57*, is found on the long arm of chromosome 21 (183). I asked if this striking conservation was also at the functional level. I cloned *C21orf57* into pBR322 and introduced it into the $\Delta ybeY$ mutant. Expression of *C21orf57* was comparable to the endogenous expression of YbeY (Fig. 12A). I tested temperature and β -lactam sensitivity and was intrigued to find that *C21orf57* did partially complement the $\Delta ybeY$ mutant (Fig. 12B). Expression of *C21orf57* conferred a near 1000 fold increase in resistance to the $\Delta ybeY$ mutant. The temperature sensitivity of the $\Delta ybeY$ mutant is bactericidal (Fig. 12B). While expression of *C21orf57* did restore growth of the $\Delta ybeY$ mutant at 42°C, the cells did survive and recover when put back to 37°C (Fig. 12B). These results suggest that YbeY and *C21orf57* share a similar activity.

The components of the human ribosome of different from those of bacteria ribosome (30). If YbeY functions in maturation of the *E. coli* ribosome I was uncertain

how the human homolog could play a similar role in maturation of the human ribosome. I examined the primary sequence of C21orf57 using mitoprot (184), which predicts mitochondrial targeting sequences, and found C21orf57 has a very strong mitochondrial targeting sequence ($p = 0.987$). Mitochondria contain their own ribosomes and are thought to have evolved from α -proteobacteria (185). This relation to bacteria made the conservation of function between C21orf57 and YbeY more understandable if C21orf57 functioned in mitochondrial ribosome maturation.

Discussion

I describe here the first report on the function of a hitherto unknown class of proteins classified as COG0319. Members of this family are highly conserved and present in every sequenced prokaryotic genome. This putative gene is part of the predicted minimal bacterial genome set (25) and agreeing with this estimation is essential in several bacteria including *Mycoplasma genitalium* (186), which has the smallest genome of any free living prokaryote.

The protein structures of homologs from *E. coli*, *Thermotoga maritima* and *Aquifex aeolicus* have recently been solved (154, 187, 188). These structures support the hypothesis that members this protein family are metal-dependent hydrolases based on structural similarities to known metallohydrolases. The *A. aeolicus* was rigorously tested for more than 15 different biochemical activities including protease, nuclease and phosphatase, however, no activity could be detected for this protein (154).

Deletion of *ybeY* perturbs ribosome maturation, specifically slowing, and potentially altering, rRNA processing (Fig. 5). Similar rRNA processing defects have been observed in *E. coli* strains depleted for essential protein Era and ObgE, which are thought to be required for ribosome maturation (81, 181). ObgE is present at approximately equal amounts to the estimated number of ribosomes per cell (83), while I have found that the total number of YbeY per cell is approximately only 1/20th the amount of ribosomes suggesting if YbeY acts in ribosome maturation it would do so catalytically with rapid turnover. ObgE has been localized to the 30S and 50S subunits *in vivo* (81), and Era has been localized to the 30S subunit (180). I have localized YbeY to the 50S subunit *in vivo*, but also to the 70S and first polysome (Fig. 8B). This suggests that YbeY may act in a step after initial assembly of 30S and 50S subunits.

Due to it binding to 70S ribosomes and polysomes, it is possible that YbeY may act as a translation factor, however, I would also then have expected it to associate with polysomes beyond the first polysome peak which I do not observe. Nonetheless I did test the effects of adding YbeY to an *in vitro* translation reaction (Fig. 13). I found that at low concentrations YbeY had no effects on translation but at higher concentrations YbeY actually inhibited translation suggesting it does not act as a translation factor but can potentially bind the ribosome inhibiting translation.

The major ribosome defect I observe in the $\Delta ybeY$ mutant is accumulation of unprocessed 16S and 23S precursors. Unprocessed 23S precursors can be assembled into active ribosomes (189). A Δrnc strain cannot process its 23S rRNA to the mature form but I have found that 50S and 30S subunits do not accumulate in that strain as I observe in $\Delta ybeY$ mutant (data not shown). This suggests that it is the unprocessed 16S rRNA

accumulation that is responsible for effects on the ribosome. Agreeing with this, it has been shown that precursor 16S rRNA does not form 30S subunits competent for translation (175).

Interestingly, final processing of the 5' end of the 23S rRNA occurs in the polysome (38). Polysome formation has also been shown to enhance the 3' maturation of 23S rRNA as well (36). The enzymes responsible for processing the 5' end of 16S rRNA have been identified but the 3' processing enzyme(s) remain elusive (37). Interestingly 16S rRNA 5' processing can be disrupted without detrimental effects to the cell (37). Taken together, these results suggest that it is the accumulation of unprocessed 3' 16S rRNA end that maybe the cause of the ribosome phenotypes observed in the $\Delta ybeY$ mutant. The extreme 3' end of the mature 16S rRNA contains that anti Shine-Dalgarno sequence required to recognize the Shine-Dalgarno sequence in the incoming mRNA (46). This recognition helps position the ribosome to begin translating at the correct start site. An immature 3' 16S rRNA end could interfere with mRNA binding possible leading to translation defects like frameshifting we observe in the $\Delta ybeY$ mutant. It may also interfere with IF2 binding causing the decrease in IF2 association with the 30S subunit we observe in the $\Delta ybeY$ mutant (Fig. 9).

All known *E. coli* RNases have been tested for 16S rRNA processing function but none have shown activity (190). Like 23S rRNA precursor 16S rRNA has been found in polysomes *in vivo* (39). Since precursor 16S rRNA are not active in translation (175), why would it be found in polysomes? I speculate that, like precursor 23S rRNA, precursor 16S rRNA final processing occurs in the polysome state. I found that YbeY associates with 70S ribosomes and polysomes. I was able to identify this localization

only after deletion of RNase III which slows maturation of 16S rRNA (Fig. 8B) (174). I also found that YbeY levels increased in the Δrnc background (Fig. 8A). These results suggest that YbeY may be involved in processing rRNA. Since precursor 23S rRNA is functional in translation and not lead to accumulation of 30S and 50S subunits, and the enzymes responsible for 5' 16S maturation are known (37), I suggest YbeY may be involved in the processing of the 3' end of 16S rRNA and have begun assays to address this possibility.

Fig. 1. Sequence alignment of COG0319 homologs from several different bacteria and eukaryotes. Alignments were performed using T-coffee (168). The red bar underlines the conserved 3 His domain that is used to classify members of this family.

The blue bar underlines a second highly conserved domain.

Fig. 2. Phenotypic analysis of the *E. coli* $\Delta ybeY$ mutant. A. Growth curves of MC4100 and the $\Delta ybeY$ mutant in LB at 37° C. Logarithmically growing cultures were diluted to OD 600 0.01 in LB. Growth was monitored by OD 600. Sensitivity of the $\Delta ybeY$ mutant to stresses DOC (B), cefotaxime (C) and H₂O₂ (D). Cultures were serially diluted and

plated on increasing concentrations of the indicated stress. Cfu were determined after 24 h of growth. MC4100 (□), $\Delta ybeY$ mutant (□).

Fig. 3. Temperature sensitivity of the $\Delta ybeY$ mutant. MC4100 and $\Delta ybeY$ mutant strains complemented by *ybeY* homologs were serially diluted and plated on LB plates. Plates were incubated at either 37°C or 45°C for 16 h. EV is empty vector.

Fig. 4. Poly some profile for MC4100 (A) and the $\Delta ybeY$ mutant (B). Cell extracts were separated on a 10 – 40% sucrose gradient. The gradient was fractionated and the A_{260} of each sample was determined. The positions of polysomes, 70S, 50S and 30S particles are indicated.

Fig. 5. A. 500ng of total RNA extracted from each indicated strain was separated on an agarose/synergel mix and stained with ethidium bromide. EV is empty vector control and “p” indicates that the gene indicated is expressed from a plasmid. B. 500ng of rRNA purified from 30S and 70S fractions of MC4100 and the $\Delta ybeY$ mutant were separated on an agarose/synergel mix and stained with ethidium bromide.

Fig. 6. A. A diagram of 17S rRNA show the location of the 5' and 3' Northern probes used in B and C relative to the maturation cut sites (_). 500ng of total RNA from MC4100 and the $\Delta ybeY$ mutant were separated on an agaorse gel, transferred to a HyBond-N+ membrane and probed for 5' (A) and 3' (B) 17S ends. D. Total RNA from

MC4100, $\Delta ybeY$ and $\Delta cafA$ mutants was separated on an agarose/synergel mix and strain with ethidium bromide.

Fig. 7. 3' ribonuclease protection (RPA) assays and 5' primer extension (PE) assays to map the 3' and 5' ends of 16S and 23S rRNA from MC4100 and $\Delta ybeY$ mutant. A. RPA for 16S rRNA. B. PE for 16S rRNA. C. RPA for 23S rRNA. D. PE for 23S rRNA.

Mature (m) and precursor (p) ends are indicated for each assay.

Fig. 8. A. Lysates from MC4100 and a Δrnc strain were blotted for the presence of FLAG-tagged YbeY. B. Western blot for YbeY-FLAG in 30S, 50S, 70S and 2X polysome fractions. Lysate from a Δrnc strain carrying a FLAG tagged *ybeY* gene at its genomic location was fractionated over a 10 – 40% sucrose gradient. Peak fractions were collected and equivalent A_{260} amounts were blotted for the FLAG epitope.

Fig. 9. Western blot for IF1, IF2 and IF3 in MC4100 and the $\Delta ybeY$ mutant. A. Total cell lysates. B. Fractionated 70S, 50S and 30S particles. OmpA was used as a control for protein load.

Fig. 10. *In vitro* translation. A. MC4100 S100 fractions were mixed with MC4100 70S or $\Delta ybeY$ mutant 70S ribosomes. Translation activity is normalized to MC4100. This assay was performed 5 times. A representative experiment is shown.

Fig. 11. Readthrough and frameshifting in the $\Delta ybeY$ mutant. Plasmids carrying *lacZ* with (A) nonsense codons or (B) frameshift were transformed into MC4100 and the $\Delta ybeY$ mutant. *LacZ* activity was assayed as described in materials and methods.

Fig. 12. Rescue of the $\Delta ybeY$ mutant by human homolog C21orf57. A. *E. coli* strains were serially diluted and plated on LB plates containing increasing concentrations of cefotaxime (Cf). Colony formation was counted after 24 h growth at 37° C. MC4100+EV (□), $\Delta ybeY$ +EV (○), $\Delta ybeY$ +pC21orf57 (◇). B. Strains were serially diluted and plated on LB plates. Plates were incubated at either 37°C or 45°C for 16 h. Plates at 45°C were then incubated at 37°C for 16h. EV is empty vector control and “p” indicates that the gene indicated is expressed from a plasmid.

Fig. 13. Effect of YbeY on *in vitro* protein translation. MC4100 S100 fractions were mixed with MC4100 70S. Purified YbeY protein was added at a final concentration of 2.0 μ M or 0.2 μ M (1:10 dilution). Control is YbeY buffer only.

Fig. 1

```

Smelliloti  --MTALDIQIS-VEAGDW-PPEDELQSFCEVLEAAADFLAREENQPLPAQAAELSLVFT
Ecoli       MSQVILDLQLA-CEDNSGLPEESQFQTWLNVA-----IPQFEESEVTIRVV
Aaeolicus   MSSTKRQKNRVLVKKIKRKVRKD-----KTEKWAELALSALGNN-VELSVYIT
Bsubtilis   MSLIIDIVDET-GSVSEE-----MLKEVENLQFAAEREGVQDQAEVSVTIV
Cfamiliaris MSLVLRVPQRA-VPVRRAP-----LRSRVELLRVLGVR-DFDLGLLVCV
Xlaevis     MSLILRNAQHA-VPLYRAH-----LRFSLDIARSCLKVK-NFDLGLICV
Hsapiens    MSLVIRNLQRV-IPVRRAP-----LRSKIEIVRRILGVQ-KFDLGLICV
consensus   mslvir-iq--v-l-kg-----i--lel---lgvq---elslv-v

Smelliloti  DDQSYRAINAENRQDNANVLSFPAPFVT-----PGRMPGPMGLGDIVVAHETLRREA
Ecoli       DTAESHSLNLTYRGKDNPTNVLSFPPEVPP-----PG-MMSLLGLVICRQVWEKEA
Aaeolicus   DDQEIRELNKTYRKKDNPTDVLSFPMGEEFGEY-----KILGDVVISQDTAERQA
Bsubtilis   SNDDIHQINKEYRGKDAPTDVLSFALEEEEGEEEIEIVGAEMP-PVLGNIIISADTRTEQA
Cfamiliaris DNEGQRLNRAYRGDDNPTDVLSFPFHENVKAGELPRPRSRDYNLGDIVLGVEYVFQRC
Xlaevis     NNARIQHINRVYRGDSVTDVLSFPFHEDLNPSLLPIATPREYNLGDIVLGVAFIYEQC
Hsapiens    DNKNIQHINRIYDNVPTDVLSFPFHEHLKAGEFPQDFPPDYNLGDIVLGVEYIFHC
consensus   dn-i--iNk-yRgkdkpTdVLSFpf-e--g-----pg--e--mLGdivva-e-l--qa

Smelliloti  AELEKPDAHLTHLVHGFLHFGYDHIEDDEAER-MEGLETRILARLGLSDPYGDQPPH
Ecoli       QEQGKPLEAHWAHMVVHGSLRLGYDHIEDDEAEE-MEALETEIMLALGYEDPYIAEKE
Aaeolicus   RELGHSLEEERLIVNGIVHLGYDHEKGGEEKKFRELENYVLSKLSAL-----
Bsubtilis   EYNHSKRELGFLAVNGFLHLGYDMTREEEEE-MTKQRELLDAYGLKRS-----
Cfamiliaris -RGDADYDALTVTAANGLCHLLGTHSTAEWRK-MYQKEKQVLEELSLTGTRLQPLS
Xlaevis     QKTQEDYRSILTITAVRGLCHLLGHKNNPEKWQ-MPEKETEILNEINRVTGSKLPLS
Hsapiens    -KENEDYNDVLTVTATRGLCHLLGTHGTAEWQQ-MPQKEKAVLDELGRRTGTRLQPLT
consensus   -e----f---lt-lavHGilHLLGydH--dde-e--mf-ke--il--lgk-----p--

Smelliloti  -----
Ecoli       -----
Aaeolicus   -----
Bsubtilis   -----
Cfamiliaris RGLF---
Xlaevis     TNHY---
Hsapiens    RGLFGGS
consensus   -----

```

Fig. 2

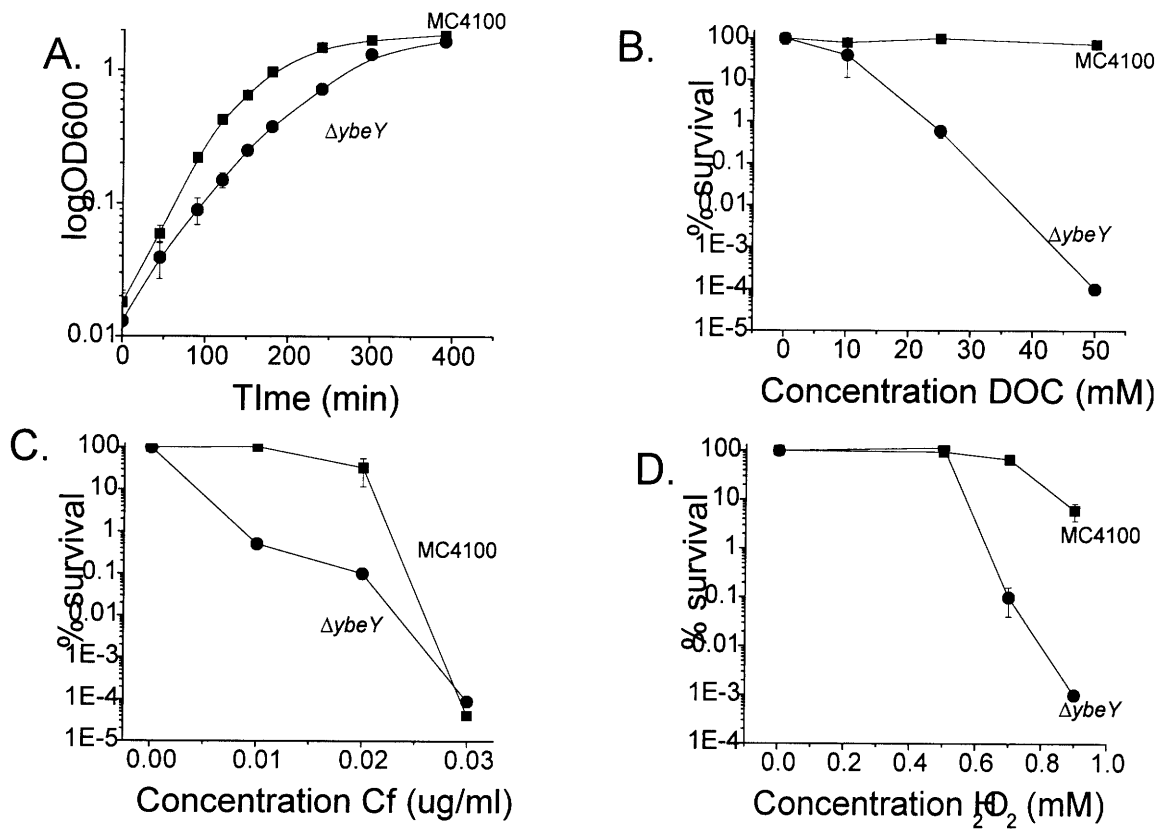


Fig. 3

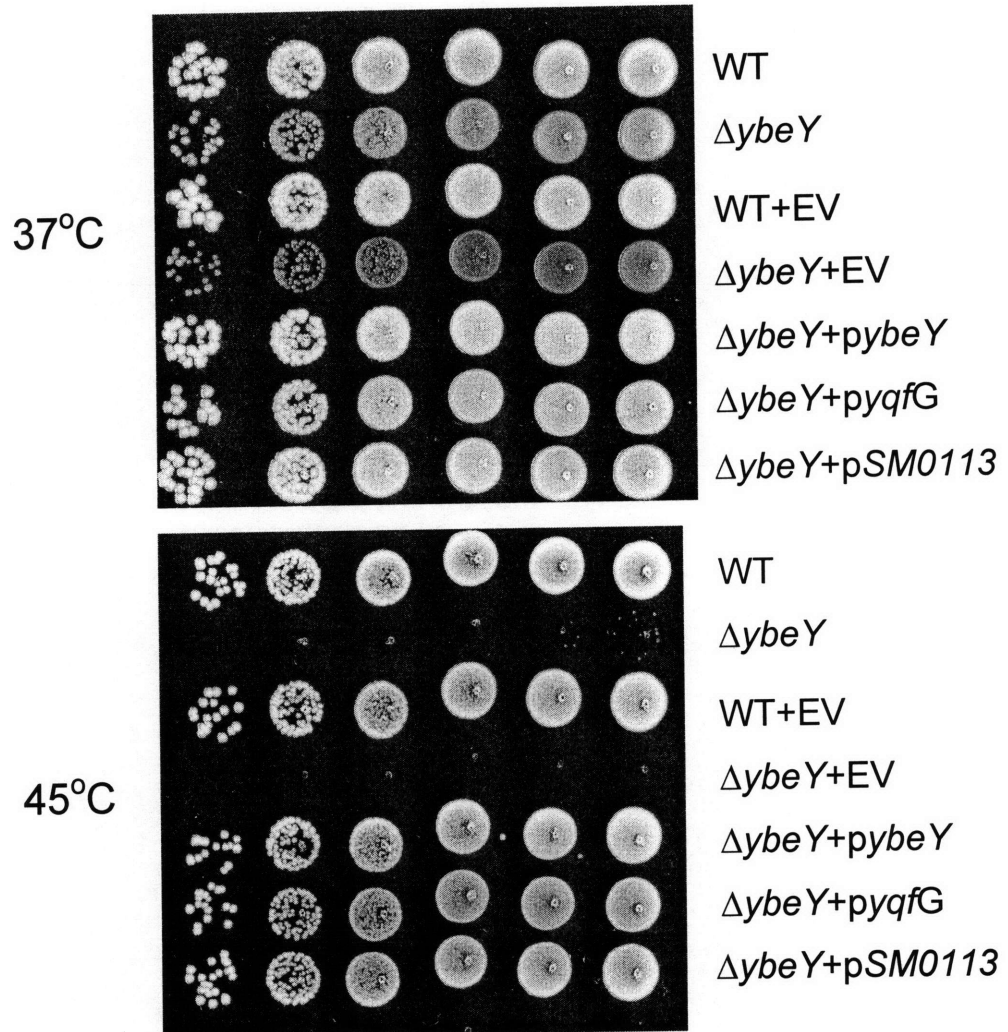


Fig. 4

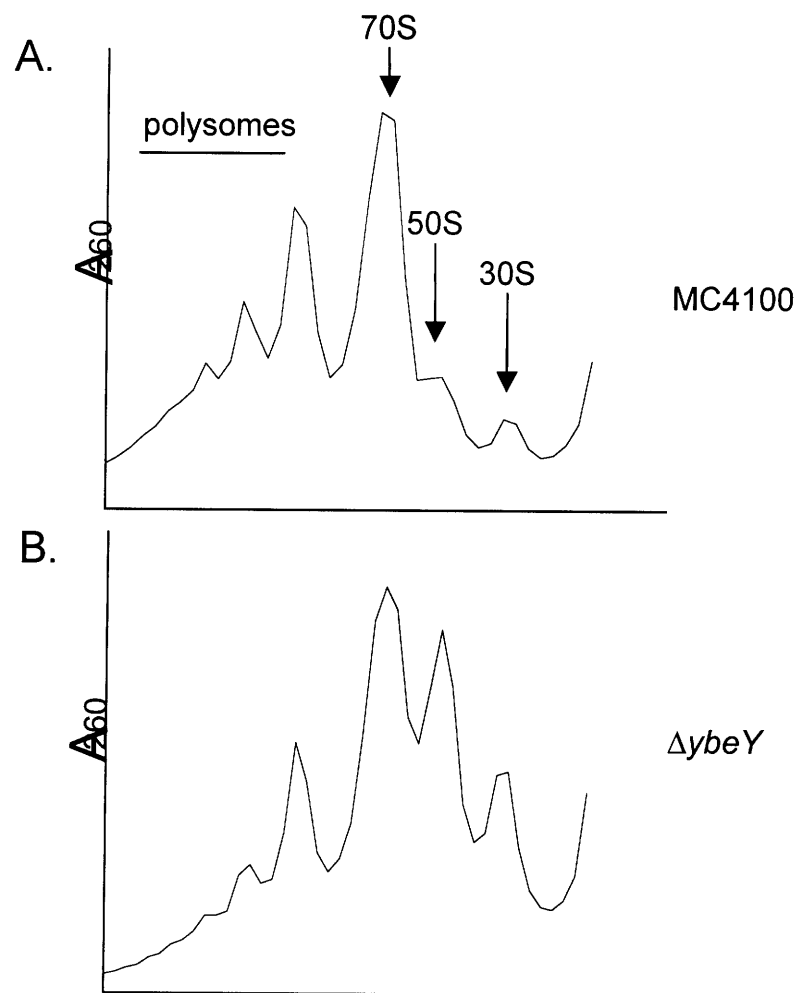


Fig. 5

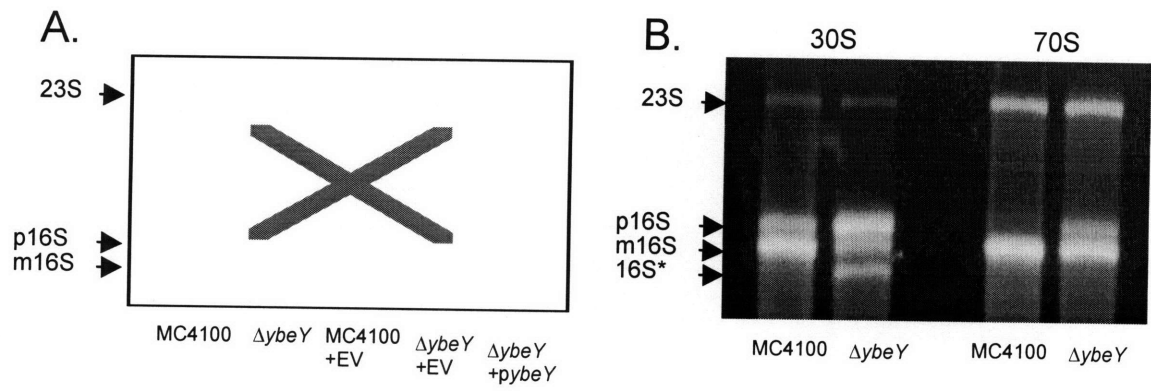


Fig. 6

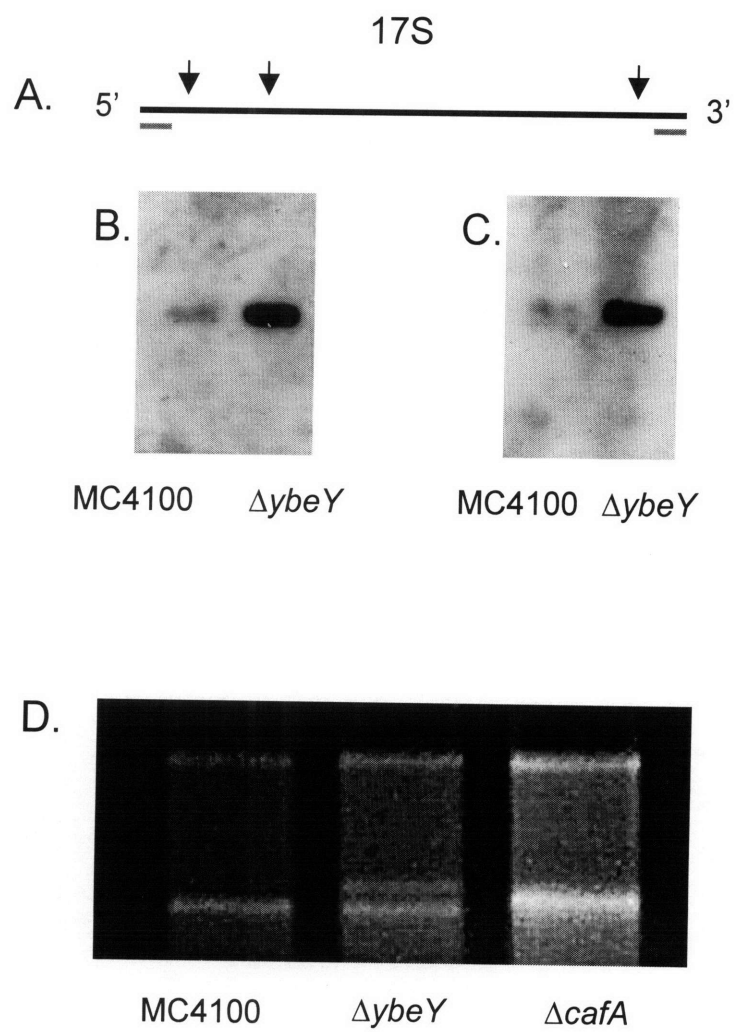


Fig. 7

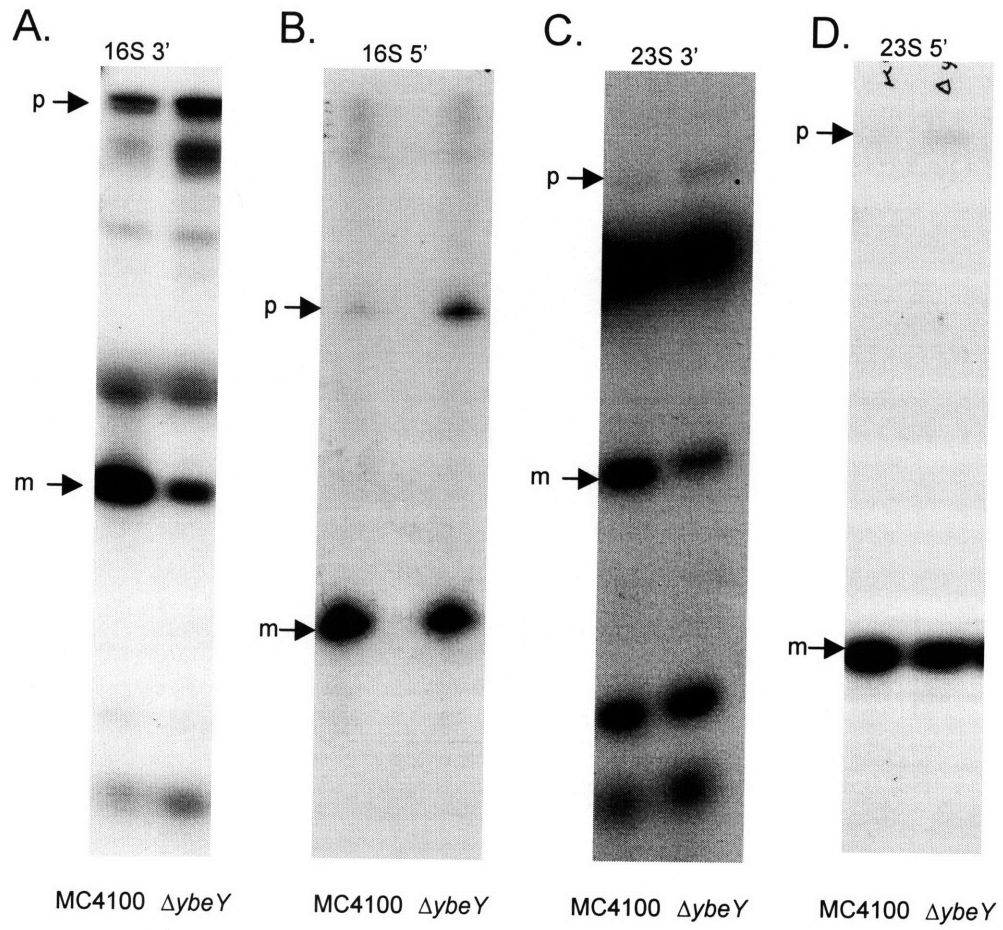


Fig. 8

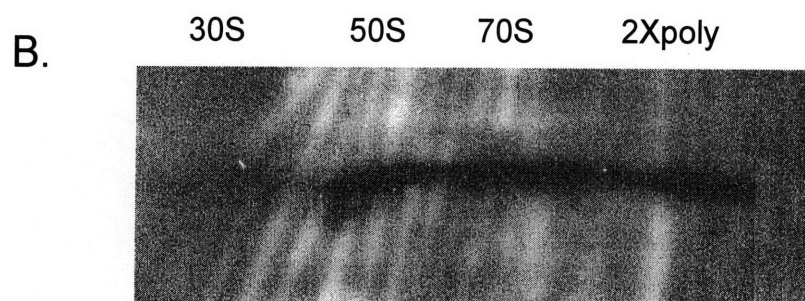
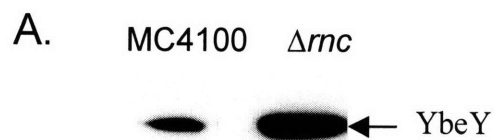


Fig. 9

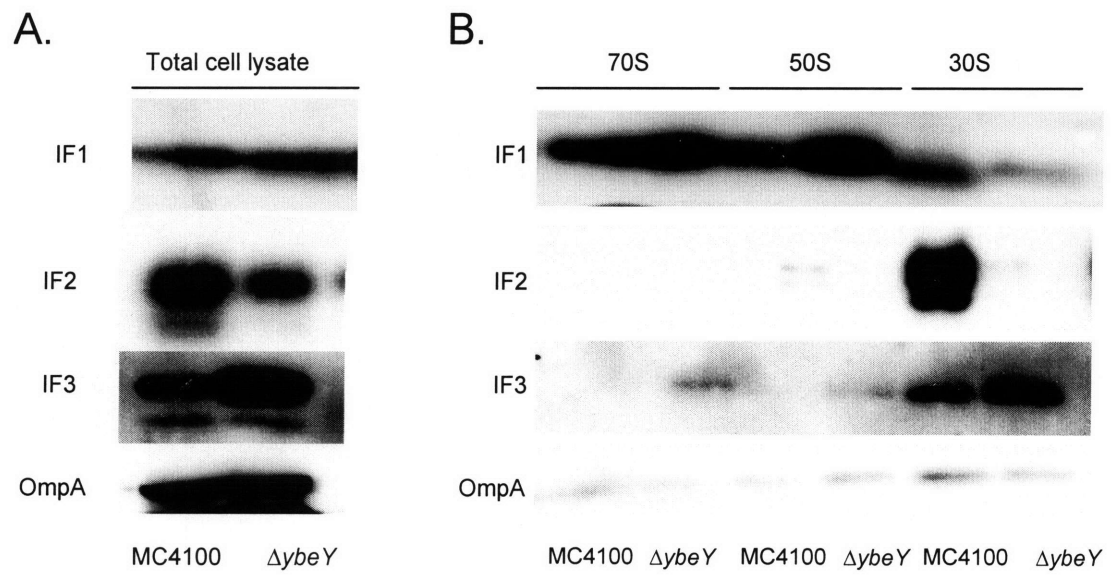


Fig. 10

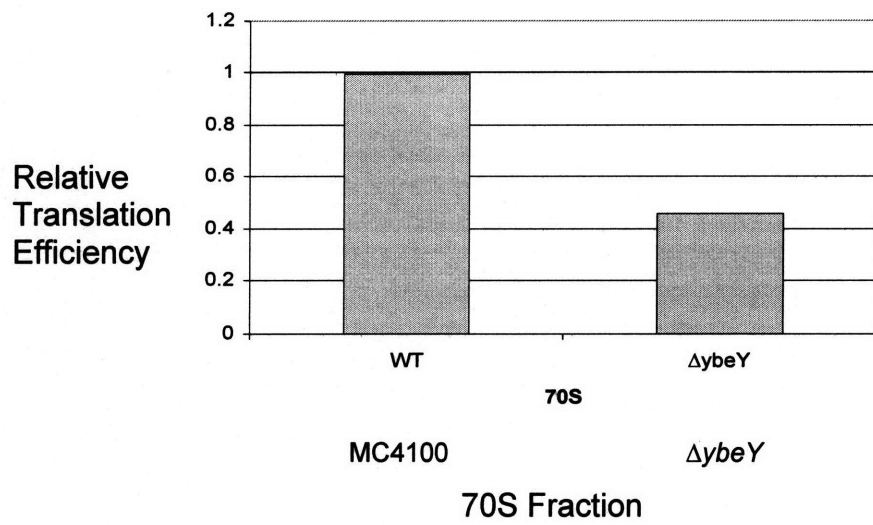


Fig. 11

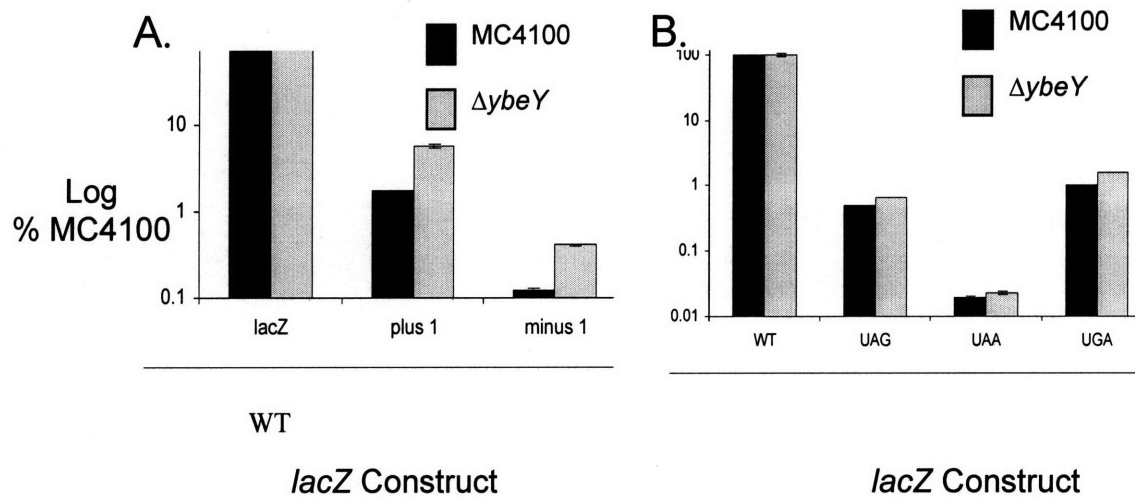
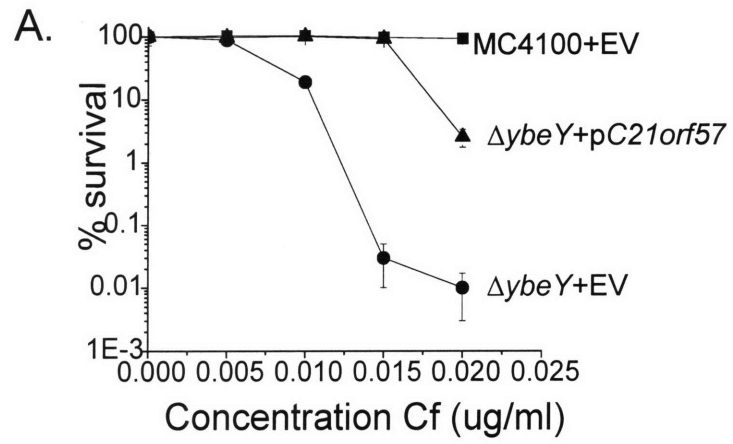


Fig. 12



B.

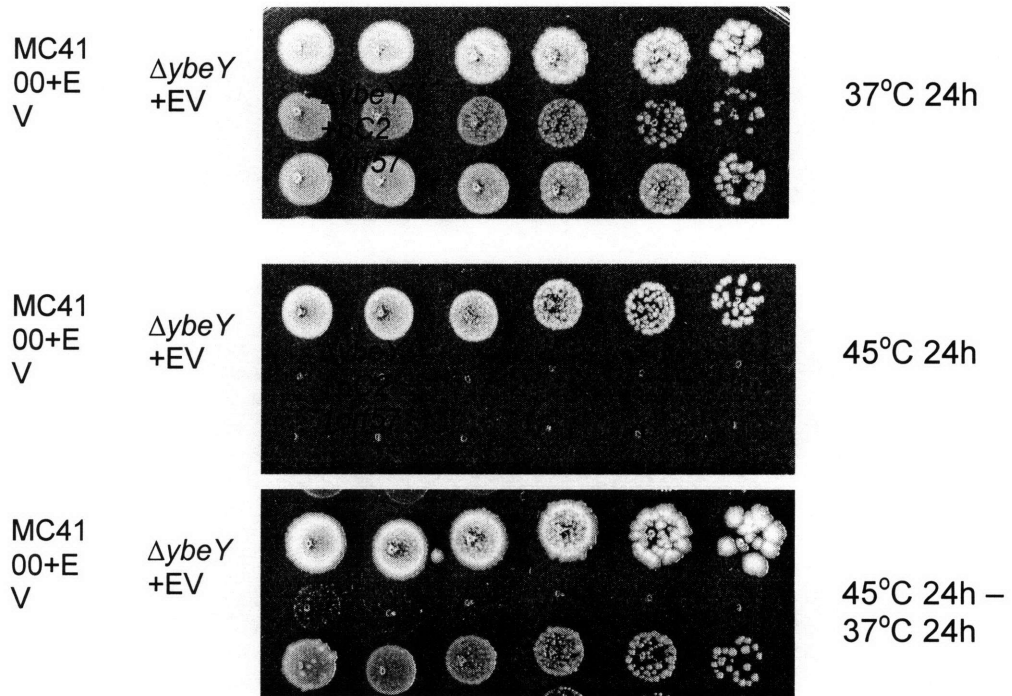
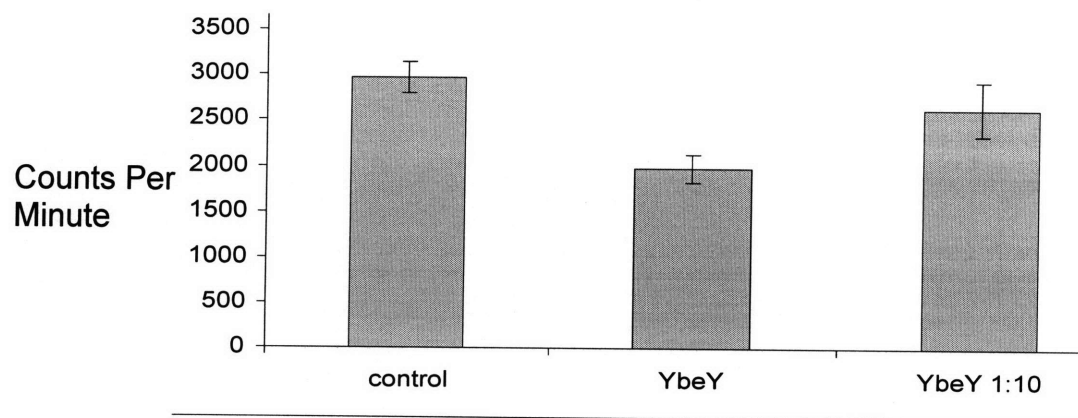


Fig. 13



Supplemental

Table S1. Bacterial strains and plasmids used in this study

Strain/plasmid	Relevant genotype and property	Source
<u>Strain</u>		
MC4100	<i>F⁻ araD139 ΔlacU169 ΔrelA1 rpsL150 thi mot flb5301 deoC7 ptsF25 rbsR</i>	Laboratory stock
<i>ΔybeY</i>	<i>ybeY</i> deletion in MC4100	This study
BWD10	MC4100 carrying pBR322	This study
BWD11	<i>ΔybeY</i> carrying pBR322	This study
BWD12	<i>ΔybeY</i> carrying pBWD1	This study
BWD13	<i>ΔybeY</i> carrying pBWD2	This study
BWD14	<i>ΔybeY</i> carrying pBWD3	This study
BWD15	<i>ΔybeY</i> carrying pBWD4	This study
Rm1021	SU47 Sm ^R	(84)
BWD16	Rm1021 carrying pMSO3	This study
GWBD12	Rm1021 <i>SMc01113::mTn5</i> transduced	Chapter 3
BWD17	GWBD12 carrying pMSO3	This study
BWD18	GWBD12 carrying pBWD5	This study
<u>Plasmid</u>		
pBR322	Ap ^R , Tc ^R	(191)
pBWD1	pBR322 expressing <i>ybeY</i>	This study

pBWD2	pBR322 expressing <i>SMc01113</i>	This study
pBWD3	pBR322 expressing <i>yqfG</i>	This study
pBWD4	pBR322 expressing <i>C21orf57</i>	This study
pMS03	Sp ^R	(192)
pBWD5	pMSO3 carrying <i>ybeY</i>	This study
pSG25	<i>lacZ</i>	(193)
pSG163	<i>lacZ</i> carrying UAG interruption	(193)
pSG853	<i>lacZ</i> carrying UAA interruption	(193)
pSG3/4	<i>lacZ</i> carrying UGA interruption	(193)
plac7	<i>lacZ</i> carrying +1 frameshift	(193)
plac10	<i>lacZ</i> carrying -1 frameshift	(193)
pET28A	T7 promoter, MBP tag, Ap ^R	Lab stock

Table S2. Complementation of the *S. meliloti* *SMc01113::mTn5* mutant symbiotic phenotype by *ybeY*. *M. sativa* seedling were inoculated with the indicated strains below. After 4 weeks of growth, plant height and nodule distribution were determined. The

decrease in plant height and increase in white nodules in the *SMc01113::mTn5* mutant are indicative of a failed symbiosis. EV is empty vector control and “p” indicates that the gene indicated is expressed from a plasmid.

Strain	Plant Height (cm)	White Nodules (%/plant)	Pink Nodules (%/plant)
Rm1021 + EV	11.1 ± 2.2	1.0 ± 0.9	8.2 ± 2.1
<i>SMc01113::mTn5</i> + EV	2.1 ± 1.2	17.8 ± 6.7	0
<i>SMc01113::mTn5</i> + <i>pybeY</i>	10.5 ± 3.0	1.0 ± 1.3	8.2 ± 2.4

Fig. S1. Complementation of the $\Delta ybeY$ mutant phenotypes with *ybeY* or the *B. subtilis* homolog, *yqfG*. A. *E. coli* strains were diluted to OD₆₀₀ 0.01 in LB at 37⁰ C. Growth over time was monitored by OD₆₀₀. *E. coli* strains were serially diluted and plated on LB plates containing increasing concentrations of (B) DOC, (C) cefotaxime (Cf) and (D) H₂O₂. Colony formation was counted after 24 h growth at 37⁰ C. MC4100+EV (□), $\Delta ybeY$ +EV (□), $\Delta ybeY$ +*pybeY* (□) and $\Delta ybeY$ +*pyqfG* (□). EV is empty vector control and “p” indicates that the gene indicated is expressed from a plasmid.

Fig. S2. Complementation of the $\Delta ybeY$ mutant phenotypes with the *S. meliloti* homolog *SMc01113*. A. *E. coli* strains were diluted to OD₆₀₀ 0.01 in LB at 37⁰ C. Growth over time was monitored by OD₆₀₀. *E. coli* strains were serially diluted and plated on LB

plates containing increasing concentrations of (B) DOC, (C) cefotaxime (Cf) and (D) H₂O₂. Colony formation was counted after 24 h growth at 37⁰ C. MC4100+EV (□), $\Delta ybeY$ +EV (□) and $\Delta ybeY$ +pSMc01113 (□). EV is empty vector control and “p” indicates that the gene indicated is expressed from a plasmid.

Fig. S3. A. Complementation of *S. meliloti* SMc01113::mTn5 mutant by *ybeY*. *S. meliloti* strains were diluted to OD₆₀₀ 0.01 in LB at 37⁰ C. Growth over time was monitored by OD₆₀₀. *S. meliloti* strains were serially diluted and plated on LB plates containing increasing concentrations of (B) DOC and (C) cefotaxime. Colony formation was counted after 96 h growth at 30⁰ C. Rm1021+EV (□), SMc01113::mTn5+EV (□) and SMc01113::mTn5+pybeY (□). EV is empty vector control and “p” indicates that the gene indicated is expressed from a plasmid.

Fig. S4. Poly some profile for MC4100+EV (A), $\Delta ybeY$ +EV (B) and $\Delta ybeY$ +pybeY. Cell extracts were separated on a 10 – 40% sucrose gradient. The gradient was fractionated and the A₂₆₀ of each sample was determined. The positions of polysomes, 70S, 50S and 30S particles are indicated. EV is empty vector control and “p” indicates that the gene indicated is expressed from a plasmid.

Fig. S5. Polysome, 70S, 50S and 30S particles were purified by sucrose gradient sedimentation from MC4100 and $\Delta ybeY$. Equal A₂₆₀ amounts of each peak for each strain were separated by SDS-PAGE and silver stained.

Fig. S1

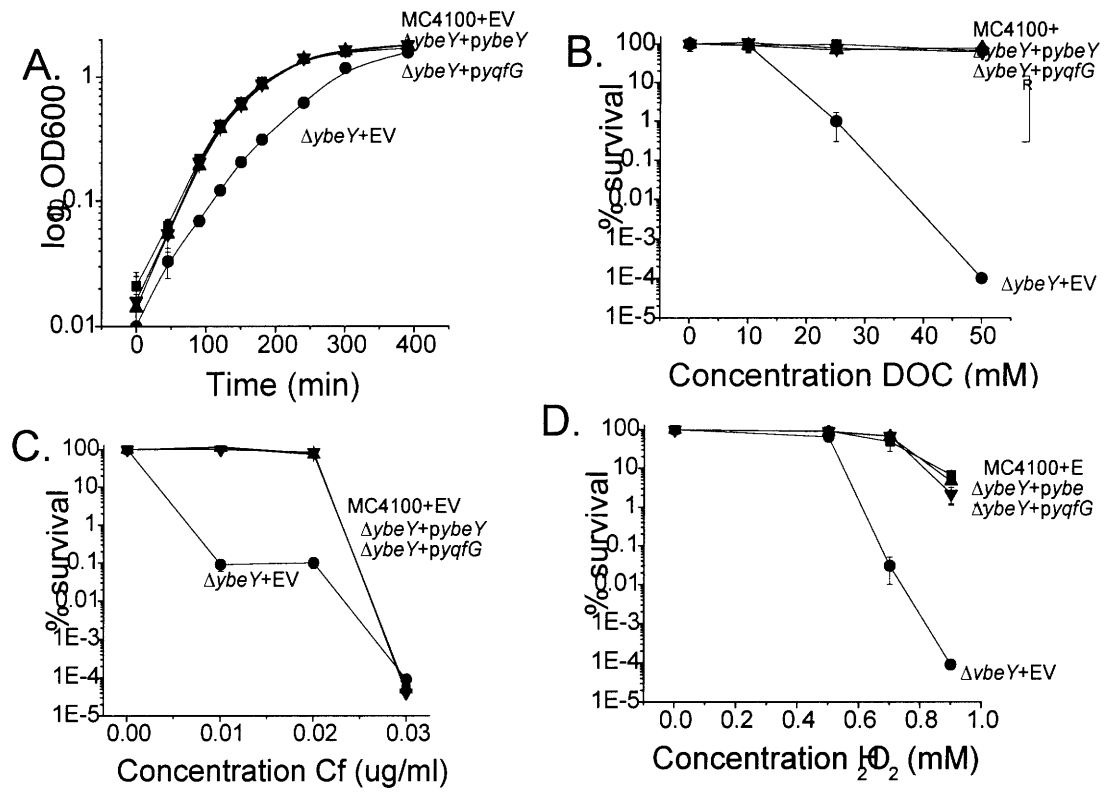


Fig. S2

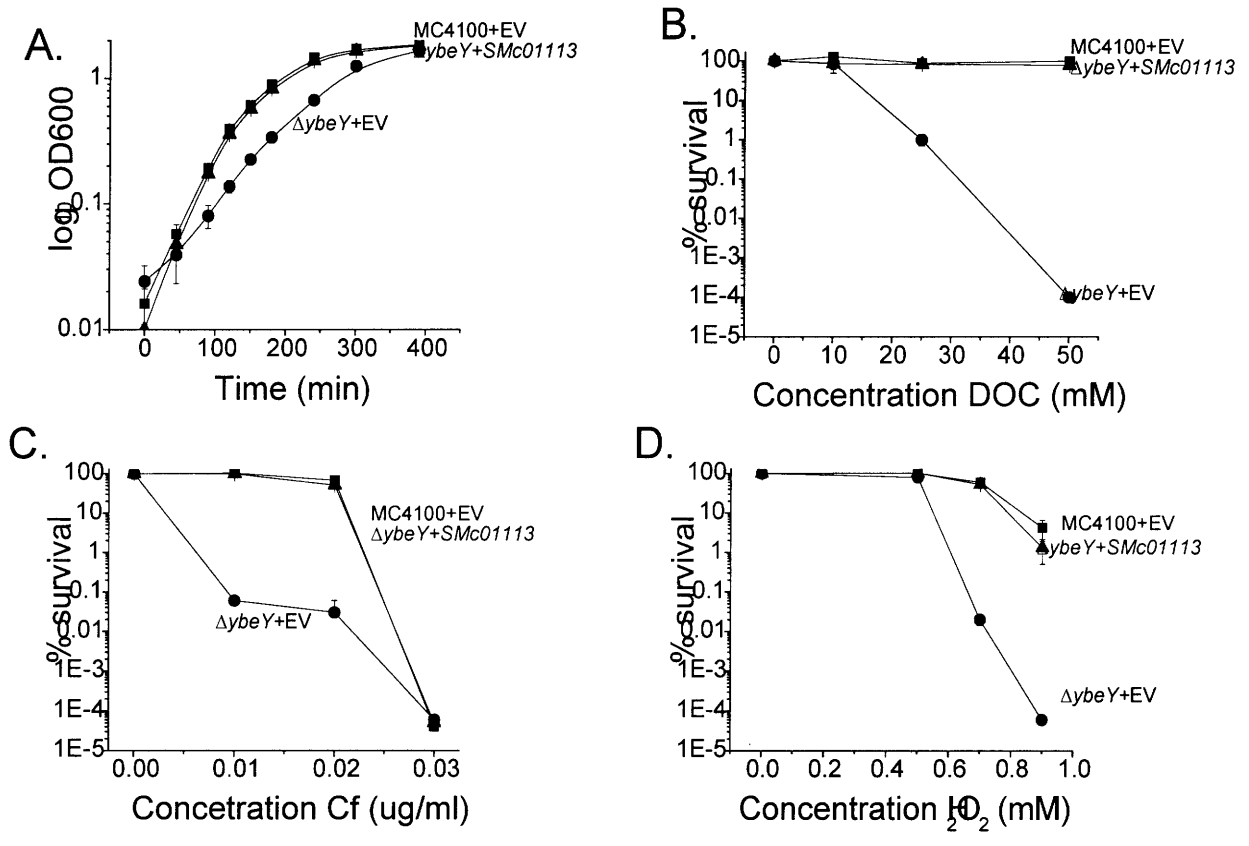


Fig. S3

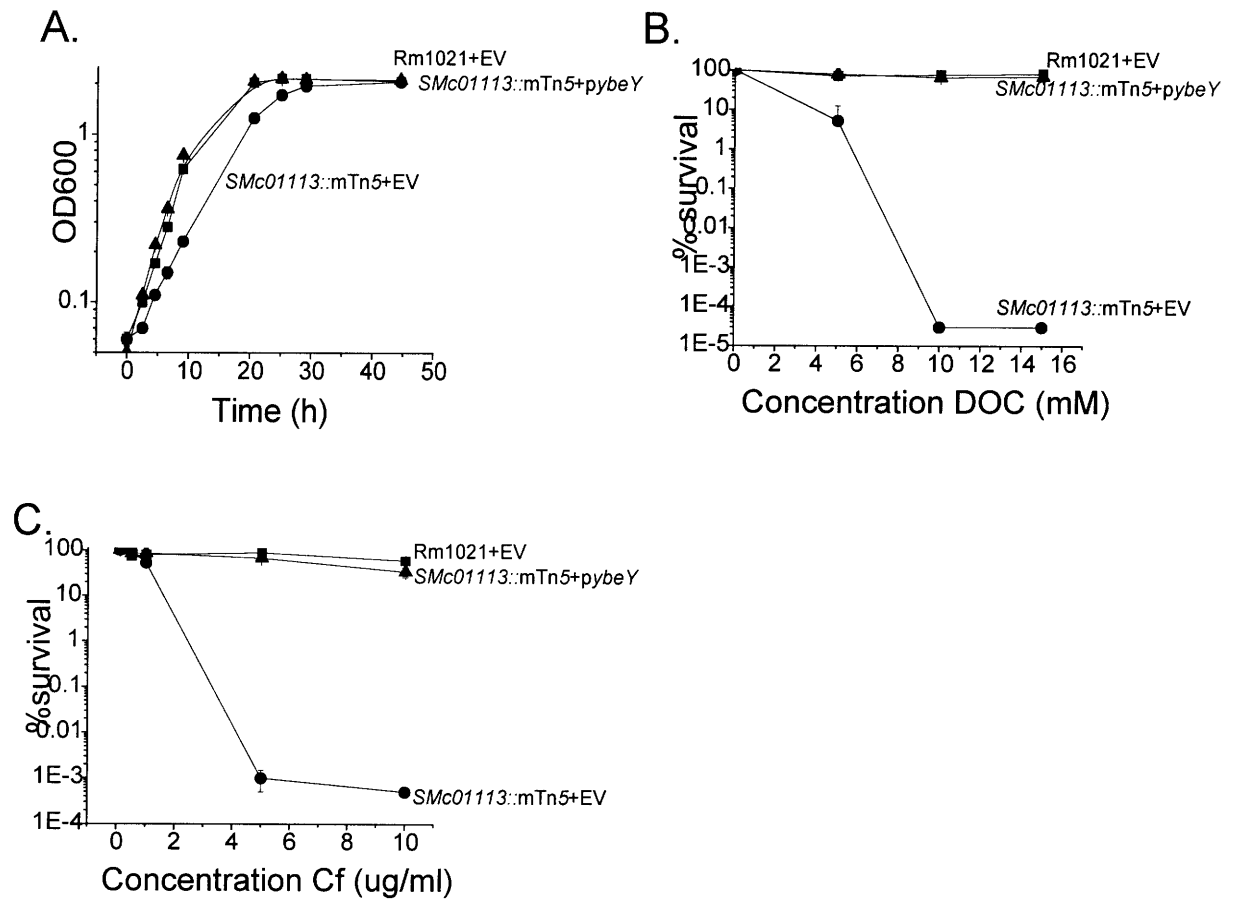


Fig. S4

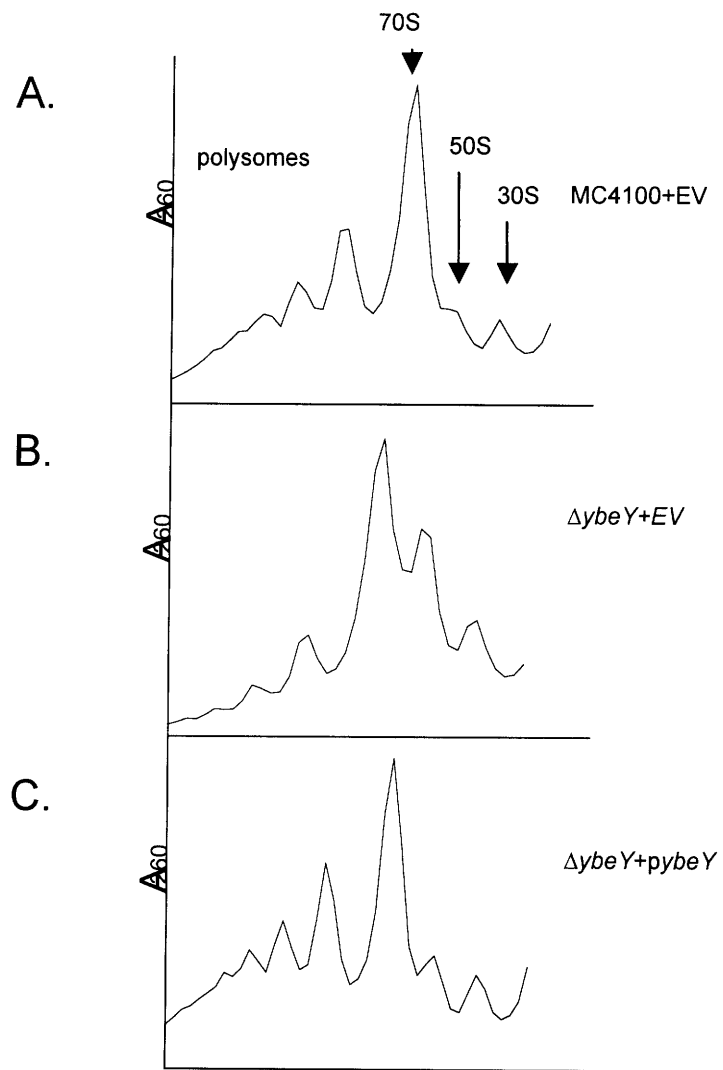
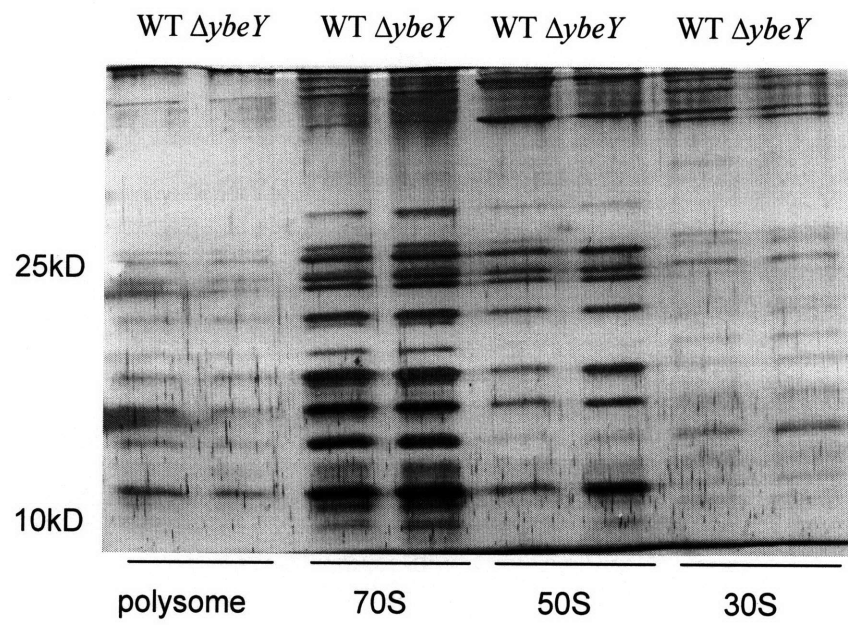


Fig. S5



Chapter 6

Damage-independent replication fork arrest in *Escherichia coli* reveals a molecular switch from cell survival to cell death*

* Davies, B. W.¹, Kohanski, M. A., Simmons, L. A., Collins, J. J. and Walker G. C. 2007. Damage-independent replication fork arrest in *Escherichia coli* reveals a molecular switch from cell survival to cell death. PNAS. in review.

Damage-independent replication fork arrest in *Escherichia coli* reveals a molecular switch from cell survival to cell death

Davies, B. W.¹, Kohanski, M. A.^{2,3}, Simmons, L. A.¹, Collins, J. J.² and Walker G. C.^{1,*}

1. Department of Biology, Massachusetts Institute of Technology, Cambridge, MA.

2. Department of Biomedical Engineering and Center for BioDynamics, Boston

University, Boston, MA.

3. Boston University School of Medicine, Boston, MA.

*Corresponding author. Mailing address: Department of Biology, Massachusetts Institute of Technology, Cambridge, MA 02139. Phone (617) 253 6711. Fax: (617) 253 2643.

Email: gwalker@mit.edu.

Classification: Biological Sciences; Genetics

Manuscript info: Text, table 23 pages; 6 figures 6 pages

Word and character count: Abstract 180, Manuscript character count: 46 748

Abstract

DNA-damaging agents induce lesions in genomic DNA that can interfere with DNA replication. Other agents that perturb replication, such as hydroxyurea (HU), can lead to fork arrest through a damage-independent mechanism by depleting the cellular concentration of deoxyribonucleotide triphosphates (dNTPs). Both DNA-damage and damage-independent methods of replication fork blockage elicit profound physiological responses including cell death. The genome-wide transcriptional response to DNA damage has been extensively examined, while the transcriptional response to damage-independent replication blockage has remained largely unexamined. In this work, we used a systems-level approach to determine the genomic and physiological responses of *E. coli* to a damage-independent mechanism of replication fork arrest. Our genome-wide analysis of the transcriptional response to HU-inducing replication fork arrest was compared to 530 different expression profiles, including the damage-dependent SOS transcriptional response. Our population and single-cell analysis shows the complex cellular response to HU triggers pathways involved in both cell survival and cell death. We suggest a model where, for any given bacterium in a population, HU can induce a molecular switch from a survival mode to a programmed cell death mode.

Introduction

Hydroxyurea (HU) is commonly used in both prokaryotes and eukaryotes to study DNA damage-independent replication fork arrest (64-66). HU is a potent inhibitor of class I ribonucleotide reductase (RNR), the enzyme responsible for the synthesis of dNTPs under aerobic conditions in many organisms. Depletion of dNTP pools through HU treatment leads to replication fork arrest, most likely through substrate starvation (66-68).

DNA damage, induced by mutagens such as UV, interferes with DNA replication through a mechanism different from that caused by HU (67, 69). When a replication fork encounters DNA damage caused by UV, replication proceeds discontinuously, leaving gaps juxtaposed to the lesions (70). The excess ssDNA generated results in formation of the RecA/ssDNA nucleoprotein filaments that facilitate auto-cleavage of the transcriptional repressor LexA and derepression of the SOS-regulon. The SOS response involves the upregulation of more than 40 genes involved in numerous aspects of DNA repair and other cellular functions (71). The genomic response to UV damage has been investigated and described in two independent studies using microarray analysis (72, 73). The majority of genes identified in these experiments belong to the SOS-regulon. The authors identified only a relatively small subset of genes that varied independently of the major SOS transcriptional repressor, LexA, or that were downregulated in response to UV. HU treatment has been shown to upregulate two genes of the SOS regulon, *recA*

and *sulA* (74). However, the extent of SOS induction, as well as other cellular responses brought about by HU-dependent fork arrest, has not been investigated in detail.

To investigate the full spectrum of cellular effects of HU treatment, we combined microarray technology with systems-level analysis to determine the genome-wide transcriptional response to HU in the model organism *Escherichia coli*. Work by several groups has shown that HU is exquisitely specific for inhibiting DNA synthesis through RNR inhibition (75, 76). However, a complete picture of the subsequent effects of dNTP pool depletion and replication fork arrest on cell physiology is lacking. In addition, it has not been known how *Escherichia coli*'s response to replication interference compares to its response to DNA damage.

Using our analysis of the transcriptional response to HU in *E. coli* to guide our investigation, we demonstrate that HU induces global molecular changes that encompass not only DNA repair but importantly pathways that extend into envelope stress, iron transport and toxin-antitoxin regulation. These data support a model that *E. coli* induces a distinctive transcriptional profile in response to damage-independent fork arrest that permits individual cells in the population to switch from a survival mode to a programmed cell death mode.

Results

Genome-wide analysis defines transcription perturbations induced by HU treatment. Treatment with 100 mM HU for 6 h in liquid culture results in less than 1%

survival of *E. coli* strain MC4100 (Fig. 1). As noted by Godoy *et al.*, the number of visible cells observed by microscopy after 5 h of HU treatment is greatly reduced (68). This indicates that HU does more than arrest replication; it sets in motion a chain of events that results not only in cell death, but also cell lysis. After only 1 h of HU treatment, MC4100 does not show a decrease in survival, but does show growth inhibition relative to the untreated culture (Fig. 1). To gain insights into the early cellular events that led to cell death and lysis, our gene expression analysis used *E. coli* MC4100 exponential cultures treated with HU for 1 h. RNA from cultures treated with or without HU were analyzed using Affymetrix Antisense Genome microarrays. The expression results were integrated into an *E. coli* microarray expression database (T Gardner, Boston University, <http://m3d.bu.edu>) for analysis comparing the HU results to over 500 additional expression profiles (194) (see experimental procedures). This procedure allowed us to identify genes that show altered transcript levels specifically in response to HU.

Treatment with HU has previously been shown to increase the expression of the two genes encoding *E. coli* class I RNR, *nrdA* and *nrdB* (195). We also observed a substantial increase in expression for these genes [Supporting Information (SI) Table 1]. We used western blots to confirm that the levels of NrdA and NrdB proteins similarly increased in response to HU treatment (SI Fig. 7A, B).

In addition, genes encoding *E. coli* anaerobic class III RNR (*nrdDG*) and a cryptic RNR (*nrdEF*) (196) showed significant transcriptional increases (SI Table 1). The *nrdEF* operon had been previously shown to respond to HU (197), however very little is known about *nrdDG* regulation other than its induction by anaerobic growth (198). We were

surprised to find substantial induction of *nrdDG*, since any NrdDG produced would be irreversibly inactivated under our aerobic conditions (196). These observations suggest that upregulation of all RNR genes in response to HU-induced dNTP pool depletion is a strong survival response.

The SOS response is induced by exposure to HU. As expected from previous work showing that HU treatment induces the expression of two SOS-regulated genes (74), our microarray analysis revealed that numerous genes in the SOS network were induced by HU treatment (SI Table 1). These include many genes involved in recombination and repair. In agreement with the transcriptional data, immunoblots for SulaA and RecA showed a significant increase of both these proteins following HU challenge (SI Fig. 8A, B).

Recent work has shown that small subpopulations of cells can account for large transcriptional changes in microarray analyses of the SOS response (199). To determine the population of SOS-induced cells after HU treatment, we used the pL(*lexO*)-GFP construct in which GFP expression is controlled by LexA (200) as a single-cell marker of SOS induction. We observed low GFP fluorescence in the untreated control cells (Fig. 2A). However, after a 1 hour exposure to HU, GFP fluorescence was clearly visible in the vast majority of cells (Fig. 2A), indicating that SOS induction occurred in the bulk of the population.

To explore the contribution of the SOS response to HU survival, we tested the sensitivity of the *lexA3* mutant strain to increasing amounts of HU (Fig. 2B). The *lexA3* strain carries a non-cleavable form of LexA resulting in a strain defective for SOS

induction (201, 202). The *lexA3* strain showed a marked increase in sensitivity to HU relative to the parental strain indicating that induction of the SOS-regulated genes helps cells survive HU exposure.

DNA damaging agents such as UV induce the expression of RecA, as well as promote formation of RecA-GFP foci at what is thought to be the replisome (203). We used RecA-GFP focus formation to compare the cellular effects of SOS induction by damage-dependent and damage-independent stresses. During growth in rich medium, we observed that RecA-GFP foci appear in approximately half of *E. coli* cells (49 %, n = 597), confirming previous observations (203). Exposure to HU results in nearly every cell containing at least one RecA-GFP focus (99 %, n = 521). In addition, these foci appeared larger in size with threads extending from most foci (SI Fig. 8C). Taken together, these results show that HU challenge induces both localization of RecA-GFP as foci and an increase in the cellular level of RecA protein (SI Fig. 8B), akin to what is observed under conditions of UV damage.

HU induces expression of genes required for DNA replication restart. Our array analysis revealed that components of the primosome, PriA and PriB, were substantially upregulated by HU treatment (SI Table 1). PriA and PriB can assemble forks on either the leading or lagging strand (204-206). The PriA pathway for replication restart is most efficient on fork structures without gaps in the leading strand. This structure could be formed after the collapse of a replication fork. An alternative PriC-dependent pathway preferentially utilizes forks with large gaps in the leading strand. We

did not observe upregulation of *priC* (SI Table 1), an observation consistent with the mode of fork damage induced by HU treatment.

Microarray analyses of the transcriptional response to UV damage did not identify genes involved in replication restart as being differentially regulated (72, 73), which suggests that induction of these genes is specific to replication fork blockage.

Considering the mode of action of UV and HU, this difference in expression pattern is reasonable. UV damage causes discontinuous DNA replication, but does not stop fork progression (70), whereas HU treatment leads to stalled replication forks that have the potential to collapse, requiring primosome function to reassemble (67).

Septum formation is perturbed by exposure to HU. A functionally linked cluster of genes involved early in cell division showed significant down-regulation in our microarray array (SI Table 1). These included several genes involved in septum formation (e.g., *ftsZ*, *ftsQ*, *zipA*) and a positive regulator of *ftsZ*, *rscB*. In agreement with the transcriptional result, we also observed a decrease in FtsZ at the protein level (SI Fig. 9A). Downregulation of genes required for septum formation offers a simple explanation for the extreme filamentation and eventual lysis observed in *E. coli* upon HU treatment (68).

To determine if the observed downregulation of genes required for septum assembly was sufficient to perturb septum formation, we analyzed Z-ring formation at the single-cell level. We used an *ftsZ*-GFP fusion under the *plac* promoter placed into the MC4100 genome at the *_ att* site (207). FtsZ-GFP does not functionally complement endogenous FtsZ, but this fusion protein is able to decorate the wild-type protein forming

Z rings allowing for visualization by fluorescence microscopy (208). Expression of FtsZ-GFP was comparable in HU-treated and non-treated cultures ensuring any observed effects were not due to unequal induction of FtsZ-GFP (SI Fig. 9B). Upon addition of IPTG, we observed septal ring formation in MC4100 cells at mid-cell (Fig. 3). When IPTG was added after HU treatment, the elongated cells did not show Z ring formation (Fig. 3). Lack of an observable Z ring in HU-treated cells correlates well with the decrease in *ftsZ* expression after HU addition (SI Table 1) and strongly suggests that the decreased expression of septum assembly genes is sufficient to perturb normal septum formation.

SOS induction upregulates expression of SulA that can bind FtsZ preventing cell division (202). HU treatment strongly upregulated SulA (SI Fig. 8A), which could result in continued cell growth without division. However, UV exposure, which also induces the SOS response and SulA upregulation, does not result in the extreme filamentation observed after HU treatment (data not shown). Previous microarray analysis has also shown that *ftsZ* expression is not perturbed by UV (72, 73). This suggests that the extreme filamentation caused by HU is not due to sequestration of FtsZ by elevated levels of SulA, but results from the HU-specific downregulation of several genes involved in formation of septum, including *ftsZ*.

HU induces the expression of genes required for iron uptake. An extremely striking observation from our microarray analysis was that *many* genes encoding several different iron uptake systems were significantly upregulated after HU treatment (SI Table 1). Several of these genes were among the most highly expressed. Upregulation of iron

mobilization genes was not observed in microarray analyses of UV-irradiated cells (72, 73).

While iron plays a catalytic role for several enzymes such as cytochromes and ribonucleotide reductases (209, 210), excess free iron can also be deleterious to *E. coli*, producing the highly destructive hydroxyl radical through Fenton chemistry (12). We postulated that such strong upregulation of many different iron uptake systems would result in a substantial increase in intracellular iron concentration that would in turn be detrimental to the cell. To test this hypothesis we disrupted *tonB*, which is required for ferric uptake through the Fep, Fec and Fhu transport systems (211), all of which were substantially upregulated in our microarray (SI Table 1). We found that, although HU induced expression of genes required for iron uptake, disruption of *tonB* greatly increased resistance of the strain to HU (Fig. 4A).

Our discovery that *tonB* expression promotes HU-induced lethality was in startling contrast to the results we described above. The induction of SOS-regulated genes and genes involved in replication restart by HU, together with the HU-induced down-regulation of genes required for cell division (SI Table 1), represent responses that would be expected to promote survival and allow the bacterium time to repair damage to its genome (202). However, the upregulation of iron transporters appear to be promoting cell death (Fig. 4A).

To understand the paradox of why cells would induce responses to promote both cell survival and cell death, we decided to determine whether only a subpopulation of cells upregulated iron transport systems after HU challenge and, if so, to examine how this subpopulation changed over time. The three major iron transport systems

upregulated in our microarray, *Fec*, *Fep* and *Fhu*, are all regulated by the iron-responsive transcriptional regulator *Fur* (212). We therefore used plasmid pL(*furO*)-GFP that expresses GFP under control of *Fur* (200, 209) as a molecular marker for induction of these systems. Strains carrying pL(*furO*)-GFP showed little fluorescence in the absence of HU (Fig. 4B). Treatment with HU resulted in a striking increase in GFP fluorescence in all cells in the population (Fig. 4B) in agreement with the upregulation of *Fur*-regulated iron transport systems we observed in our microarray results.

However, there was heterogeneity to the response, as our microscopy indicated that there were two populations of GFP-expressing cells in the HU-treated sample. Both subpopulations showed GFP fluorescence well above the untreated control, however one subpopulation was more fluorescent than the other (Fig. 4B). Taken together, these observations showed that induction of iron transport systems occurs in the bulk of the population but does so in a strikingly non-uniform fashion.

To explore this phenomenon in more detail, we used FACS analysis to follow *Fur*-regulated GFP expression over time after HU challenge (Fig. 4C). We observed increased GFP expression in all cells after 1 h (Fig. 4C, peak **B**) in agreement with our microscopy results. However the differentiation into two subpopulations was not observed until 2 h at which point the overall fluorescence of the culture had reached maximum (peak **C**). This offset in timing (2 h vs. 1 h) of observing two subpopulations is most likely due to the lower sensitivity of the FACS analysis. Cell survival began to decrease 2 h post HU treatment (Fig. 1), which correlates with the appearance of peak **C** (Fig. 4C). This suggests that cells in peak **C** have entered a cell death pathway. This inference is supported by our observation that the number of cells in peak **C** decreases

with time after HU exposure. We also observe increased side scattering in the FACS analysis over this period of time, consistent with increased cell debris from lysis. The bacteria are not reverting to a lower level of GFP expression as peak **B** does not increase in size as peak **C** decreases after 3 h. We suggest the transition of cells from peak **B** to peak **C** represents a profound switch in cell physiology from a state that promotes survival to a state that commits cells to death.

The *rpoE-rseA-rseB-rseC* operon is downregulated by HU. We were intrigued to find that the operon containing the alternative sigma factor, *rpoE*, was strongly downregulated after HU treatment (SI Table 1). RpoE controls a stress response pathway that regulates the expression of genes encoding periplasmic chaperons, proteases, biosynthetic enzymes for lipid A and proteins that produce components of the envelope (213). In HU-treated cells, the entire *rpoE* operon was downregulated. This includes *rseA* and *rseB*, which encode regulators of RpoE activity. We performed immunoblots for RpoE and RseA on samples from HU-treated cultures and found that indeed both RpoE and RseA levels decreased in HU-treated cultures relative to the untreated control (SI Fig. 10A, B).

Decreased RpoE levels would affect a bacterium's ability to manage envelope stress. Downregulation of the *rpoE* operon, like increased iron accumulation, could promote cell death. In fact, recent work has shown that cells that have lost RpoE function die because they overreact to the absence of this sigma factor by triggering a cell death signal (214).

***mazEF* and *relBE* toxin-antitoxin systems show a synergistic affect with HU treatment and act separately from iron-induced cell death.** Toxin-antitoxin systems have been identified in several different bacteria (215, 216). Each pair consists of a stable toxin and an unstable antitoxin that interferes with the toxin activity. When conditions lead to a decrease in antitoxin synthesis, it is rapidly degraded exposing the cell to the lethal effects of the toxin.

It has previously been shown that disruption of the toxin-antitoxin pairs, *mazEF* or *relBE*, in certain strains of *E. coli* increases HU resistance (68). Our observations of increased iron uptake and downregulation of *rpoE* after HU treatment led us to ask whether the MazF and/or RelE toxin were activated under our conditions and contribute to the eventual death of the HU-treated MC4100. Our microarray results showed only small perturbations in expression of *mazF* relative to *mazE* and *relE* relative to *relB* in the direction that would promote toxin activity (SI Table 1). However, these changes were so small as to leave their biological significance questionable.

We constructed strains carrying deletions of each of the *mazEF* and *relBE* toxin-antitoxin pairs and also a strain deleted for both toxin-antitoxin pairs. When challenged with HU, we found that in MC4100, deletion of *mazEF* led to increased resistance to HU in agreement with previous work (Fig. 5A) (68). Our MC4100 Δ *relBE* strain, however, was indistinguishable from the parental strain for HU survival (Fig. 5B). Strikingly, we found that deletions of both *mazEF* and *relBE* act synergistically to promote HU resistance to levels well above that observed in a Δ *mazEF* strain alone (Fig. 5C). Our results suggest that both *mazEF* and *relBE* contribute to a toxin-induced cell death pathway initiated by HU challenge. Since HU causes only very small changes in

transcript level of the toxin-antitoxin pairs, HU treatment appears to be affecting toxin activation at a post-transcriptional level.

We showed above that HU challenge causes a striking upregulation of iron transport genes in MC4100 (SI Table 1), and that disruption of iron uptake, through deletion of *tonB*, increased the strain's resistance to HU (Fig. 4A). We asked if the cell death program promoted by increased iron uptake was part of the cell death pathway through which *mazF* and *relE* toxins operated. To address this question, we constructed a strain carrying deletions for *mazEF* and *relBE* as well as *tonB*, and tested its sensitivity to HU (Fig. 5D). Our $\Delta mazEF\Delta relBE\Delta tonB$ was even more resistant to HU than our $\Delta mazEF\Delta relBE$ strain (Fig. 5D). The increase in resistance of our $\Delta mazEF\Delta relBE\Delta tonB$ strain above that of our $\Delta mazEF\Delta relBE$ strain is comparable in magnitude to the increase in resistance observed of our $\Delta tonB$ strain above the parental strain, MC4100 (Fig. 4A). Thus the HU resistance conferred by deletion of $\Delta mazEF\Delta relBE$ and $\Delta tonB$ are additive suggesting they induce cell death through different pathways.

Discussion

Our systems-level analysis of the transcriptional response of *E. coli* to HU stress has revealed an intricate response, coordinating events that first promote cell survival but that later can switch to promoting cell death. Consistent with a response promoting cell survival, HU-challenged *E. coli* show clear induction of the SOS response in all cells in the population. This also demonstrates that replication fork interference by either DNA

damage-dependent or damage-independent means results in upregulation of this defense pathway. Our analysis showed that HU treatment also induced additional mechanisms to promote cell survival that are not induced by DNA-damaging agents such as UV irradiation (SI Table 1) (72, 73). This includes upregulation of *priA* and *priB* for replication restart and downregulation of cell division genes, such as *ftsZ*, *ftsQ* and *zipA* that would allow the bacterium added time to repair its genome before dividing. These results indicate that damage-dependent (i.e., UV) and damage-independent (i.e., HU) fork interference share some overlap in DNA damage response, however damage-independent events invoke additional levels of protective responses.

Besides the activation of these protective responses, we were intrigued to find that a set of cellular responses which promote cell death were also activated by HU (SI Table 1). Our analysis showed that, following HU treatment, *E. coli* strain MC4100 cell death is mediated in part by MazF and RelE since deletion of *mazEF* and *relBE* results in a significant increase in survival (Fig. 5C). The dependence of cell death on toxin/antitoxin pairs after HU treatment suggests a mechanism similar to thymineless death which also results from depletion of substrate for DNA replication and is dependent on MazF (217).

We also identified two additional mediators of cell death. HU treatment induced several iron uptake systems (SI Table 1). Deletion of the gene encoding the common outer membrane component for these transport systems, *tonB*, resulted in a significant increase in HU resistance (Fig. 4A), suggesting that iron uptake also contributes to cell death. The resistance against HU afforded by deleting *tonB* was additive with the

resistance given by disruption of *mazEF* and *relBE* (Fig. 5D), suggesting two distinct pathways activated by HU that can lead to cell death.

The major iron transport systems upregulated in our array, *Fec*, *Fep* and *Fhu*, are *Fur* regulated. *Fur* acts as a repressor when bound to ferrous ions. While *Fur* binds ferrous iron, the *Fec*, *Fep* and *Fhu* transport systems uptake ferric iron (209). De-repression of *Fur*-regulated genes implies a lowered level of active *Fur* repressor. This could arise by an HU-induced reduction in the concentration of ferrous ions available to bind *Fur*. HU treatment may affect the reduction of ferric iron to the ferrous form. In this model, increased intracellular ferric ion concentration may then activate a cell death response.

An alternative explanation is that HU induces a reduction in *Fur* protein levels by *fur* mRNA being targeted for degradation by *MazF* or *RelE*. We did not observe a decrease in *fur* transcript in our microarray analysis. However our analysis only examined the transcriptional response after 1 h of HU treatment. We did not observe cell death beginning until 2 h after HU treatment, the same time we observed maximum *Fur*-regulated GFP expression. Measurable degradation of *fur* mRNA by *MazF* or *RelE* might not occur until after 1 h of HU treatment. With this model, intracellular ferrous ions could accumulate without activating *Fur* repression. Accumulation of ferrous ions may help activate a cell death pathway by entering into a redox cycle producing destructive hydroxyl radicals (218). This mode of killing may be similar to that observed in early stage treatment with bactericidal antibiotics (219). Kohanski *et al.* showed that bactericidal antibiotics caused accumulation of intracellular iron that activated hydroxyl radical formation eventually causing cell death. However, the

increase in iron from bactericidal antibiotic treatment was found to come from release of iron from iron-sulfur containing proteins rather than external iron sources as we observe for HU treatment. It will be interesting to test if the cell death induced by increased uptake of iron following HU treatment is also due to radical formation.

HU treatment also induced the downregulation of the *rpoE* operon (SI Table 1). Recent work has suggested that, in the absence of RpoE, *E. coli* activates a cell death pathway that could function by activating MazF (214). Thus the activation of toxin-dependent cell death we observe after HU treatment may be the consequence of several cell signals including downregulation of *rpoE*. In addition, loss of RpoE would hinder the cell's ability to respond to membrane stress, possibly, making it more susceptible to lysis which we observed after HU treatment.

Our single-cell analyses offered insights that could not be gained from microarray studies, which report population averages. Our single-cell analysis of the SOS response revealed that all cells in the population experience a similar induction of a protective response that promotes survival soon after HU treatment. However, the situation is different with respect to the HU induction of Fur-regulated iron transport, which appears to promote cell death. In this case, the HU-induced increase in Fur-regulated genes is heterogeneous within the population. Initially, all the cells in the population experience an increase in the expression of Fur-regulated genes. Then, between 1-2 h after HU treatment, a second population of cells is observed that expresses extreme levels of Fur-regulated genes. These cells slowly disappear, presumably by lysis, while additional cells switch from the lower level of Fur-regulated gene expression to the higher state.

Our killing curve shows that HU treatment halts growth by 1 h, and by 2 h the bacteria begin to lose viability (Fig. 1).

From these observations, we have developed a model (Fig. 6) where the SOS response is initiated early in the population after HU treatment in an attempt to save each individual bacterium. At some point after initial exposure, some bacteria may no longer be able to repair themselves and switch to a complex cell death mode. As this switch is not synchronized in the population, different bacteria initiate this process at different times. We observe this differential switch as a heterogeneous increase in expression of iron-regulated GFP fluorescence that increases in intensity over time as more bacteria switch on programmed cell death. It will be interesting to determine if a bimodal distribution, similar to iron uptake in a population, is also observed for activation of toxin/antitoxins and for repression of *rpoE* after HU treatment.

Programmed cell death is observed in higher organisms following dNTP depletion, suggesting that eukaryotes and prokaryotes share a similar response to this stress (220). In a multicellular organism there are clear reasons for elimination of individual cells if it benefits the organism as a whole (221). Rationales have also been suggested for bacterial programmed cell death as in the case of cannibalism during *B. subtilis* sporulation (222). Considering the cannibalism model, we were intrigued to find that genes responsible for the utilization of hexauronates showed significant upregulation in response to HU (SI Table 1). We hypothesize that degraded peptidoglycan components, released from lysed bacteria, are shuttled through the hexauronate system to provide precursors for dNTPs synthesis and energy supplies for the surviving cells.

Thymine starvation provokes DNA damage involving a unique breaking/twisting of the chromosome into a configuration that defies all the repair systems (223, 224) which is thought to activate the MazF toxin. Both HU and thymine starvation interfere with DNA replication suggesting that both may lead to a common class of events that then leads to an activation of the complex cell death program. We have reported that the activation of both DNA polIV (DinB) and DNA polV (UmuD'₂C) carrying out limited mutagenic DNA synthesis is able to make cells resistant to killing by HU, presumably by stabilizing the replication fork under conditions of dNTP depletion (68). These observations suggest that some type of replication fork problem or collapse may be the event that triggers a cell death response. It is not yet clear what signal transduction events lead the replication fork problem to activation of the cell death program. By activating a cell death program, cells that have terminally lost the ability to replicate because of an insurmountable DNA problem are able to lyse and release their nutrients to aid the surviving members of the population in their battle to withstand stress.

Materials and Methods

Strains, plasmids and growth conditions. Strains and plasmids are shown in SI Table

2. All strains were grown aerobically in Luria-Berani (LB) at 37 °C. For *ftsZ*-GFP assays, LB was supplemented with 0.2 % glucose and 1.0 μM to 2.5 μM IPTG. Where indicated, antibiotics were used at the following concentrations: ampicillin (100 μg/ml except for BWD05 that used 25 μg/ml), kanamycin (30 μg/ml) and spectinomycin (100 μg/ml). Allele transfers were done by P1 transduction.

RNA isolation and microarray analysis. MC4100 was grown to mid-exponential phase. Cultures were diluted and grown +/- 100mM hydroxyurea (Sigma) for 1 h after which RNA was isolated using the Qiagen RNeasy extraction kit and samples were treated with DNase treated using *dna-free* (Ambion). cDNA preparation and microarray analysis were performed as described (200).

Hydroxyurea sensitivity assays. Liquid culture assays were done as described (68).

For chronic assays, strains were serially diluted and plated on LB agar containing increasing amounts of hydroxyurea. Cfus were counted after 24 h growth at 37°C.

Protein lysates and immunoblots. Strains were grown in mid-log +/- 100 mM hydroxyurea for 1 h. Cultures were lysed by two passages through a bead beater with glass beads. Immunoblotting was performed as previously described (126), loading equal amounts of protein for each sample.

Microscopy and FACS analysis. Strains were grown to mid-exponential phase, diluted, and grown for 1 h +/- 100 mM hydroxyurea. Preparation of cells for live-cell microscopy was done essentially as described (68). FACS analysis was performed as described (200).

Acknowledgements

We would like to thank Dr. Carol Gross for anti-RpoE and anti-RseA antibodies and Dr. Joe Lutkenhaus for anti-FtsZ antibodies. This work was supported by National Institutes of Health grants GM31010, CA21615-27 (to G.C.W.) and DP10D003644 (to J.J.C.), National Science Foundation FIBR program (to J.J.C.), National Sciences and Engineering Research Council of Canada graduate scholarship (to B.W.D.), NCI postdoctoral fellowship (to L.A.S) and Massachusetts Institute of Technology Center for Environmental Health Sciences National Institute of Environmental Health Sciences Grant P30 ES002109. G.C.W. is an American Cancer Society Research Professor.

Fig. 1. Exponentially growing MC4100 cultures were treated with (□) or without (○) 100 mM HU.

Fig. 2. (A) MC4100 pL(*lexO*)-GFP treated with or without HU. (B) WT AB1157 (□) and AB1157 *lexA3* (○) were spotted on LB agar plates containing increasing concentrations of HU.

Fig. 3. MC4100 carrying P_{lac}*ftsZ*-GFP treated with 2.0 μM IPTG in the presence or absence of 100 mM HU.

Fig. 4. (A) MC4100 (□) and MC4100 Δ *tonB*::Km^R (○) were serially diluted and spotted on LB agar plates containing increasing concentrations of HU. (B) MC4100 pL(*furO*)-GFP treated with or without 100 mM HU. Each panel is a merge of the membrane (red) and GFP (green) images. (C) MC4100 pL(*furO*)-GFP treated with 100 mM HU and sorted by FACS as previously described (200).

Fig. 5. (A) MC4100 (□) and MC4100 Δ *mazEF*::Km^R (○). (B) MC4100 (□) and MC4100 Δ *relBE* (○). (C) MC4100 (□) and MC4100 Δ *relBE* Δ *mazEF*::Km^R (○). (D) Δ *relBE* Δ *mazEF*::Km^R (○) and Δ *relBE* Δ *mazEF*::Km^R Δ *tonB* (○). In each experiment the strains were spotted on LB agar plates containing increasing concentrations of HU.

Fig. 6. Model of *E. coli* cellular response to HU. Following HU exposure, *E. coli* activates a series of survival mechanisms. At a later time point, cells that are unable to repair their damaged genomes activate a complex cell death program.

Fig. 1

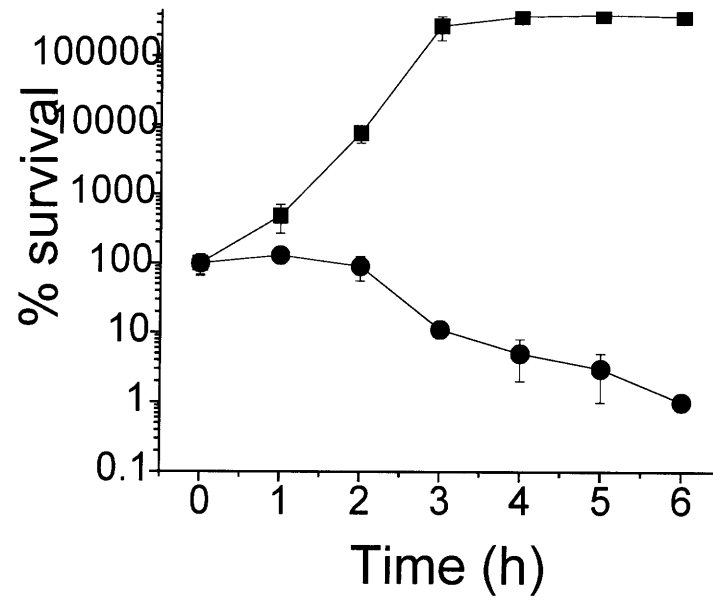


Fig. 2

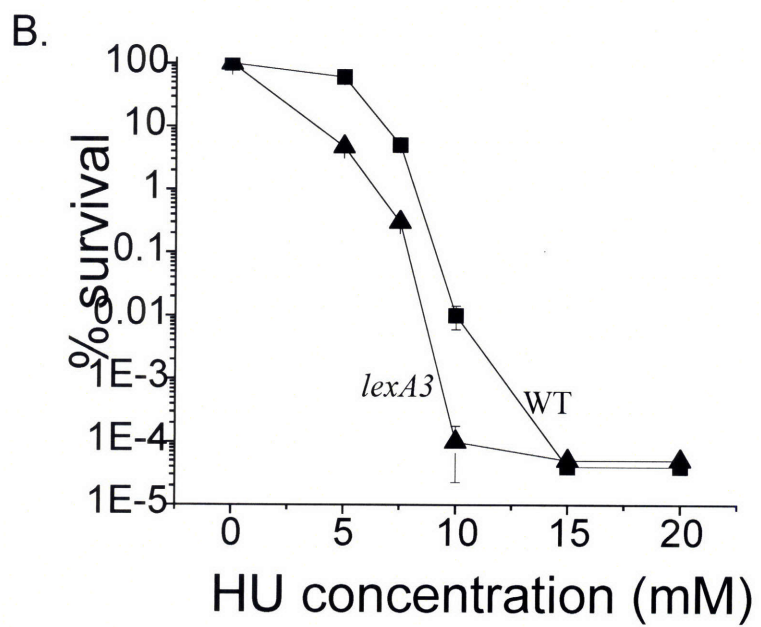
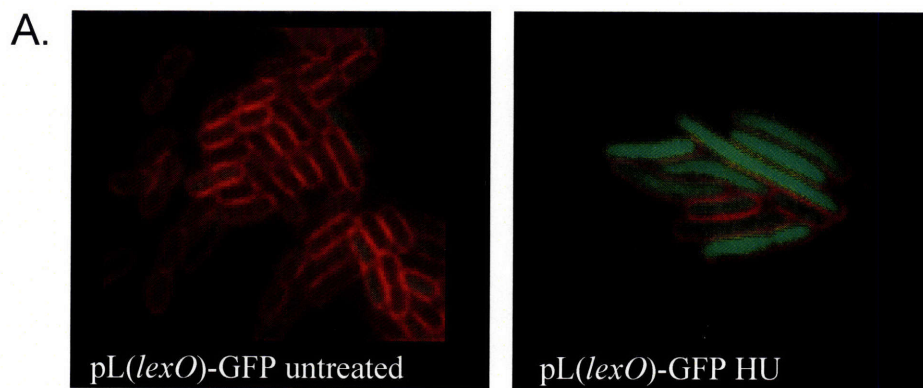


Fig. 3

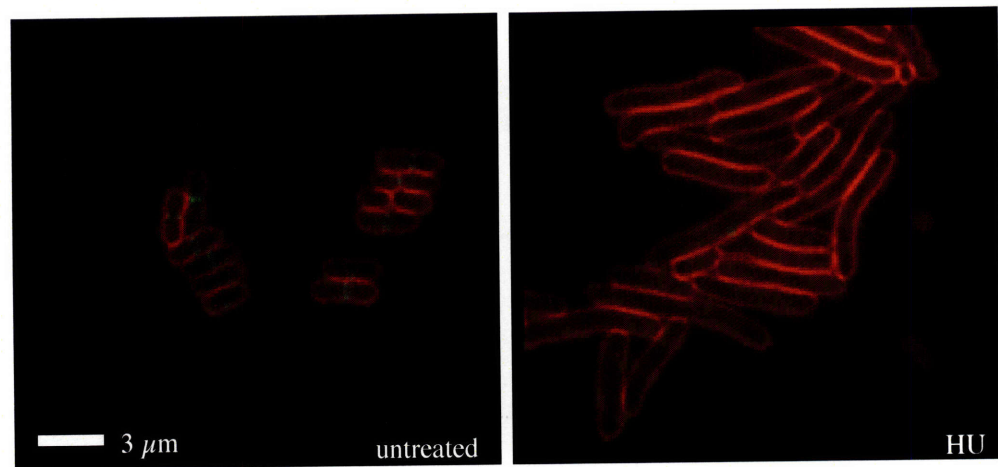
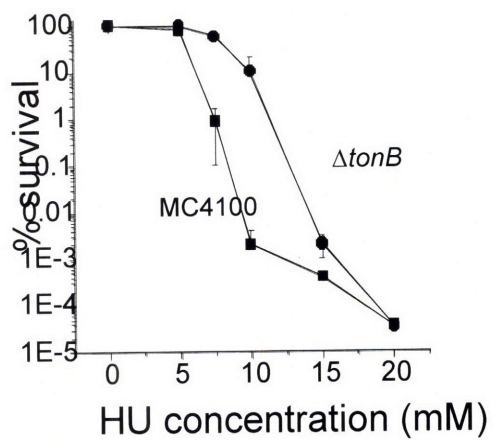
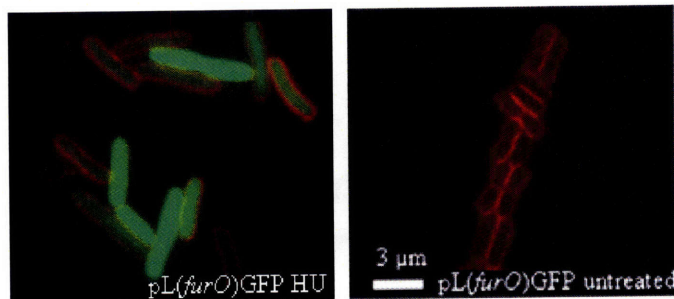


Fig. 4

A.



B.



C.

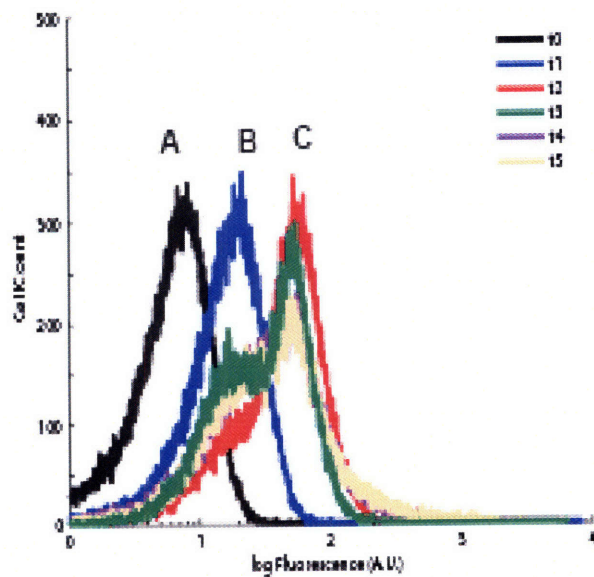


Fig. 5

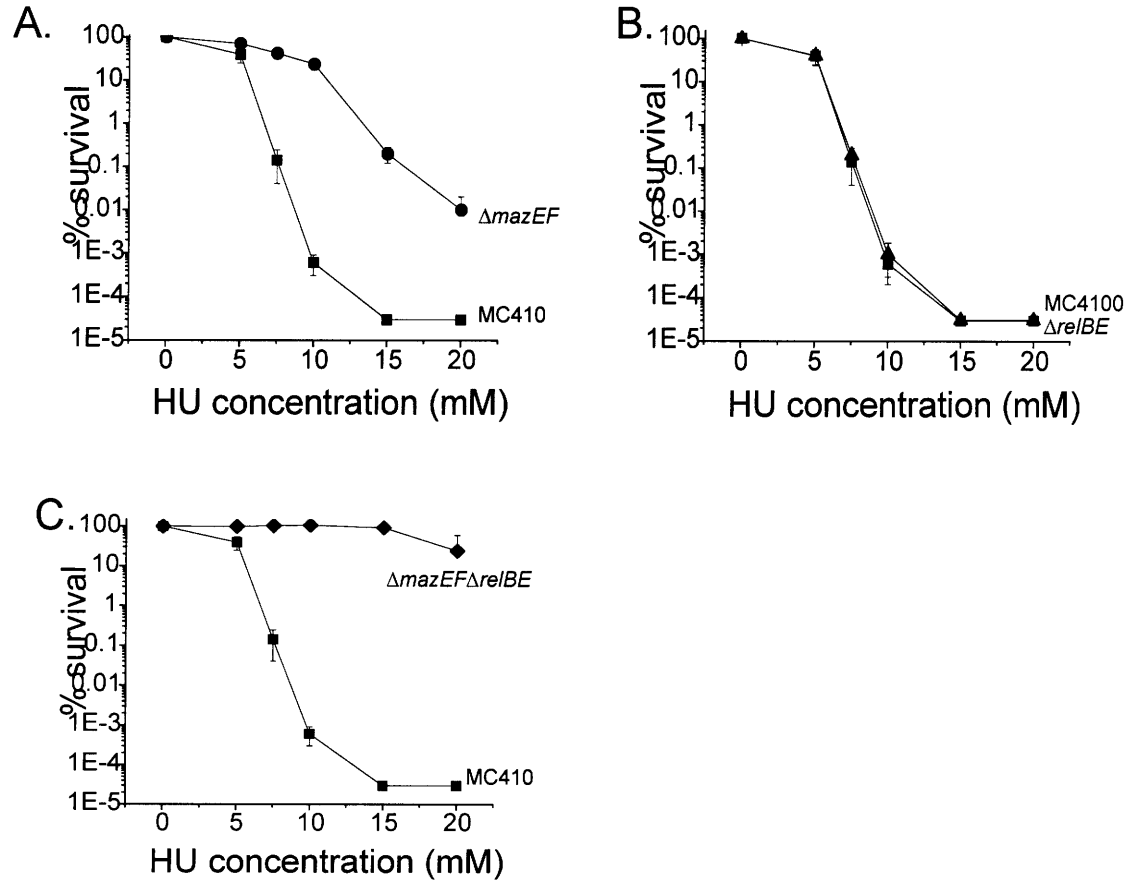
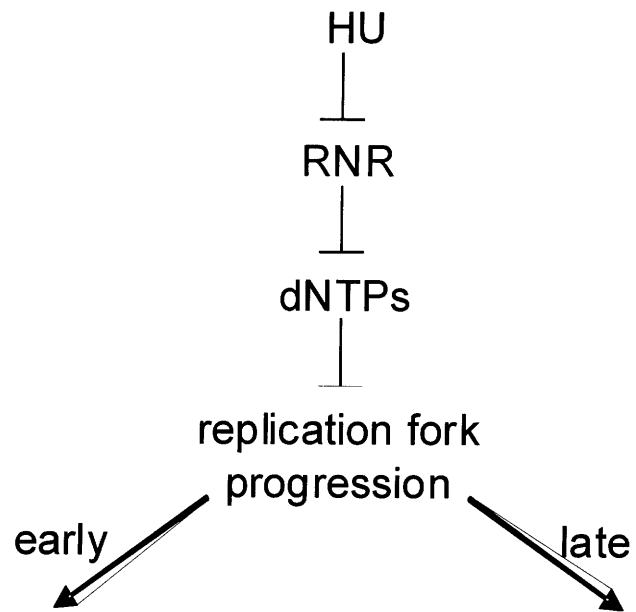


Fig. 6



Survival Response

1. SOS response
2. Primosome Upregulation
3. Arrest cell division

Cell Death Response

1. Toxin activation
2. Iron uptake
3. RpoE downregulation

Supplemental

SI Table 1. Functional grouping for differentially regulated genes identified by microarray analysis.

Gene	Gene Product/Function	Z Score (+HU vs. -HU)
Ribonucleotide Reductase		
<i>nrdA</i>	subunit A class I ribonucleotide reductase	+3.16
<i>nrdB</i>	subunit B class I ribonucleotide reductase	+4.34
<i>nrdD</i>	class III ribonucleotide reductase, anaerobic	+3.76
<i>nrdG</i>	NrdD activating enzyme	+3.99
<i>nrdH</i>	electron transport system for NrdEF	+4.07
<i>nrdI</i>	part of <i>nrdHIEF</i> operon; function unknown	+4.39
<i>nrdE</i>	subunit _ cryptic class I ribonucleotide reductase	+3.98
<i>nrdF</i>	subunit _ cryptic class I ribonucleotide reductase	+4.23
SOS Network		
<i>sulA</i>	inhibits FtsZ ring formation	+2.55
<i>dinB</i>	DNA polymerase IV	+1.48
<i>recA</i>	recombinational repair	+1.75
<i>recN</i>	recombinational repair	+1.33
<i>umuC</i>	DNA polymerase V	+2.70
<i>umuD</i>	DNA polymerase V	+2.62

<i>ruvA</i>	Holliday junction recognition	+2.04
<i>ruvB</i>	Branch migration of Holliday structures	+2.69
<i>uvrB</i>	Excision nuclease subunit B	+2.62
<i>uvrD</i>	DNA-dependent ATPaseI-DNA helicase II	+1.50
DNA Replication Restart		
<i>priA</i>	primosome factor Y	+2.16
<i>priB</i>	primosome protein	+1.76
<i>dnaB</i>	helicase	+0.70
<i>dnaC</i>	sliding clamp subunit	+1.65
<i>dnaN</i>	sliding clamp subunit	+2.58
Cell Division		
<i>ftsZ</i>	initiates septum ring formation	-2.14
<i>zipA</i>	septal ring structural protein	-2.59
<i>ftsQ</i>	growth of cell wall at septum	-1.58
<i>rcsB</i>	<i>ftsZ</i> regulator	-1.20
Iron Uptake		
<i>fecA</i>	receptor, citrate-dependent ferric iron transport	+3.48
<i>fecB</i>	periplasmic protein, ferric iron transport	+3.09
<i>fecC</i>	ferric iron transport	+3.08
<i>fecD</i>	membrane protein, ferric iron transport	+2.31

<i>fecE</i>	ferric iron transport	+2.72
<i>fecI</i>	ferric iron transport	+3.73
<i>fecR</i>	regulator of ferric iron transport	+1.97
<i>feoA</i>	ferrous iron uptake system	+1.11
<i>feoB</i>	membrane protein, ferrous iron uptake system	+1.23
<i>fepA</i>	outer membrane protein, ferribactin transport	+3.16
<i>fepB</i>	periplasmic protein, ferrienterbactin transport	+2.07
<i>fepC</i>	inner membrane protein, ferrienterobactin transport	+2.55
<i>fepD</i>	ferrienterobactin permease	+2.19
<i>fepE</i>	ferric enterobactin uptake	+0.73
<i>fepG</i>	ferrienterobactin permease	+2.47
<i>fhuA</i>	ferrichrome OMP	+2.72
<i>fhuB</i>	hydroxamate-dependent ferric uptake	+3.59
<i>fhuC</i>	hydroxamate-dependent ferric uptake	+2.72
<i>fhuD</i>	hydroxamate-dependent ferric uptake	+2.31
<i>fhuE</i>	ferric-rhodotorulic acid outer membrane receptor	+1.45
<i>fhuF</i>	ferric hydroxamate transport	+4.12
<i>tonB</i>	iron uptake	+3.25
<i>exbB</i>	iron uptake	+4.19
<i>exbD</i>	iron uptake	+3.64
	RpoE Related	
<i>rpoE</i>	alternative sigma factor, envelope stress response	-4.02

<i>rseA</i>	negative regulator of RpoE	-3.43
<i>rseB</i>	binds RseA, negative regulator of RpoE	-4.78
<i>rseC</i>	positively regulates RpoE	-3.07
<i>fkpA</i>	periplasmic chaperone	-2.23
<i>surA</i>	periplasmic chaperone	-1.86
Toxin-Antitoxin Pairs		
<i>mazE</i>	suppressor of MazF activity	-0.57
<i>mazF</i>	toxic protein, growth inhibitor	+0.19
<i>relB</i>	suppressor of RelE activity	-0.34
<i>relE</i>	toxic protein, growth inhibitor	-0.07
Hexauronate Metabolism		
<i>uxaA</i>	altronate hydrolase galacturonate	+4.63
<i>uxaC</i>	uronate isomerase galacturonate	+3.87
<i>uxuA</i>	mannonate hydrolase glucuronate	+3.54
<i>uxuB</i>	mannonate oxidoreductase glucuronate	+3.17

SI Table 2. Bacterial strains and plasmids used in this study

Strain/plasmid	Relevant genotype and property	Source
<u>Strain</u>		
MC4100	<i>F⁻ araD139 ΔlacU169 ΔrelA1 rpsL150 thi mot flb5301 deoC7 ptsF25 rbsR</i>	Laboratory stock
AB1157	<i>F⁻ thr-1 leuB6 proA2 his4 thi1 argE3 lacY1 galK2 rpsL supE44 ara-14 xyl-15 mtl-1 txs-33</i>	Laboratory stock
DM49	AB1157 <i>lexA3</i>	(201)
DFJ135	AB1157 <i>lexA(Def), sulA11</i>	Laboratory stock
CH971	CH113 <i>ΔmazEF::Km^R</i>	(225)
CH972	CH113 <i>ΔrelBE::Km^R</i>	(225)
JW1224	BW25113 <i>ΔtonB::Km^R</i>	(226)
BWD01	MC4100 <i>ΔmazEF::Km^R</i>	This study
BWD02	MC4100 <i>ΔrelBE</i>	This study
BWD03	MC4100 <i>ΔmazEF::Km^R, ΔrelBE</i>	This study
BWD04	MC4100 <i>ΔtonB::Km^R</i>	This study
EC448	MC4100 <i>Δ(attL-lom)::bla lacI^P P₂₀₈-ftsZ-gfp</i>	(207)
BWD05	MC4100 <i>Δ(attL-lom)::bla lacI^P P₂₀₈-ftsZ-gfp</i>	This study
SS1744	<i>recA4136-gfp</i>	(203)
BWD06	MC4100 <i>recA4136-gfp</i>	This study
BWD07	MC4100 <i>lexA-gfp</i> plasmid	This study

BWD08	MC4100 <i>fur</i> -gfp plasmid	This study
BWD09	MC4100 Δ <i>seqA</i> ::Cm ^R	This study
<u>Plasmids</u>		
pL(<i>lexO</i>)GFP	GFP under LexA control	(200)
pL(<i>furO</i>)GFP	GFP under Fur control	(200)

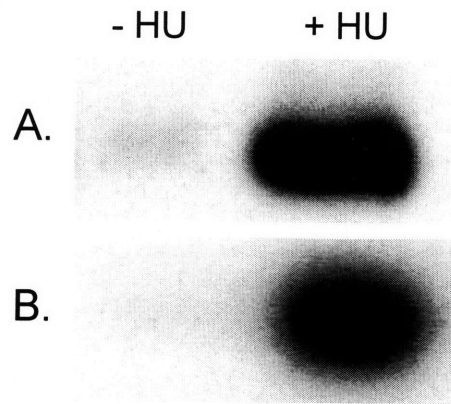
SI Fig. 7. Whole cell lysates from MC4100 treated +/-100 mM HU immunoblotted for (A) NrdA or (B) NrdB.

SI Fig. 8. Whole cell lysates from MC4100 treated +/- 100 mM HU immunoblotted for SulA-GFP (A) using anti-GFP antibodies or RecA (B) using a monoclonal antibody against RecA. (C) RecA-GFP localization in MC4100 with, and without, HU treatment. For cell images in (C), the membrane was visualized using FM4-64 (“experimental procedures”).

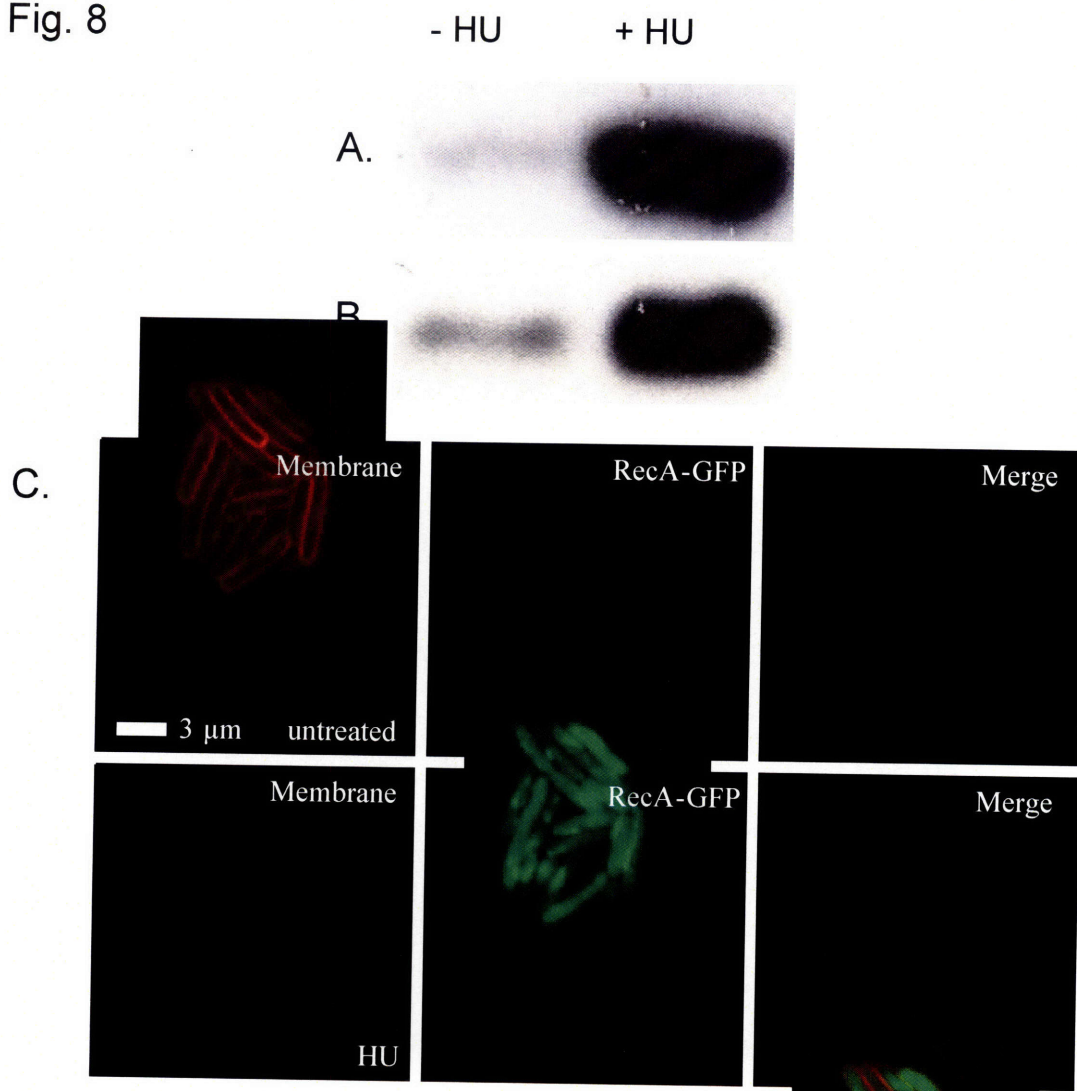
SI Fig. 9. (A) Whole cell lysates from MC4100 treated +/- 100 mM HU immunoblotted for FtsZ. (B) Whole cell lysates from MC4100 carrying P_{lac}*ftsZ*-GFP treated with IPTG in the presence or absence of 100 mM HU followed by immunoblotting for FtsZ-GFP using monoclonal anti-GFP antibodies.

SI Fig. 10. Whole cell lysates from MC4100 treated +/- 100 mM HU immunoblotted for (A) RpoE or (B) RseA.

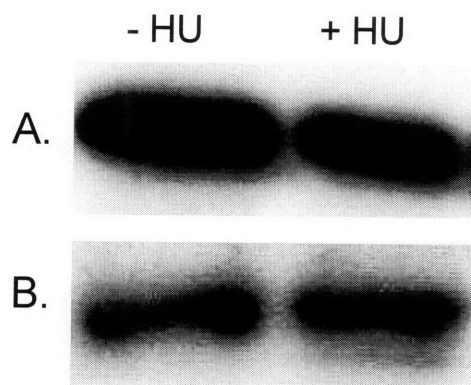
SI Fig. 7



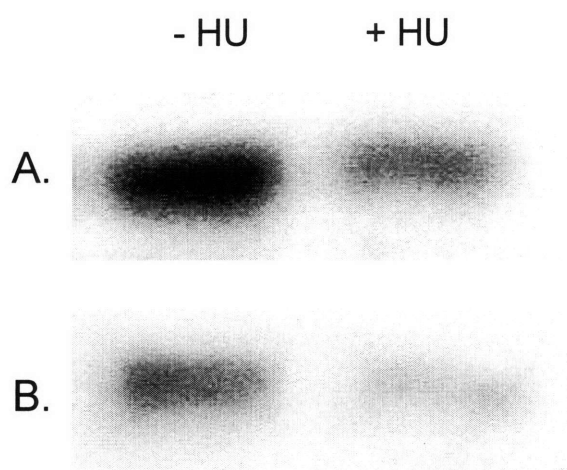
SI Fig. 8



SI Fig. 9



SI Fig. 10



Chapter 7

Investigations into the Mechanism of Hydroxyurea Resistance Conferred by Loss of
YbeY Activity

Abstract

While investigating the $\Delta ybeY$ mutant (Chapter 5), I found that, in contrast to the wide range of stresses it was sensitive to, the $\Delta ybeY$ mutant was very resistant to the DNA replication inhibitor hydroxyurea. In Chapter 6, I presented a model where, for any given bacterium in a population, hydroxyurea can induce a molecular switch from a survival mode to a programmed cell death mode. Here, I use that model to explore possible mechanisms for the increased resistance of the $\Delta ybeY$ mutant to hydroxyurea. I demonstrate that the $\Delta ybeY$ mutant induces a cell-survival pathway in response to HU but is much less sensitive to triggering activation of cell death pathways. Furthermore, I show that the increased resistance to HU cannot be simply explained by the decreased growth rate of the $\Delta ybeY$ mutant and offer evidence that YbeY may act more directly in sensing HU-related stress.

Introduction

Hydroxyurea (HU) is commonly used in both prokaryotes and eukaryotes to study DNA damage-independent replication fork arrest (64-66). HU is a potent inhibitor of class I ribonucleotide reductase (RNR), the enzyme responsible for the synthesis of dNTPs under aerobic conditions in many organisms. Depletion of dNTP pools through HU treatment leads to replication fork arrest, most likely through substrate starvation (66-68)

DNA damage, induced by mutagens such as UV, interferes with DNA replication through a mechanism different from that caused by HU (67, 69). When a replication fork encounters DNA damage caused by UV, replication proceeds discontinuously, leaving gaps juxtaposed to the lesion (70). The excess ssDNA generated results in formation of the RecA/ssDNA nucleoprotein filaments that facilitate auto-cleavage of the transcriptional repressor LexA and derepression of the SOS-regulon. The SOS response involves the upregulation of more than 40 genes involved in numerous aspects of DNA repair and other cellular functions (71). The genomic response to UV damage has been investigated and described in two independent studies using microarray analysis (72, 73). The majority of genes identified in these experiments belong to the SOS-regulon. The authors identified only a small subset of genes that varied independently of the major SOS transcriptional repressor, LexA, or that were downregulated in response to UV. HU treatment had been shown to upregulate two genes of the SOS-regulon, *recA* and *sulA* (74), however the extent of SOS induction as well as other cellular responses brought about by HU-dependent fork arrest had not been investigated in detail.

In Chapter 6, I investigated the cellular response of *E. coli* to HU. Using a systems-level analysis of the transcriptional perturbations induced by HU to guide my experiments, I showed that HU induces global molecular changes that encompass not only DNA repair but importantly pathways that extend into envelope stress, iron transport and toxin-antitoxin regulation. These data support the model that *E. coli* induces a distinctive transcriptional profile in response to damage-independent fork arrest that permits individual cells in the population to switch from a survival mode to a programmed cell death mode.

In Chapter 5, I presented my study of a previously undescribed family of proteins designated as COG0319. I demonstrated that the *E. coli* homolog, YbeY, is required for ribosome maturation. The $\Delta ybeY$ mutant is very pleiotropic displaying increased sensitivity to a wide variety of environmental stresses (Chapter 5). During my study of the $\Delta ybeY$ mutant I was intrigued to find that it was also highly resistant to HU. I present here my investigation into the mechanism(s) of HU resistance of the $\Delta ybeY$ mutant. I demonstrate that the $\Delta ybeY$ mutant is capable of activating HU-inducible cell death pathways but requires higher doses of HU to trigger their activation, which suggest that YbeY may act to enhance the signal to activate cell death pathways.

Materials and Methods

Strains, plasmids and growth conditions. Strains and plasmids are shown in Table 1.

All strains were grown aerobically in Luria-Berani (LB) at 37 °C. Where indicated,

antibiotics were used at the following concentrations: ampicillin (100 µg/ml), kanamycin (30 µg/ml) and chloramphenicol (20 µg/ml). Allele transfers were done by P1 transduction.

RNA isolation and microarray analysis. MC4100 was grown to mid-exponential phase. Cultures were diluted and grown +/- 100mM hydroxyurea (Sigma) for 1 h after which RNA was isolated using the Qiagen RNeasy extraction kit and samples were treated with DNase using *dna-free* (Ambion). cDNA preparation and microarray analysis were performed as described (200).

Hydroxyurea sensitivity assays. Liquid culture assays were done as described (68). For chronic assays, strains were serially diluted and plated on LB agar containing increasing amounts of hydroxyurea. Cfu were counted after 24 h growth at 37⁰C.

Protein lysates and immunoblots. Strains were grown in mid-log +/- 100 mM hydroxyurea for 1 h. Cultures were lysed by two passages through a bead beater with glass beads. Immunoblotting was performed as previously described (126), loading equal amounts of protein for each sample.

Microscopy and FACS analysis. Strains were grown to mid-exponential phase, diluted, and grown for 1 h +/- 100 mM hydroxyurea. Preparation of cells for live-cell microscopy was done essentially as described (68). FACS analysis and run-out assays were performed as described (67).

Co-immunoprecipitation assays. Co-immunoprecipitation assays were performed using $\Delta ybeY$ mutant strains carrying *ybeY* (+/- FLAG-tag) on a plasmid. Assays were performed as described by manufacture (Sigma FLAG-tag system).

Results

The $\Delta ybeY$ mutant is highly resistant to drugs that induce DNA damage-independent replication arrest. In Chapter 5, I described a novel, universally conserved protein in bacteria, YbeY, required for ribosome maturation. I constructed a strain carrying a deletion of *ybeY*, which I refer to as the $\Delta ybeY$ mutant. The $\Delta ybeY$ mutant is very pleiotropic with increased sensitivity to a wide-range of environmental stresses (Chapter 5). While investigating the physiology of the $\Delta ybeY$ mutant, I made the striking observation that the mutant was very resistant to the DNA replication inhibitor hydroxyurea (HU) (Fig. 1A). HU specifically inhibits class I ribonucleotide reductase (RNR) (57), depleting cellular dNTP pools and causing replication fork arrest, presumably through substrate level starvation (68). The $\Delta ybeY$ mutant was also resistant to a derivative of HU, guanozle (Fig. 1B), which also inhibits RNR (57). These results suggest that disruption of *ybeY* confers resistance against DNA-damage independent fork arrest from substrate starvation by RNR inhibition. The resistance to HU was fully complemented by ectopic expression of *ybeY* from a plasmid (Fig. 1C).

The $\Delta ybeY$ mutant induces the SOS-regulon in response to HU but fails to downregulate cell division genes and upregulate replication restart genes. We began to investigate the striking resistance of the $\Delta ybeY$ mutant to HU using a system-level analysis of its genome-wide transcriptional response to HU as we had previously in Chapter 6. In Chapter 6, I presented a model for affects of HU that eventually led to cell death and lysis in MC4100. I used this model as a comparison to determine similarities and differences in the $\Delta ybeY$ mutant's transcriptional response to HU that could account for its resistance to HU (Table 2).

Like the parental strain MC4100, the $\Delta ybeY$ mutant activates the genes involved in the SOS response when challenged with HU (Table 2). Many genes in the SOS-regulon were strongly upregulated in the $\Delta ybeY$ mutant following HU treatment and to approximately the same levels observed in MC4100 after HU treatment. Recent work has shown that small subpopulations of cells can account for large transcriptional changes in microarray analyses of the SOS response (199). To determine the population of SOS induced cells after HU treatment, we used a construct pL(*lexO*)-GFP in which GFP expression is controlled by LexA (200) as a single cell marker of SOS induction. We observed low GFP fluorescence in the untreated control cells (Fig. 2A). However, after a 1 hour exposure to HU, GFP fluorescence was clearly visible in the vast majority of cells (Fig. 2A) indicating that SOS induction occurred in the bulk of the $\Delta ybeY$ mutant population.

After 1 h exposure to HU, MC4100 downregulates genes required for cell division (Table 2). In Chapter 5, I suggested that this could account for the filamentation of MC4100 induced by HU and may contribute to the eventual lysis of the cell. I was

intrigued to find that expression of cell division genes were unaffected in the $\Delta ybeY$ mutant after 1 h of HU treatment (Table 2). This observation agrees with the decreased filamentation observed in a $\Delta ybeY$ mutant cell after 1 h of HU treatment, compared to MC4100 (Fig. 4A vs. 4B).

In my model for the *E. coli* HU response, I showed that genes involved in primosome assembly are upregulated, most likely as part of a survival response (Chapter 6, and Table 2). Interestingly, I found that $\Delta ybeY$ mutant did not show a significant transcriptional increase of primosome components in response to HU (Table 2). If primosome genes are upregulated in response to replication arrest caused by HU, then the absence of their upregulation would imply that the replication forks in the $\Delta ybeY$ mutant do not require as much repair. This observation would agree with the increased resistance of the $\Delta ybeY$ mutant to HU if the signal to activate cell death in MC4100 is replication fork blockage and/or possibly collapse.

The $\Delta ybeY$ mutant requires increased levels of HU to activate cell death programs promoted by MazF and increased iron uptake. In Chapter 6, I showed that, after prolonged exposure, HU induces a molecular switch activating cell death pathways in *E. coli*. At least three mechanisms are involved in cell death and lysis following HU treatment: activation of toxins, increased iron uptake and downregulation of the *rpoE* operon. Analysis of the transcriptional response of the $\Delta ybeY$ mutant following HU treatment showed a stark divergence in these systems compared with the response from the parental strain (Table 2).

Much of the cell death induced by HU is mediated by MazF toxin. The action of MazF is negated by the antitoxin MazE. In the $\Delta ybeY$ mutant, I found that *mazE* transcript levels were much higher than in MC4100 after 1 h of HU treatment (Table 2). Genetic analysis showed that deleting *mazEF* still did enhance survival of the $\Delta ybeY$ mutant, however this effect was not observed until much higher levels of HU were used (Fig. 3A). This suggests that MazF can still be activated in the $\Delta ybeY$ mutant but the signal activating it requires a much higher dose of HU. We also tested the affect of deleting toxin/antitoxin *relBE* and found that, as in MC4100, it did not affect survival of the $\Delta ybeY$ mutant (Fig. 3B).

In Chapter 6, I made an interesting discovery that HU treatment increased iron uptake, which was detrimental to cell survival. I showed data suggesting that the increased iron uptake was due to strong upregulation of Fur-dependent transporters Fhu, Fep and Fec. Our transcriptional analysis of the $\Delta ybeY$ mutant following HU treatment showed these transport systems were upregulated, but to a lesser extent than in MC4100 (Table 2). In MC4100, upregulation of iron transport systems is heterogeneous in the population (Chapter 6). To determine if the $\Delta ybeY$ mutant population had a similar heterogeneous distribution, I observed GFP fluorescence from a $\Delta ybeY$ mutant population carrying Fur-regulated GFP construct (pL(*furO*)-GFP) as a marker of Fur-dependent iron transporter activation.

Under non HU-treated conditions I observed only background fluorescence in from MC4100 and $\Delta ybeY$ mutant population carrying pL*furO*-GFP (Fig. 4A, B; -HU). After HU treatment I observed heterogeneous GFP fluorescence in the MC4100 population (Fig. 4A; +HU). In contrast, the pattern of GFP expression in the $\Delta ybeY$

mutant population did not significantly change following HU treatment (Fig. 4B; +HU). There was a general increase in overall fluorescence, but far less than observed with MC4100. This result is consistent with the transcriptional data showing a significantly smaller induction of iron transport genes in the $\Delta ybeY$ mutant following HU treatment (Table 2) and the increased resistance to HU of the $\Delta ybeY$ mutant (Fig. 1A).

I tested if iron uptake still affected the $\Delta ybeY$ mutant survival following HU-treatment by deleting *tonB*. I found that deletion of *tonB* in the $\Delta ybeY$ mutant did promote survival in the $\Delta ybeY$ mutant following HU treatment but, like *mazF*, the effects were not observed until higher levels of HU were used (Fig. 4C). This suggests that increased iron uptake following HU-treatment is detrimental to the $\Delta ybeY$ mutant, however, compared to MC4100, higher levels of HU are required to induce iron uptake in the $\Delta ybeY$ mutant. Taken together, these results suggest that the $\Delta ybeY$ mutant can activate cell death pathways involving toxins and iron uptake following HU treatment, however the signal to activate these pathways requires a higher dose of HU.

The $\Delta ybeY$ mutant shows decreased replication initiation. Given that HU inhibits RNR which in turn depletes dNTP pools and leads to replication blockage through substrate level starvation (68, 210), it is possible that the signal to activate cell death programs in response to HU is initiated by blocked or damaged replication forks. This would suggest that a cell with more blocked replication forks may induce a stronger signal. The $\Delta ybeY$ mutant grows slower than MC4100 in rich media at 37°C (40 ± 2 min vs. 28 ± 3 min, Chapter 5). As replication initiation is coupled to cell mass (227), the slower growing $\Delta ybeY$ mutant could be expected to have fewer initiated replication forks

during logarithmic growth compared to MC4100. This could in turn account for the increased resistance to HU.

I used FACS analysis to determine the DNA content of MC4100 and $\Delta ybeY$ mutant cells during logarithmic growth (Fig. 5). I used the *dnaA46* TS allele to determine the 1N DNA content position using run-out assays (Fig. 5A) (67). At the non-permissive temperature, the *dnaA46* strain should arrest with one chromosome (67). During logarithmic growth, MC4100 shows a DNA content distribution around the 2N position (Fig. 5B). Run-out experiments, which allow origin replication to complete but inhibits new rounds of initiation, showed that MC4100 cells contain either 2N or 4N genome contents (Fig. 5C). In contrast, during logarithmic growth, the $\Delta ybeY$ mutant shows a DNA content distribution around 1N (Fig. 5D) and run-out experiments show that $\Delta ybeY$ mutant cells contain either 1N or 2N content of DNA (Fig. 5E). This suggests that fewer initiation events are occurring in the $\Delta ybeY$ mutant during logarithmic growth.

To more clearly define the number of replisomes in MC4100 compared to the $\Delta ybeY$ mutant I used microscopy to visualize the localization patterns of SeqA fused to GFP in the cell. SeqA binds hemi-methylated DNA following replication, in part, to prevent aberrant reinitiation events (227, 228). During logarithmic growth, SeqA-GFP foci were clearly evident in both MC4100 and $\Delta ybeY$ mutant cell, however there were more foci, on average, observed in MC4100 cells (Fig. 6A, B; -HU). When treated with HU for 1 h, MC4100 cells showed increased numbers of SeqA-GFP foci per cell on average, as well as more diffuse foci (Fig. 6A; +HU). As HU can lead to fork collapse, reinitiation may occur at *oriC* before full replication of the chromosome can occur. This could lead to an increase number of blocked forks in MC4100 following HU treatment

that could activate a cell death signal. In contrast, HU treatment did not greatly affect the SeqA-GFP localization pattern of the $\Delta ybeY$ mutant (Fig. 7B; +HU). This result agrees with the decreased DNA content of the $\Delta ybeY$ mutant (Fig. 5E) and suggests that the mutant contains fewer replisomes than MC4100.

Translation defects and decreased growth rate alone do not account for increased HU resistance. My results from Fig. 5 and Fig. 6 support a model where the increased resistance of the $\Delta ybeY$ mutant is due to its decreased growth rate. The decreased growth rate could be attributed to the translation defects of the $\Delta ybeY$ mutant (Chapter 5). If the increased HU resistance of the $\Delta ybeY$ mutant is solely a consequence of defective protein translation and subsequent slowed growth rate, then all slow growing strains should show increased HU resistance. I should also be able to induce resistance in MC4100 by disrupting protein translation and slowing its growth rate.

To test this theory, I began by examining if inhibition of protein translation would increase resistance to HU in MC4100. I assayed the survival of MC4100 on 7.5 mM and 15 mM HU in the presence of subinhibitory concentrations of chloramphenicol (Cm). Cm functions by inhibiting peptidyl transferase and preventing peptide bond formation (229). I found that subinhibitory concentrations of Cm did dramatically increase survival of MC4100 at 7.5 mM HU, however it had little affect on survival at 15 mM HU (Fig. 7A). This suggests the resistance of the $\Delta ybeY$ mutant at low levels of HU can be attributed to defective translation, however this does not account for the increased resistance I observe in the $\Delta ybeY$ mutant at higher HU doses.

I followed this result by testing the sensitivity of a Δrnc strain I constructed in MC4100. *rnc* codes for the RNase III enzyme that initially separates 16S, 23S and 5S into their respective precursors (174). Loss of RNase III activity greatly slows the maturation of 16S rRNA, prevents proper maturation of 23S rRNA and decreases the translation rate (38). I found that the Δrnc and $\Delta ybeY$ mutants both grew at the same rate in rich media (dT: $\Delta rnc = 41 \pm 1$ min, $\Delta ybeY = 40 \pm 2$ min). Therefore, the Δrnc strain phenocopies the $\Delta ybeY$ mutant in that it has a decreased growth and rRNA maturation defects compared to MC4100. Interestingly, I found that disruption of *rnc* conferred only a very minor increase in resistance to HU (Fig. 7B) and this was not substantial relative to the effect of deleting *ybeY* (Fig. 1A). Taken together, these results suggest that a defect in translation or a decrease in growth rate cannot fully account for the increased HU resistance of the $\Delta ybeY$ mutant.

YbeY is downregulated in response to HU and associates with RNR. Given the striking resistance of the $\Delta ybeY$ mutant to HU, I questioned if HU treatment affected the expression of YbeY. I blotted protein extracts from MC4100, carrying an epitope tagged *ybeY* gene, treated with or without HU treatment and found that YbeY expression substantially decreased following HU treatment (Fig. 8A).

The $\Delta ybeY$ mutant can activate cell death pathways following HU treatment but requires much higher doses of HU to trigger the activation than MC4100 (Fig. 3 and 4). It also appears that slower growth rates and decreased DNA initiation cannot fully account for increased resistance to HU (Fig. 7). I speculated that, in addition to its role in ribosome maturation, YbeY may also play a role in DNA replication. Although UV and

HU induce DNA damage, UV does not induce the cell death programs and lysis we observe after HU treatment (72, 73). RNR is the target of HU inhibition and loss of RNR activity leads to the subsequent blockage of replication forks. I questioned if the state of RNR could be acting as the signal to activate cell death and if YbeY somehow influences this. I performed co-immunoprecipitation experiments to determine if RNR interacted with YbeY. I immunoprecipitated YbeY and found the α -subunit of RNR, NrdA, bound YbeY (Fig. 8B). I also observed a much weaker interaction with the β -subunit, NrdB (Fig. 8B). These results suggest that the expression of YbeY is responsive to HU and that it may act directly in monitoring the state of RNR.

Discussion

Recently a body of work has emerged suggesting an intricate coupling of protein translation and DNA replication (67, 77, 78). The highly conserved GTPase, ObgE/CtgA, exemplifies this association. ObgE/CtgA has been shown to bind the ribosome (79, 80) and is required for ribosome assembly (78, 81). ObgE/CtgA has also been shown to regulate chromosome partitioning (67, 82, 83). These results prompted me to explore the possibility that, like ObgE/CtgA, YbeY may act in both translation and replication and how this role may lead to the increased resistance to HU observed in the $\Delta ybeY$ mutant.

My systems-level and single cell analysis of the $\Delta ybeY$ mutant's response to HU showed clear induction of SOS response. This result suggests that HU is causing

sufficient DNA damage in the $\Delta ybeY$ mutant to induce the SOS-regulon. However, I do not observe induction of genes involved in replication restart or downregulation of genes for cell division as I had for MC4100 (Table 2). This suggests that, while HU causes DNA-damage in the $\Delta ybeY$ mutant significant enough to induce the SOS-response, it is either interpreted differently by the cell or not sufficient to induce the additional cell survival response of replication restart activation and downregulation of cell division.

The $\Delta ybeY$ mutant appears able to activate cell death programs but requires higher doses of HU to do so (Fig. 3 and 4). I had suggested perhaps this was due to the slower growth rate of the $\Delta ybeY$ mutant. A slower growth rate would imply fewer replication initiation events, which is supported by FACS analysis and SeqA-GFP localization (Fig. 5 and 6). As HU inhibits RNR preventing dNTP synthesis, having fewer replication forks would decrease the rate at which dNTP pools are depleted. The depletion of dNTPs causes replication fork arrest, and potentially collapse (67, 68). Accumulation of collapsed replication forks could be the signal to activate cell death pathways. MC4100 has more replication forks following HU treatment (Fig. 6), and therefore more potential to accumulate collapsed replication forks. This could then lead to more rapid activation of cell death pathways compared to the $\Delta ybeY$ mutant (Fig. 3 and 4). Thus, this model suggests how the decreased growth rate of the $\Delta ybeY$ mutant can account for its increased resistance to HU.

However, I found that slowing protein translation does not affect HU resistance at high levels (Fig. 7A). More importantly, the Δrnc mutant, which grows at the same rate as the $\Delta ybeY$ mutant, does not show a substantial increase in resistance to HU (Fig. 7B). These observations, suggest that the decreased growth rate of the $\Delta ybeY$ mutant cannot

fully account for its dramatically increased resistance to HU. In addition, I found that YbeY expression decreased upon HU treatment and that YbeY physically interacted with RNR subunits (Fig. 8) suggesting a more direct role for YbeY in the cellular response to HU. It will be interesting to determine if YbeY modulates the activity of RNR.

A recent proteome-wide protein interaction map for *Campylobacter jejuni* identified NrdB interacting with several ribosomal proteins (230). This study was unable to determine if NrdB interacts with the ribosomal proteins in isolation or as part of the ribosome. Growth rate and DNA replication are intimately coupled (227). It is possible that the specific ribosome defects of the $\Delta ybeY$ mutant may also contribute to the increased resistance of the mutant by interfering with a signaling event transduced through RNR.

Table 1. Bacterial strains and plasmids used in this study

Strain/plasmid	Relevant genotype and property	Source
<u>Strain</u>		
MC4100	<i>F⁻ araD139 ΔlacU169 ΔrelA1 rpsL150 thi mot flb5301 deoC7 ptsF25 rbsR</i>	Laboratory stock
<i>ΔybeY</i>	<i>ybeY</i> deletion in MC4100	Chapter 4
BWD10	MC4100 carrying pBR322	Chapter 4
BWD11	<i>ΔybeY</i> carrying pBR322	Chapter 4
BWD12	<i>ΔybeY</i> carrying pBWD1	Chapter 4
BWD19	<i>ΔybeY</i> carrying pBWD5	This study
BWD01	MC4100 <i>ΔmazEF::Km^R</i>	Chapter 5
BWD02	MC4100 <i>ΔrelBE</i>	Chapter 5
BWD04	MC4100 <i>ΔtonB::Km^R</i>	Chapter 5
BWD20	<i>ΔybeYΔmazEF::Km^R</i>	This study
BWD21	<i>ΔybeYΔrelBE</i>	This study
BWD22	<i>ΔybeYΔtonB::Km^R</i>	This study
BWD23	MC4100 <i>Δrnc</i>	This study
<u>Plasmids</u>		
pBR322	<i>Ap^R, Tc^R</i>	(191)
pBWD1	pBR322 expressing <i>ybeY</i>	Chapter 4
pBWD5	pBR322 expressing <i>ybeY-FLAG</i>	This study

pL(<i>lexO</i>)GFP	GFP under LexA control	(200)
pL(<i>furO</i>)GFP	GFP under Fur control	(200)

Table 2. Functional grouping for differentially regulated genes identified by microarray analysis.

Gene	Gene Product/Function	Z Score	
		(Δ <i>ybeY</i> +HU vs. Δ <i>ybeY</i> -HU)	(WT +HU vs. WT -HU)
SOS Network			
<i>sulA</i>	inhibits FtsZ ring formation	+1.38	+1.48
<i>dinB</i>	DNA polymerase IV	+1.36	+1.54
<i>recA</i>	recombinational repair	+1.31	+0.97
<i>recN</i>	recombinational repair	+1.12	+0.71
<i>umuC</i>	DNA polymerase V	+1.16	+1.57
<i>umuD</i>	DNA polymerase V	+1.00	+1.49
Cell Division			
<i>ftsZ</i>	initiates septum ring formation	-0.48	-1.29
<i>zipA</i>	septal ring structural protein	-0.85	-1.53
<i>ftsQ</i>	growth of cell wall at septum	+0.03	-0.93
<i>rcsB</i>	<i>ftsZ</i> regulator	-0.85	-0.71

DNA Replication Restart

<i>priA</i>	primosome factor Y	-0.17	+1.20
<i>priB</i>	primosome protein	+0.31	+1.03
<i>dnaB</i>	helicase	+0.03	+0.41
<i>dnaC</i>	sliding clamp subunit	+0.08	+0.95
<i>dnaN</i>	sliding clamp subunit	+0.77	+1.52

Toxin-Antitoxin Pairs

<i>mazE</i>	suppressor of MazF activity	+0.79	-0.38
<i>mazF</i>	toxic protein, growth inhibitor	-0.17	+0.10
<i>relB</i>	suppressor of RelE activity	-0.52	-0.21
<i>relE</i>	toxic protein, growth inhibitor	-0.49	-0.04

Iron Uptake

<i>fecA</i>	citrate-dependent ferric iron transport	+1.95	+2.20
<i>fecB</i>	periplasmic protein, ferric iron transport	+1.65	+1.80
<i>fecC</i>	ferric iron transport	+1.56	+1.77
<i>fecD</i>	membrane protein, ferric iron transport	+1.80	+1.33
<i>fecE</i>	ferric iron transport	+1.47	+1.58
<i>fecI</i>	ferric iron transport	+1.66	+2.16
<i>fecR</i>	regulator of ferric iron transport	+1.43	+1.12
<i>feoA</i>	ferrous iron uptake system	-0.15	+0.60

<i>feoB</i>	ferrous iron uptake system	+0.36	+0.76
<i>fepA</i>	ferribactin transport	+1.45	+1.84
<i>fepB</i>	ferrienterbactin transport	+0.72	+1.19
<i>fepC</i>	ferrienterobactin transport	+0.90	+1.50
<i>fepD</i>	ferrienterobactin permease	+1.39	+1.23
<i>fepE</i>	ferric enterobactin uptake	+0.16	+0.40
<i>fepG</i>	ferrienterobactin permease	+1.50	+1.40
<i>fhuA</i>	ferrichrome OMP	+0.73	+1.59
<i>fhuB</i>	hydroxamate-dependent ferric uptake	+0.80	+2.07
<i>fhuC</i>	hydroxamate-dependent ferric uptake	+1.06	+1.59
<i>fhuD</i>	hydroxamate-dependent ferric uptake	+0.30	+1.34
<i>fhuE</i>	ferric-rhodotorulic acid receptor	+0.70	+0.86
<i>fhuF</i>	ferric hydroxamate transport	+1.51	+2.38
<i>tonB</i>	iron uptake	+0.75	+1.88
<i>exbB</i>	iron uptake	+1.72	+2.49
<i>exbD</i>	iron uptake	+1.63	+2.11

RpoE Related

<i>rpoE</i>	alternative sigma factor, stress response	-0.88	-2.29
<i>rseA</i>	negative regulator of RpoE	-0.83	-1.95
<i>rseB</i>	binds RseA, negative regulator of RpoE	-0.50	-2.75
<i>rseC</i>	positively regulates RpoE	-0.08	-1.82

Fig. 1. Sensitivity of the $\Delta ybeY$ mutant to (A) HU and (B) guanazole. Cultures were serially diluted and plated on increasing concentrations of the indicated stress. Cfu were determined after 24 h of growth. MC4100 (□), $\Delta ybeY$ (□). (C) Ectopic express of *ybeY* in the $\Delta ybeY$ mutant complements the HU phenotype. Same assay as used in A and B. MC4100+EV (□), $\Delta ybeY$ +EV (□), $\Delta ybeY$ +*pybeY* (□). EV is empty vector control and “p” indicates that the gene indicated is expressed from a plasmid.

Fig. 2. (A) MC4100 pL(*lexO*)-GFP and (B) $\Delta ybeY$ mutant pL(*lexO*)-GFP treated with or without HU.

Fig. 3. (A) MC4100 (□), $\Delta ybeY$ (□), MC4100 $\Delta mazEF::Km^R$ (□) and $\Delta ybeY\Delta mazEF::Km^R$ (□). (B) MC4100 (□), $\Delta ybeY$ (□), MC4100 $\Delta relBE$ (□) and $\Delta ybeY\Delta relBE$ (□). In each experiment the strains were spotted on LB agar plates containing increasing concentrations of HU.

Fig. 4. (A) MC4100 pL(*furO*)-GFP and (B) $\Delta ybeY$ pL(*furO*)-GFP, treated with or without 100 mM HU. (C) MC4100 (□) and MC4100 $\Delta tonB::Km^R$ (□) were serially diluted and spotted on LB agar plates containing increasing concentrations of HU.

Fig. 5. FACS analysis of the DNA content MC4100 and the $\Delta ybeY$ mutant. (A) Run-out experiment using *dnaA46* strain to mark 1N DNA content. (B) DNA content of logarithmically growing MC4100. (C) Run-out experiment of logarithmically growing

MC4100. (D) DNA content of logarithmically growing $\Delta ybeY$ mutant. (E) Run-out experiment of logarithmically growing $\Delta ybeY$ mutant.

Fig. 6. SeqA-GFP localization in (A) MC4100 and (B) $\Delta ybeY$ mutant with and without treatment with 100 mM HU.

Fig. 7. (A) Affect of sub-inhibitory concentrations on survival of MC4100 on LB plates containing 7.5 mM or 15 mM HU. (B) Sensitivity of MC4100 (□), the $\Delta ybeY$ mutant (○) and MC4100 Δrnc (△) to increasing concentrations of HU.

Fig. 8. (A) Immunoblot for YbeY using whole cell lysates from MC4100 treated with out without 100 mM HU. (B) Western blots for NrdA and NrdB from YbeY-FLAG immunoprecipitated complex. The control strain carried a non-FLAG tagged *ybeY* gene and was assayed side-by-side the *ybeY*-FLAG tagged strain.

Fig. 1

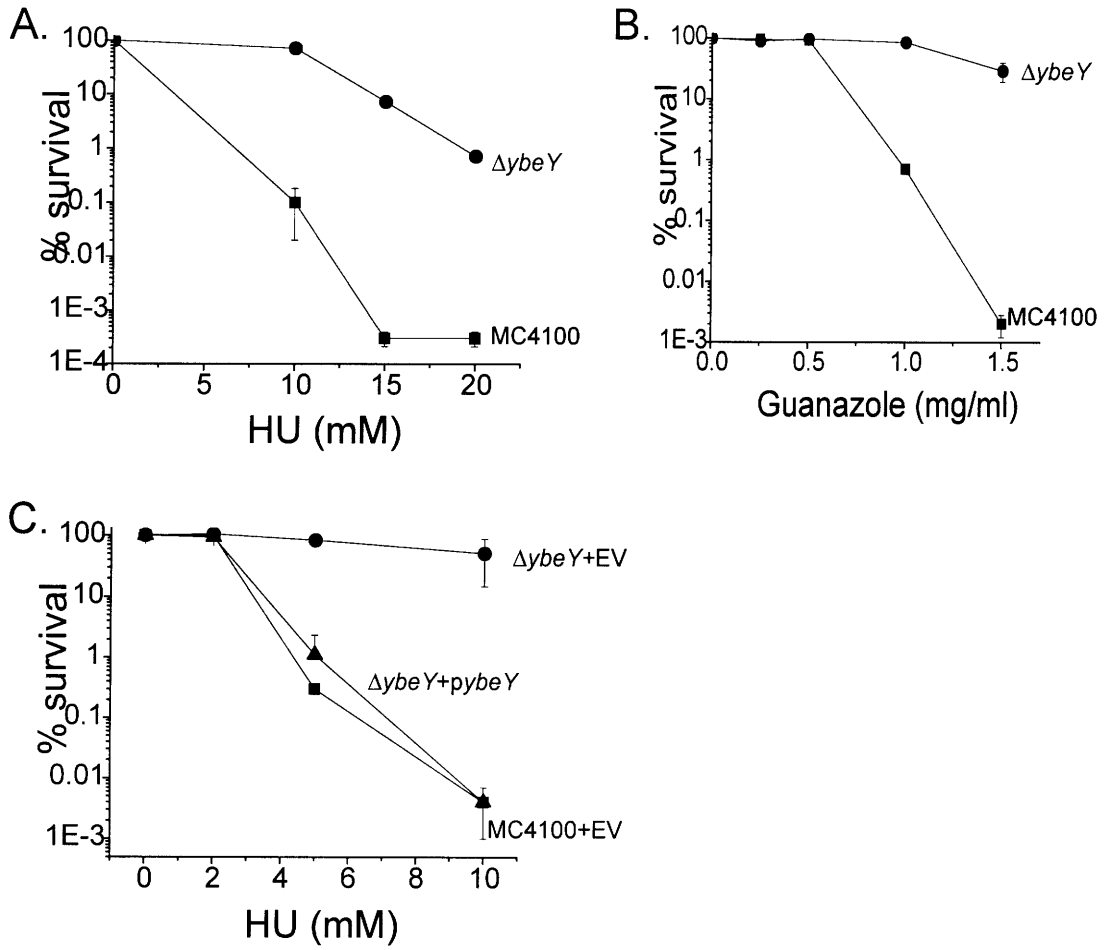


Fig. 2

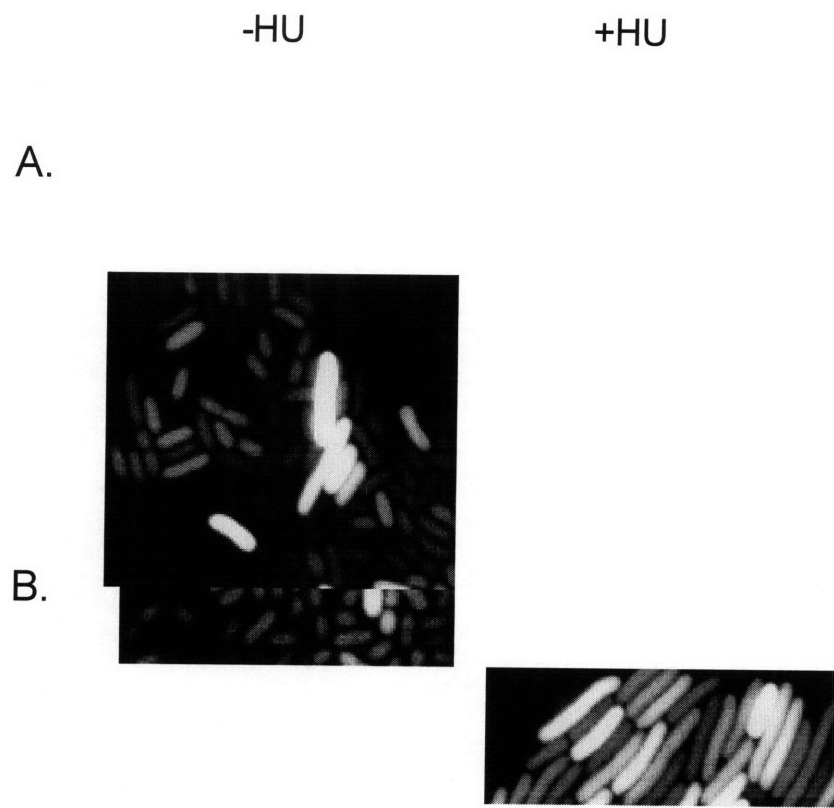


Fig. 3

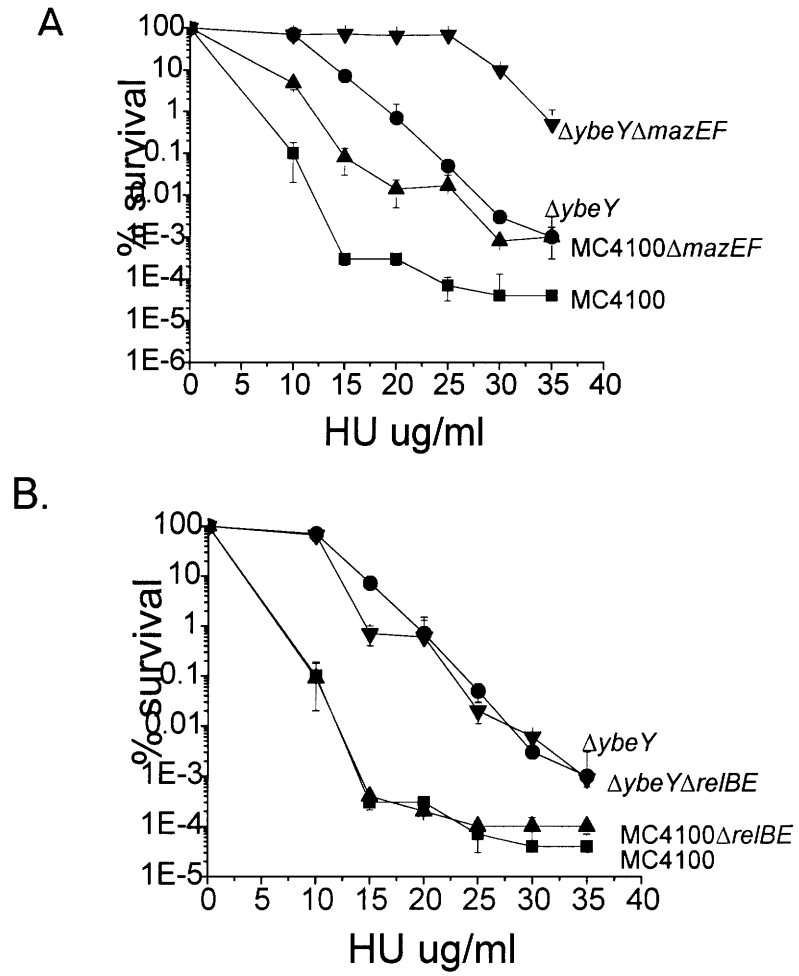


Fig. 4

-HU

+HU

A.

B.

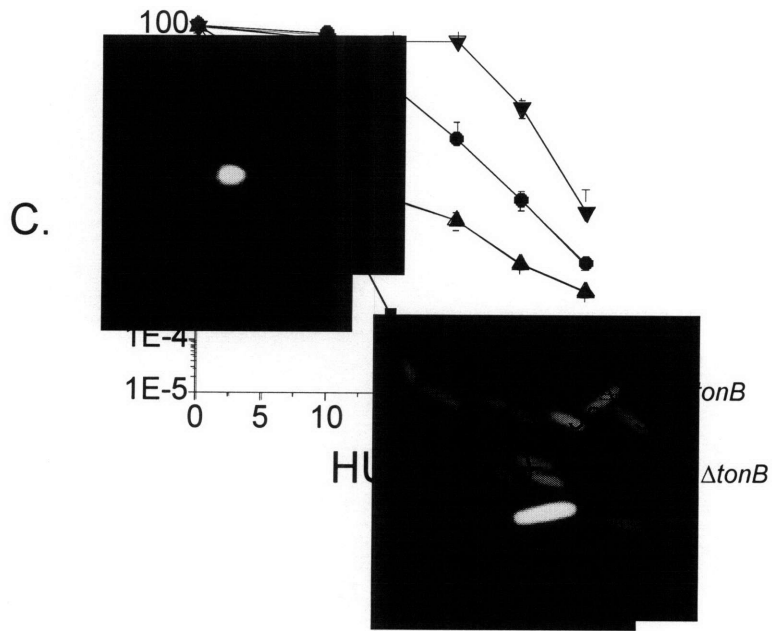


Fig. 5

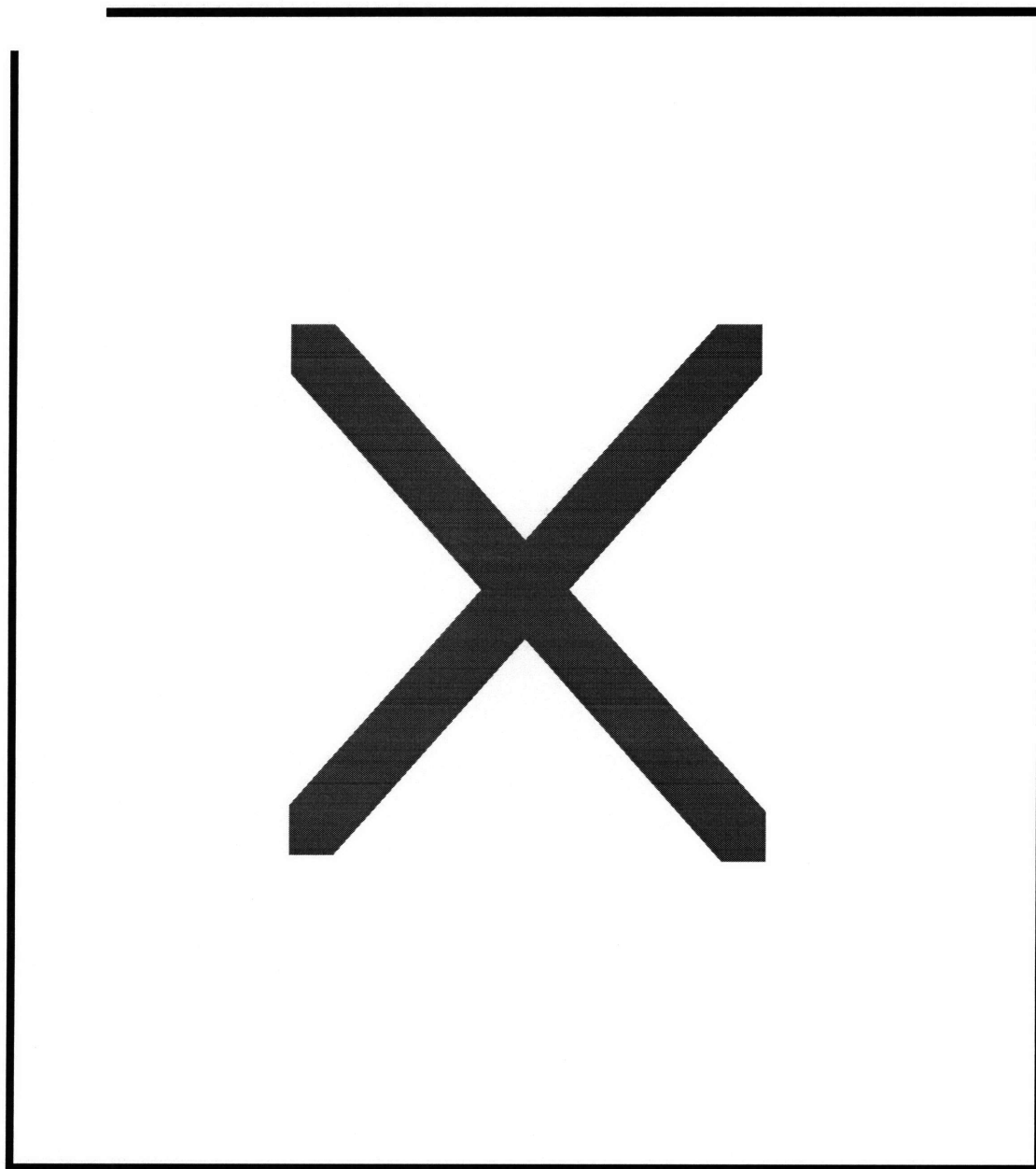


Fig. 6

-HU

+HU

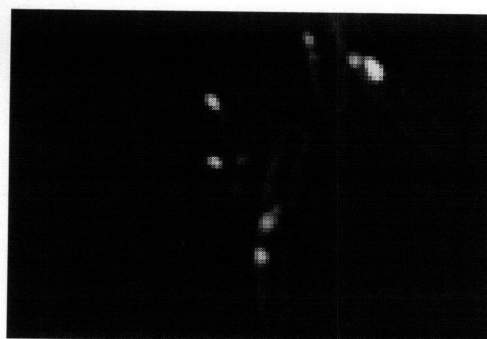
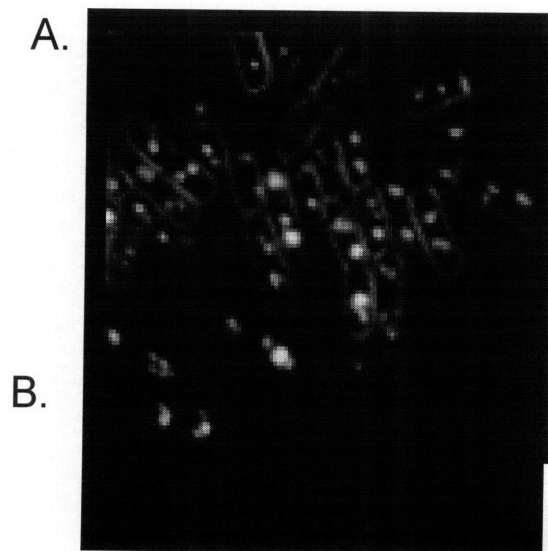


Fig. 7

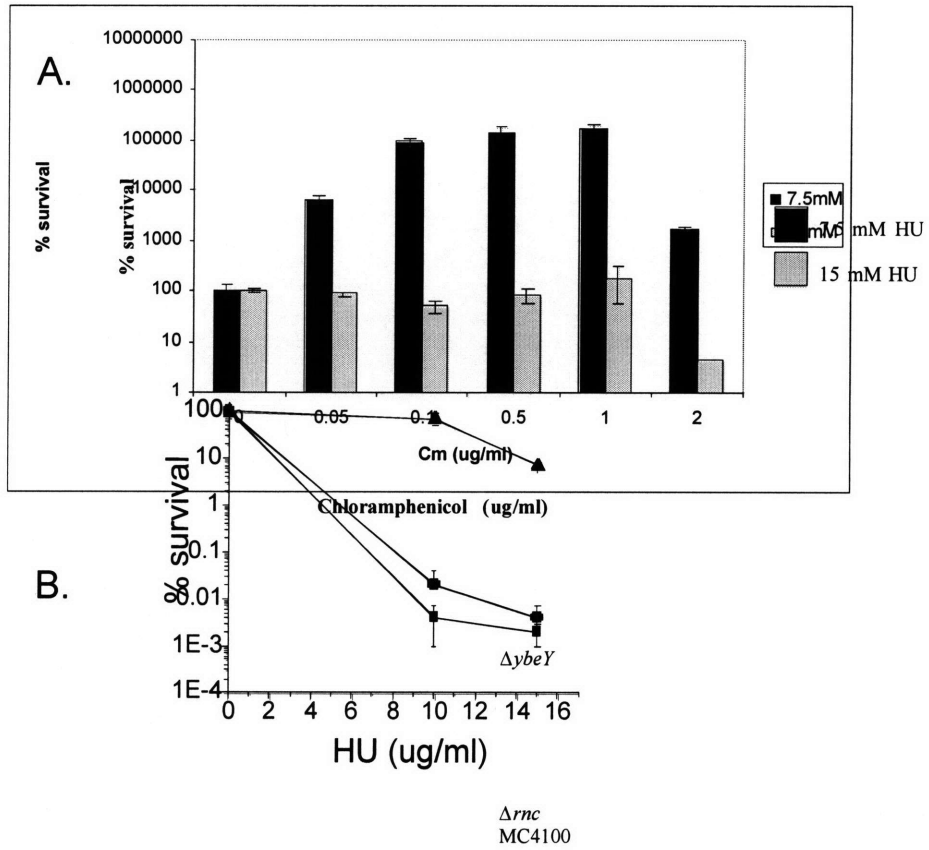
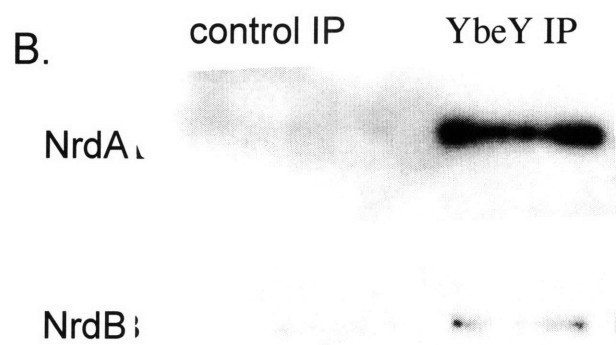
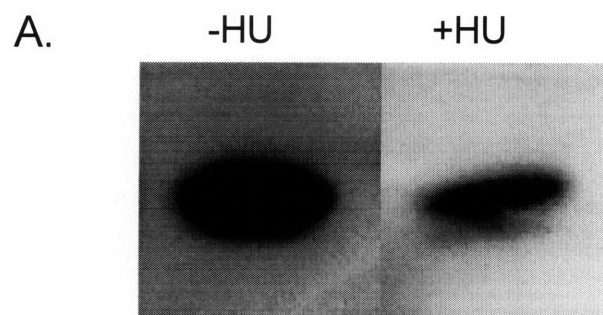


Fig. 8



Chapter 8

Perspectives and Future Direction

My thesis work has covered several areas of research. I will focus on YbeY and its family members in this Chapter.

Antibiotic resistant bacteria are becoming an increasing public health problem. A recent study has shown that drug-resistant *Staphylococcus aureus* deaths are now exceeding death due to AIDS in the U.S. (231). Nearly 70% of bacteria that cause infections in hospitals are resistant to at least one of the antibiotics most commonly used to treat infections (232). While several “new” antibiotics have emerged over the past two decades, the vast majority of these are derivatives of previously known antibiotics that bacteria rapidly gain resistance to (233, 234). A great challenge confronting the medical community is to identify new bacterial targets for antimicrobial action (233, 234).

Ideally, an antibiotic should target an essential bacterial function. Targeting of a non-essential function may slow bacterial growth in hopes that the immune system can then clear the infection, however this also allows a bacterium more time to develop resistance. Recently, several novel GTPases have been identified that are essential in bacteria, including Era and ObgE (29), and have been advocated as potential drug targets (235). However, it has been difficult to suggest how to specifically inhibit these bacterial GTPases without also harming the host.

YbeY homologs are found in all sequenced prokaryotes. A screen for essential genes in *B. subtilis* identified the YbeY homolog YqfG, suggesting it is essential in this organism and possibly in all gram-positive bacteria (236). I attempted to specifically delete *yqfG* in *B. subtilis* but was unsuccessful supporting its possible essential role in this bacterium (unpublished data). I have shown that while YbeY has a human homolog,

they are not completely equivalent, suggesting there is possible divergence in the active or substrate binding sites. Indeed primary sequence analysis shown in Chapter 5 shows several areas of divergence between human and bacterial homologs. Structural similarity searches show that the putative active site of YbeY resembles that of matrix metalloproteases (154). Many different protease inhibitors have been developed over the years, demonstrating the tractability of a protease-like active site as a potential drug target. I suggest that the YbeY protein family would make an excellent drug target and am in the processes of developing a screen to identify small molecule inhibitors of YbeY.

I was struck to find that the human homolog C21orf57 was able to partially complement the $\Delta ybeY$ mutant. The discovery of a mitochondrial signaling sequence on C21orf57 clarified how a bacterial protein involved in ribosome maturation could have such a strong human homolog. Mitochondria synthesize their own ribosomes and are thought to have evolved from α -proteobacteria (237). C21orf57 is located near the telomere on the long arm of chromosome 21 (238). This region is classified as the critical region in Down Syndrome as it is thought that genes located in this distal portion of 21q are responsible for the physical manifestations of the genetic abnormality (239). The function of very few genes on chromosome 21 have been identified and, while no single gene is thought to be responsible for the pathology of Down syndrome, knowledge of the gene products on chromosome 21 will greatly help elucidate the mechanisms (240). I hypothesize that, like YbeY in *E. coli*, C21orf57 plays a role in ribosome maturation in human mitochondria. In Chapter 5, I speculated that YbeY may be

involved in 3' maturation of 16S rRNA. Interestingly, the enzyme responsible for 3' processing of mitochondrial rRNA is also unknown (241).

There is general agreement in the field that a disturbance in the balance of reactive oxygen species (ROS) may be a key point in the pathogenesis of Down Syndrome (242). The mitochondrial respiration chain is the most important intracellular source of ROS (242). The mitochondria have a central role in apoptosis, and numerous studies have demonstrated that the accumulation of mitochondrial DNA mutations is a major contributor to neurodegenerative diseases and aging (242). Interestingly, most Down syndrome patients develop Alzheimer's disease neuropathology (243). This development of Alzheimer's disease in Down syndrome patients may be related to the overexpression of the amyloid _ precursor protein due to increased gene dosage (244). Recent studies have shown that mitochondrial dysfunction may play a significant role in development of Alzheimer's disease in Down syndrome patients by promoting aberrant amyloid _ precursor protein processing (242).

I have begun experiments in human 293T cells to look at the effect of knocking down *C21orf57* expression. I have achieved a 4 fold knockdown of *C21orf57* mRNA using siRNA technology and will shortly be assaying the affect on mitochondrial activity and rRNA processing. If an effect is observed it will be very interesting to overexpress *C21orf57* in human 293T cells and determine if detrimental cellular affects ensue.

References

1. Brewin, N. J. (1991) *Annu Rev Cell Biol* **7**, 191-226.
2. Fisher, R. F. & Long, S. R. (1992) *Nature* **357**, 655-60.
3. Foucher, F. & Kondorosi, E. (2000) *Plant Mol Biol* **43**, 773-86.
4. Jones, K. M., Kobayashi, H., Davies, B. W., Taga, M. E. & Walker, G. C. (2007) *Nat Rev Microbiol* **5**, 619-33.
5. Gage, D. J. (2004) *Microbiol Mol Biol Rev* **68**, 280-300.
6. Santos, R., Herouart, D., Sigaud, S., Touati, D. & Puppo, A. (2001) *Mol Plant Microbe Interact* **14**, 86-9.
7. Galibert, F., Finan, T. M., Long, S. R., Puhler, A., Abola, P., Ampe, F., Barloy-Hubler, F., Barnett, M. J., Becker, A., Boistard, P., Bothe, G., Boutry, M., Bowser, L., Buhrmester, J., Cadieu, E., Capela, D., Chain, P., Cowie, A., Davis, R. W., Dreano, S., Federspiel, N. A., Fisher, R. F., Gloux, S., Godrie, T., Goffeau, A., Golding, B., Gouzy, J., Gurjal, M., Hernandez-Lucas, I., Hong, A., Huizar, L., Hyman, R. W., Jones, T., Kahn, D., Kahn, M. L., Kalman, S., Keating, D. H., Kiss, E., Komp, C., Lelaure, V., Masuy, D., Palm, C., Peck, M. C., Pohl, T. M., Portetelle, D., Purnelle, B., Ramsperger, U., Surzycki, R., Thebault, P., Vandebol, M., Vorholter, F. J., Weidner, S., Wells, D. H., Wong, K., Yeh, K. C. & Batut, J. (2001) *Science* **293**, 668-72.
8. Jamet, A., Sigaud, S., Van de Sype, G., Puppo, A. & Herouart, D. (2003) *Mol Plant Microbe Interact* **16**, 217-25.

9. Sigaud, S., Becquet, V., Frendo, P., Puppo, A. & Herouart, D. (1999) *J Bacteriol* **181**, 2634-9.
10. Jamet, A., Kiss, E., Batut, J., Puppo, A. & Herouart, D. (2005) *J Bacteriol* **187**, 376-81.
11. Ardisson, S., Frendo, P., Laurenti, E., Jantschko, W., Obinger, C., Puppo, A. & Ferrari, R. P. (2004) *Biochemistry* **43**, 12692-9.
12. Jakubovics, N. S. & Jenkinson, H. F. (2001) *Microbiology* **147**, 1709-18.
13. Archibald, F. S. & Fridovich, I. (1981) *J Bacteriol* **145**, 442-51.
14. Archibald, F. S. & Fridovich, I. (1982) *Arch Biochem Biophys* **214**, 452-63.
15. Horsburgh, M. J., Wharton, S. J., Karavolos, M. & Foster, S. J. (2002) *Trends Microbiol* **10**, 496-501.
16. Stadtman, E. R., Berlett, B. S. & Chock, P. B. (1990) *Proc Natl Acad Sci U S A* **87**, 384-8.
17. Barynin, V. V., Whittaker, M. M., Antonyuk, S. V., Lamzin, V. S., Harrison, P. M., Artymiuk, P. J. & Whittaker, J. W. (2001) *Structure (Camb)* **9**, 725-38.
18. Santos, R., Bocquet, S., Puppo, A. & Touati, D. (1999) *J Bacteriol* **181**, 4509-16.
19. Boyer, E., Bergevin, I., Malo, D., Gros, P. & Cellier, M. F. (2002) *Infect Immun* **70**, 6032-42.
20. Janulczyk, R., Ricci, S. & Bjorck, L. (2003) *Infect Immun* **71**, 2656-64.
21. Riley, M., Abe, T., Arnaud, M. B., Berlyn, M. K., Blattner, F. R., Chaudhuri, R. R., Glasner, J. D., Horiuchi, T., Keseler, I. M., Kosuge, T., Mori, H., Perna, N. T., Plunkett, G., 3rd, Rudd, K. E., Serres, M. H., Thomas, G. H., Thomson, N. R., Wishart, D. & Wanner, B. L. (2006) *Nucleic Acids Res* **34**, 1-9.

22. Roberts, R. J. (2004) *PLoS Biology* **2**, 293-294.
23. Galperin, M. Y. & Koonin, E. V. (2004) *Nucleic Acids Res* **32**, 5452-63.
24. Tatusov, R. L., Natale, D. A., Garkavtsev, I. V., Tatusova, T. A., Shankavaram, U. T., Rao, B. S., Kiryutin, B., Galperin, M. Y., Fedorova, N. D. & Koonin, E. V. (2001) *Nucleic Acids Res* **29**, 22-8.
25. Gil, R., Silva, F. J., Pereto, J. & Moya, A. (2004) *Microbiol Mol Biol Rev* **68**, 518-37.
26. Davies, B. W. & Walker, G. C. (2007) *in review - The Journal of Bacteriology*.
27. Green, R. & Noller, H. F. (1997) *Annu Rev Biochem* **66**, 679-716.
28. Nomura, M., Gourse, R. & Baughman, G. (1984) *Annu Rev Biochem* **53**, 75-117.
29. Wilson, D. N. & Nierhaus, K. H. (2007) *Crit Rev Biochem Mol Biol* **42**, 187-219.
30. Noller, H. F. & Nomura, M. (1987) *Escherichia coli and Salmonella Typhimurium; Cellular and Molecular Biology* (American Society for Microbiology, Washington D. C.).
31. Wilson, D. N. & Nierhaus, K. H. (2005) *Crit Rev Biochem Mol Biol* **40**, 243-67.
32. Nomura, M. & Erdmann, V. A. (1970) *Nature* **228**, 744-8.
33. Traub, P. & Nomura, M. (1968) *Proc Natl Acad Sci U S A* **59**, 777-84.
34. Kaczanowska, M. & Ryden-Aulin, M. (2007) *Microbiol Mol Biol Rev* **71**, 477-94.
35. Klein, F. & Evguenieva-Hackenberg, E. (2002) *Biochem Biophys Res Commun* **299**, 780-6.
36. Li, Z., Pandit, S. & Deutscher, M. P. (1999) *Rna* **5**, 139-46.
37. Li, Z., Pandit, S. & Deutscher, M. P. (1999) *Embo J* **18**, 2878-85.
38. Srivastava, A. K. & Schlessinger, D. (1988) *Proc Natl Acad Sci U S A* **85**, 7144-8.

39. Mangiarotti, G., Turco, E., Ponzetto, A. & Altruda, F. (1974) *Nature* **247**, 147-8.
40. Laursen, B. S., Sorensen, H. P., Mortensen, K. K. & Sperling-Petersen, H. U. (2005) *Microbiol Mol Biol Rev* **69**, 101-23.
41. Carter, A. P., Clemons, W. M., Jr., Brodersen, D. E., Morgan-Warren, R. J., Hartsch, T., Wimberly, B. T. & Ramakrishnan, V. (2001) *Science* **291**, 498-501.
42. Dahlquist, K. D. & Puglisi, J. D. (2000) *J Mol Biol* **299**, 1-15.
43. Allen, G. S., Zavialov, A., Gursky, R., Ehrenberg, M. & Frank, J. (2005) *Cell* **121**, 703-12.
44. Gualerzi, C. O., Severini, M., Spurio, R., La Teana, A. & Pon, C. L. (1991) *J Biol Chem* **266**, 16356-62.
45. La Teana, A., Gualerzi, C. O. & Dahlberg, A. E. (2001) *Rna* **7**, 1173-9.
46. Shine, J. & Dalgarno, L. (1974) *Proc Natl Acad Sci U S A* **71**, 1342-6.
47. La Teana, A., Gualerzi, C. O. & Brimacombe, R. (1995) *Rna* **1**, 772-82.
48. Gualerzi, C., Risuleo, G. & Pon, C. L. (1977) *Biochemistry* **16**, 1684-9.
49. Pon, C. L. & Gualerzi, C. O. (1984) *FEBS Lett* **175**, 203-7.
50. Antoun, A., Pavlov, M. Y., Lovmar, M. & Ehrenberg, M. (2006) *Embo J* **25**, 2539-50.
51. Kurland, C. G., Hughes, D. & Ehrenberg, M. (1996) *In Escherichia coli and Salmonella typhimurim: Cellular and Molecular Biology* (Am. Soc. Microbiol. Press, Washinton, D. C.).
52. Fersht, A. R. & Dingwall, C. (1979) *Biochemistry* **18**, 2627-31.
53. Freist, W., Pardowitz, I. & Cramer, F. (1985) *Biochemistry* **24**, 7014-23.

54. Rodnina, M. V., Daviter, T., Gromadski, K. & Wintermeyer, W. (2002) *Biochimie* **84**, 745-54.
55. Ogle, J. M. & Ramakrishnan, V. (2005) *Annu Rev Biochem* **74**, 129-77.
56. Gregory, S. T., Lieberman, K. R. & Dahlberg, A. E. (1994) *Nucleic Acids Res* **22**, 279-84.
57. Larsen, I. K., Sjoberg, B. M. & Thelander, L. (1982) *Eur J Biochem* **125**, 75-81.
58. Leipuviene, R. & Bjork, G. R. (2007) *J Bacteriol* **189**, 7024-31.
59. O'Connor, M., Gregory, S. T. & Dahlberg, A. E. (2004) *Nucleic Acids Res* **32**, 5750-6.
60. Ortiz, P. A., Ulloque, R., Kihara, G. K., Zheng, H. & Kinzy, T. G. (2006) *J Biol Chem* **281**, 32639-48.
61. Urbonavicius, J., Stahl, G., Durand, J. M., Ben Salem, S. N., Qian, Q., Farabaugh, P. J. & Bjork, G. R. (2003) *Rna* **9**, 760-8.
62. Farabaugh, P. J. (2000) *Prog Nucleic Acid Res Mol Biol* **64**, 131-70.
63. Craigen, W. J. & Caskey, C. T. (1986) *Nature* **322**, 273-5.
64. Lopes, M., Cotta-Ramusino, C., Pelliccioli, A., Liberi, G., Plevani, P., Muzi-Falconi, M., Newlon, C. S. & Foiani, M. (2001) *Nature* **412**, 557-61.
65. Sogo, J. M., Lopes, M. & Foiani, M. (2002) *Science* **297**, 599-602.
66. Timson, J. (1975) *Mutat Res* **32**, 115-32.
67. Foti, J. J., Schienda, J., Sutera, V. A., Jr. & Lovett, S. T. (2005) *Mol Cell* **17**, 549-60.
68. Godoy, V. G., Jarosz, D. F., Walker, F. L., Simmons, L. A. & Walker, G. C. (2006) *Embo J* **25**, 868-79.

69. Tercero, J. A., Longhese, M. P. & Diffley, J. F. (2003) *Mol Cell* **11**, 1323-36.
70. Rupp, W. D. & Howard-Flanders, P. (1968) *J Mol Biol* **31**, 291-304.
71. Sutton, M. D., Smith, B. T., Godoy, V. G. & Walker, G. C. (2000) *Annu Rev Genet* **34**, 479-497.
72. Courcelle, J., Khodursky, A., Peter, B., Brown, P. O. & Hanawalt, P. C. (2001) *Genetics* **158**, 41-64.
73. Quillardet, P., Rouffaud, M. A. & Bouige, P. (2003) *Res Microbiol* **154**, 559-72.
74. Barbe, J., Villaverde, A. & Guerrero, R. (1987) *Mutat Res* **192**, 105-8.
75. Rosenkranz, H. S., Winshell, E. B., Mednis, A., Carr, H. S. & Ellner, C. J. (1967) *J Bacteriol* **94**, 1025-33.
76. Sinha, N. K. & Snustad, D. P. (1972) *J Bacteriol* **112**, 1321-4.
77. Datta, K., Skidmore, J. M., Pu, K. & Maddock, J. R. (2004) *Mol Microbiol* **54**, 1379-92.
78. Jiang, M., Datta, K., Walker, A., Strahler, J., Bagamasbad, P., Andrews, P. C. & Maddock, J. R. (2006) *J Bacteriol* **188**, 6757-70.
79. Lin, B., Thayer, D. A. & Maddock, J. R. (2004) *J Bacteriol* **186**, 481-9.
80. Wout, P., Pu, K., Sullivan, S. M., Reese, V., Zhou, S., Lin, B. & Maddock, J. R. (2004) *J Bacteriol* **186**, 5249-57.
81. Sato, A., Kobayashi, G., Hayashi, H., Yoshida, H., Wada, A., Maeda, M., Hiraga, S., Takeyasu, K. & Wada, C. (2005) *Genes Cells* **10**, 393-408.
82. Foti, J. J., Persky, N. S., Ferullo, D. J. & Lovett, S. T. (2007) *Mol Microbiol* **65**, 569-81.
83. Kobayashi, G., Moriya, S. & Wada, C. (2001) *Mol Microbiol* **41**, 1037-51.

84. Ausubel, F. M., R. Brent, R.E. Kingston, D.D. Moore, J.G. Seidman, J.A. Smith and K. Struhl (1991) *Current Protocols in Molecular Biology* (John Wiley & Sons Inc., New York).
85. Reeve, W. G., Tiwari, R. P., Worsley, P. S., Dilworth, M. J., Glenn, A. R. & Howieson, J. G. (1999) *Microbiology* **145 (Pt 6)**, 1307-16.
86. de Lorenzo, V., Herrero, M., Jakubzik, U. & Timmis, K. N. (1990) *J Bacteriol* **172**, 6568-72.
87. Campbell, G. R., Sharypova, L. A., Scheidle, H., Jones, K. M., Niehaus, K., Becker, A. & Walker, G. C. (2003) *J Bacteriol* **185**, 3853-62.
88. Leigh, J. A., Signer, E. R. & Walker, G. C. (1985) *Proc Natl Acad Sci U S A* **82**, 6231-5.
89. Finan, T. M., Hartweig, E., LeMieux, K., Bergman, K., Walker, G. C. & Signer, E. R. (1984) *J Bacteriol* **159**, 120-4.
90. Turner, G. L. a. A. H. G. (1980) *Measurment of nitrogen fixation by indirect means*, (John Wiley and Sons, Chichester).
91. Herouart, D., Sigaud, S., Moreau, S., Frendo, P., Touati, D. & Puppo, A. (1996) *J Bacteriol* **178**, 6802-9.
92. Berg, D. E., Weiss, A. & Crossland, L. (1980) *J Bacteriol* **142**, 439-46.
93. Reeve, W. G. (2003).
94. Davies, B. W. & Walker, G. C. (2006) *J Bacteriol*.
95. Aman, P., M. McNeil, L.-E., Frazen, A., Darvill, G., and Albersheim, P. (1981) *Carbohydrate Research* **95**, 263-282.

96. Reinhold, B. B., Chan, S. Y., Reuber, T. L., Marra, A., Walker, G. C. & Reinhold, V. N. (1994) *J Bacteriol* **176**, 1997-2002.
97. Battisti, L., Lara, J. C. & Leigh, J. A. (1992) *Proc Natl Acad Sci U S A* **89**, 5625-9.
98. Urzainqui, A. & Walker, G. C. (1992) *J Bacteriol* **174**, 3403-6.
99. Wang, L. X., Wang, Y., Pellock, B. & Walker, G. C. (1999) *J Bacteriol* **181**, 6788-96.
100. Gonzalez, J. E., York, G. M. & Walker, G. C. (1996) *Gene* **179**, 141-6.
101. Reuber, T. L. & Walker, G. C. (1993) *Cell* **74**, 269-80.
102. D'Haese, W., Glushka, J., De Rycke, R., Holsters, M. & Carlson, R. W. (2004) *Mol Microbiol* **52**, 485-500.
103. van Niel, E. W., Hofvendahl, K. & Hahn-Hagerdal, B. (2002) *Appl Environ Microbiol* **68**, 4350-6.
104. Reed, J. W. & Walker, G. C. (1991) *J Bacteriol* **173**, 664-77.
105. White, D. (2000) *The Physiology and Biochemistry of Prokaryotes* (Oxford University Press, New York).
106. Boada, J., Roig, T., Perez, X., Gamez, A., Bartrons, R., Cascante, M. & Bermudez, J. (2000) *FEBS Lett* **480**, 261-4.
107. Hwang, K., Jeong, D. W., Lee, J. W., Kim, I. H., Chang, H. I., Kim, H. J. & Kim, I. Y. (1999) *Mol Cells* **9**, 429-35.
108. Juhnke, H., Krems, B., Kotter, P. & Entian, K. D. (1996) *Mol Gen Genet* **252**, 456-64.

109. Marroqui, S., Zorreguieta, A., Santamaria, C., Temprano, F., Soberon, M., Megias, M. & Downie, J. A. (2001) *J Bacteriol* **183**, 854-64.
110. Liu, Y., Tsinoremas, N. F., Golden, S. S., Kondo, T. & Johnson, C. H. (1996) *Mol Microbiol* **20**, 1071-81.
111. Buendia-Claveria, A. M., Moussaid, A., Ollero, F. J., Vinardell, J. M., Torres, A., Moreno, J., Gil-Serrano, A. M., Rodriguez-Carvajal, M. A., Tejero-Mateo, P., Peart, J. L., Brewin, N. J. & Ruiz-Sainz, J. E. (2003) *Microbiology* **149**, 1807-18.
112. Kerppola, T. K. & Kahn, M. L. (1988) *J Gen Microbiol* **134**, 913-9.
113. Malek, W. & Kowalski, M. (1983) *Acta Microbiol Pol* **32**, 19-24.
114. Davies, B. W. & Walker, G. C. (2006) *J Bacteriol*.
115. Heurgue-Hamard, V., Mora, L., Guarneros, G. & Buckingham, R. H. (1996) *Embo J* **15**, 2826-33.
116. Delgado, M. J., Yeoman, K. H., Wu, G., Vargas, C., Davies, A. E., Poole, R. K., Johnston, A. W. & Downie, J. A. (1995) *J Bacteriol* **177**, 4927-34.
117. Kereszt, A., Slaska-Kiss, K., Putnoky, P., Banfalvi, Z. & Kondorosi, A. (1995) *Mol Gen Genet* **247**, 39-47.
118. Tabche, M. L., Garcia, E. G., Miranda, J., Escamilla, J. E. & Soberon, M. (1998) *Gene* **208**, 215-9.
119. Tiwari, R. P., Reeve, W. G., Dilworth, M. J. & Glenn, A. R. (1996) *Microbiology* **142 (Pt 7)**, 1693-704.
120. Maurer, L. M., Yohannes, E., Bondurant, S. S., Radmacher, M. & Slonczewski, J. L. (2005) *J Bacteriol* **187**, 304-19.
121. Posey, J. E. & Gherardini, F. C. (2000) *Science* **288**, 1651-3.

122. Miller, J. H. (1972) *Experiments in Molecular Cloning* (Cold Spring Harbor Laboratory, Cold Spring Harbor, N.Y.).
123. Sambrook, J. a. D. W., Russel (2001) *Molecular Cloning. A Laboratory Manual* (Cold Spring Harbor Laboratory, Cold Spring Harbour, N.Y.).
124. Beauchamp, C. & Fridovich, I. (1971) *Anal Biochem* **44**, 276-87.
125. Gregory, E. M. & Fridovich, I. (1974) *Anal Biochem* **58**, 57-62.
126. Robichon, C., Vidal-Ingigliardi, D. & Pugsley, A. P. (2005) *J Biol Chem* **280**, 974-83.
127. Cheng, H. P. & Walker, G. C. (1998) *J Bacteriol* **180**, 5183-91.
128. Hirsch, A. M., Long, S. R., Bang, M., Haskins, N. & Ausubel, F. M. (1982) *J Bacteriol* **151**, 411-9.
129. Gibson, K. E., Campbell, G. R., Lloret, J. & Walker, G. C. (2006) *J Bacteriol* **188**, 4508-21.
130. Appleby, C. A. (1974) *Biological Nitrogen Fixation* (North Holland Publishing Co., Amsterdam).
131. Chao, T. C., Becker, A., Buhrmester, J., Puhler, A. & Weidner, S. (2004) *J Bacteriol* **186**, 3609-20.
132. Engelke, T., Jording, D., Kapp, D. & Puhler, A. (1989) *J Bacteriol* **171**, 5551-60.
133. Hirsch, A. M., Bang, M. & Ausubel, F. M. (1983) *J Bacteriol* **155**, 367-80.
134. Lopez, J. C., Grasso, D. H., Frugier, F., Crespi, M. D. & Aguilar, O. M. (2001) *Mol Plant Microbe Interact* **14**, 55-62.
135. Brouwer, D. J. & Osborn, T. C. (1999) *Theoretical and Applied Genetics* **99**, 1194-1200.

136. Imlay, J. A. & Linn, S. (1987) *J Bacteriol* **169**, 2967-76.
137. Seaver, L. C. & Imlay, J. A. (2001) *J Bacteriol* **183**, 7173-81.
138. Gutteridge, B. H. a. J. M. C. (1999) *Free Radicals in Biology and Medicine* (Oxford University Press, Oxford).
139. Kehres, D. G. & Maguire, M. E. (2003) *FEMS Microbiol Rev* **27**, 263-90.
140. Platero, R. A., Jauregui, M., Battistoni, F. J. & Fabiano, E. R. (2003) *FEMS Microbiol Lett* **218**, 65-70.
141. Kehres, D. G., Janakiraman, A., Slauch, J. M. & Maguire, M. E. (2002) *J Bacteriol* **184**, 3159-66.
142. Winkler, W. C. (2005) *Curr Opin Chem Biol* **9**, 594-602.
143. Santos, R., Herouart, D., Puppo, A. & Touati, D. (2000) *Mol Microbiol* **38**, 750-9.
144. Wells, D. H. & Long, S. R. (2002) *Mol Microbiol* **43**, 1115-27.
145. Prell, J. & Poole, P. (2006) *Trends Microbiol* **14**, 161-8.
146. Niehaus, K. & Becker, A. (1998) *Subcell Biochem* **29**, 73-116.
147. Campbell, G. R., Reuhs, B. L. & Walker, G. C. (2002) *Proc Natl Acad Sci U S A* **99**, 3938-43.
148. Davies, B. W. & Walker, G. C. (2007) *J Bacteriol* **189**, 2110-3.
149. Ferguson, G. P., Roop, R. M., 2nd & Walker, G. C. (2002) *J Bacteriol* **184**, 5625-32.
150. Davies, B. W. & Walker, G. C. (2007) *J Bacteriol* **189**, 2101-9.
151. Leigh, J. A., Reed, J. W., Hanks, J. F., Hirsch, A. M. & Walker, G. C. (1987) *Cell* **51**, 579-87.

152. Tatusov, R. L., Fedorova, N. D., Jackson, J. D., Jacobs, A. R., Kiryutin, B., Koonin, E. V., Krylov, D. M., Mazumder, R., Mekhedov, S. L., Nikolskaya, A. N., Rao, B. S., Smirnov, S., Sverdlov, A. V., Vasudevan, S., Wolf, Y. I., Yin, J. J. & Natale, D. A. (2003) *BMC Bioinformatics* **4**, 41.
153. Koonin, E. V. (2003).
154. Oganessian, V., Busso, D., Brandsen, J., Chen, S., Jancarik, J., Kim, R. & Kim, S. H. (2003) *Acta Crystallogr D Biol Crystallogr* **59**, 1219-23.
155. Beranek, D. T. (1990) *Mutat Res* **231**, 11-30.
156. Pegg, A. E. (1984) *Cancer Invest* **2**, 223-31.
157. Boiteux, S., Huisman, O. & Laval, J. (1984) *Embo J* **3**, 2569-73.
158. Tse-Dinh, Y. C. (2007) *Infect Disord Drug Targets* **7**, 3-9.
159. Ross, J. I., Eady, E. A., Cove, J. H. & Cunliffe, W. J. (1998) *Antimicrob Agents Chemother* **42**, 1702-5.
160. Maxwell, I. H. (1967) *Biochim Biophys Acta* **138**, 337-46.
161. Coutsogeorgopoulos, C. (1966) *Biochim Biophys Acta* **129**, 214-7.
162. Bochner, B. R., Gadzinski, P. & Panomitros, E. (2001) *Genome Res* **11**, 1246-55.
163. Madigan, M. T., Martinko, J. M. & Parker, J. P. (1997) *Biology of Microorganisms* (Prentice Hall, Upper Saddle River).
164. Snel, B., Lehmann, G., Bork, P. & Huynen, M. A. (2000) *Nucleic Acids Res* **28**, 3442-4.
165. von Mering, C., Jensen, L. J., Kuhn, M., Chaffron, S., Doerks, T., Kruger, B., Snel, B. & Bork, P. (2007) *Nucleic Acids Res* **35**, D358-62.

166. Kazakov, A. E., Vassieva, O., Gelfand, M. S., Osterman, A. & Overbeek, R. (2003) *In Silico Biol* **3**, 3-15.
167. Harvey, R. J. (1970) *J Bacteriol* **101**, 574-83.
168. Poirot, O., O'Toole, E. & Notredame, C. (2003) *Nucleic Acids Res* **31**, 3503-6.
169. Datsenko, K. A. & Wanner, B. L. (2000) *Proc Natl Acad Sci U S A* **97**, 6640-5.
170. Gibson, K. E. & Silhavy, T. J. (1999) *J Bacteriol* **181**, 563-71.
171. Etchegaray, J. P. & Inouye, M. (1999) *J Biol Chem* **274**, 10079-85.
172. Wachi, M., Umitsuki, G., Shimizu, M., Takada, A. & Nagai, K. (1999) *Biochem Biophys Res Commun* **259**, 483-8.
173. Matthaei, H. & Nirenberg, M. W. (1961) *Biochem Biophys Res Commun* **4**, 404-8.
174. Gegenheimer, P., Watson, N. & Apirion, D. (1977) *J Biol Chem* **252**, 3064-73.
175. Wireman, J. W. & Sypherd, P. S. (1974) *Nature* **247**, 552-4.
176. Bram, R. J., Young, R. A. & Steitz, J. A. (1980) *Cell* **19**, 393-401.
177. Sirdeshmukh, R. & Schlessinger, D. (1985) *J Mol Biol* **186**, 669-72.
178. March, P. E., Lerner, C. G., Ahnn, J., Cui, X. & Inouye, M. (1988) *Oncogene* **2**, 539-44.
179. Pierrel, F., Bjork, G. R., Fontecave, M. & Atta, M. (2002) *J Biol Chem* **277**, 13367-70.
180. Sayed, A., Matsuyama, S. & Inouye, M. (1999) *Biochem Biophys Res Commun* **264**, 51-4.
181. Inoue, K., Alsina, J., Chen, J. & Inouye, M. (2003) *Mol Microbiol* **48**, 1005-16.
182. Karimi, R., Pavlov, M. Y., Buckingham, R. H. & Ehrenberg, M. (1999) *Mol Cell* **3**, 601-9.

183. Reymond, A., Friedli, M., Henrichsen, C. N., Chapot, F., Deutsch, S., Ucla, C., Rossier, C., Lyle, R., Guipponi, M. & Antonarakis, S. E. (2001) *Genomics* **78**, 46-54.
184. Claros, M. G. & Vincens, P. (1996) *Eur J Biochem* **241**, 779-86.
185. Gray, M. W., Burger, G. & Lang, B. F. (2001) *Genome Biol* **2**, REVIEWS1018.
186. Glass, J. I., Assad-Garcia, N., Alperovich, N., Yooseph, S., Lewis, M. R., Maruf, M., Hutchison, C. A., 3rd, Smith, H. O. & Venter, J. C. (2006) *Proc Natl Acad Sci USA* **103**, 425-30.
187. Penhoat, C. H., Li, Z., Atreya, H. S., Kim, S., Yee, A., Xiao, R., Murray, D., Arrowsmith, C. H. & Szyperski, T. (2005) *J Struct Funct Genomics* **6**, 51-62.
188. Zhan, C., Fedorov, E. V., Shi, W., Ramagopal, U. A., Thirumuruhan, R., Manjasetty, B. A., Almo, S. C., Fiser, A., Chance, M. R. & Fedorov, A. A. (2005) *Acta Crystallograph Sect F Struct Biol Cryst Commun* **61**, 959-63.
189. King, T. C., Sirdeshmukh, R. & Schlessinger, D. (1984) *Proc Natl Acad Sci USA* **81**, 185-8.
190. Deutscher, M. P. (2007).
191. Bolivar, F., Rodriguez, R. L., Greene, P. J., Betlach, M. C., Heyneker, H. L. & Boyer, H. W. (1977) *Gene* **2**, 95-113.
192. Barnett, M. J., Oke, V. & Long, S. R. (2000) *Biotechniques* **29**, 240-2, 244-5.
193. O'Connor, M., Goring, H. U. & Dahlberg, A. E. (1992) *Nucleic Acids Res* **20**, 4221-7.
194. Faith, J. J., Hayete, B., Thaden, J. T., Mogno, I., Wierzbowski, J., Cottarel, G., Kasif, S., Collins, J. J. & Gardner, T. S. (2007) *PLoS Biol* **5**, e8.

195. Gibert, I., Calero, S. & Barbe, J. (1990) *Mol Gen Genet* **220**, 400-8.
196. Jordan, A. & Reichard, P. (1998) *Annu Rev Biochem* **67**, 71-98.
197. Jordan, A., Aragall, E., Gibert, I. & Barbe, J. (1996) *Mol Microbiol* **19**, 777-90.
198. Tamarit, J., Mulliez, E., Meier, C., Trautwein, A. & Fontecave, M. (1999) *J Biol Chem* **274**, 31291-6.
199. Britton, R. A., Kuster-Schock, E., Auchtung, T. A. & Grossman, A. D. (2007) *J Bacteriol* **189**, 4359-66.
200. Dwyer, D. J., Kohanski, M. A., Hayete, B. & Collins, J. J. (2007) *Molecular Systems Biology* **3**, 1-15.
201. Mount, D. W., Low, K. B. & Edmiston, S. J. (1972) *J Bacteriol* **112**, 886-93.
202. Friedberg, E. C., Walker, G. C., Siede, W., Wood, R. D., Schultz, R. A., and T. Ellenberger (2006) *DNA Repair and Mutagenesis* (ASM Press, Washington, DC).
203. Renzette, N., Gumlaw, N., Nordman, J. T., Krieger, M., Yeh, S. P., Long, E., Centore, R., Boonsombat, R. & Sandler, S. J. (2005) *Mol Microbiol* **57**, 1074-85.
204. Heller, R. C. & Marians, K. J. (2005) *Mol Cell* **17**, 733-43.
205. Heller, R. C. & Marians, K. J. (2006) *Nature* **439**, 557-62.
206. Lovett, S. T. (2005) *Mol Cell* **17**, 751-2.
207. Weiss, D. S., Chen, J. C., Ghigo, J. M., Boyd, D. & Beckwith, J. (1999) *J Bacteriol* **181**, 508-20.
208. Ma, X., Ehrhardt, D. W. & Margolin, W. (1996) *Proc Natl Acad Sci U S A* **93**, 12998-3003.
209. Andrews, S. C., Robinson, A. K. & Rodriguez-Quinones, F. (2003) *FEMS Microbiol Rev* **27**, 215-37.

210. Stubbe, J. (2003) *Curr Opin Chem Biol* **7**, 183-8.
211. Postle, K. & Larsen, R. A. (2007) *Biometals*.
212. Simmons, L. A., Breier, A. M., Cozzarelli, N. R. & Kaguni, J. M. (2004) *Mol Microbiol* **51**, 349-58.
213. Alba, B. M. & Gross, C. A. (2004) *Mol Microbiol* **52**, 613-9.
214. Button, J. E., Silhavy, T. J. & Ruiz, N. (2007) *J Bacteriol* **189**, 1523-30.
215. Engelberg-Kulka, H., Amitai, S., Kolodkin-Gal, I. & Hazan, R. (2006) *PLoS Genet* **2**, e135.
216. Engelberg-Kulka, H., Sat, B., Reches, M., Amitai, S. & Hazan, R. (2004) *Trends Microbiol* **12**, 66-71.
217. Sat, B., Reches, M. & Engelberg-Kulka, H. (2003) *J Bacteriol* **185**, 1803-7.
218. Imlay, J. A. (2003) *Annu Rev Microbiol* **57**, 395-418.
219. Kohanski, M. A., Dwyer, D. J., Hayete, B., Lawrence, C. A. & Collins, J. J. (2007) *Cell* **130**, 797-810.
220. Kerr, J. F., Wyllie, A. H. & Currie, A. R. (1972) *Br J Cancer* **26**, 239-57.
221. LeGrand, E. K. (2001) *Perspect Biol Med* **44**, 509-21.
222. Gonzalez-Pastor, J. E., Hobbs, E. C. & Losick, R. (2003) *Science* **301**, 510-3.
223. Ahmad, S. I., Kirk, S. H. & Eisenstark, A. (1998) *Annu Rev Microbiol* **52**, 591-625.
224. Nakayama, K., Kusano, K., Irino, N. & Nakayama, H. (1994) *J Mol Biol* **243**, 611-20.
225. Hayes, C. S. & Sauer, R. T. (2003) *Mol Cell* **12**, 903-11.

226. Baba, T., Ara, T., Hasegawa, M., Takai, Y., Okumura, Y., Baba, M., Datsenko, K. A., Tomita, M., Wanner, B. L. & Mori, H. (2006) *Mol Syst Biol* **2**, 2006 0008.
227. Boye, E., Stokke, T., Kleckner, N. & Skarstad, K. (1996) *Proc Natl Acad Sci U S A* **93**, 12206-11.
228. Nievera, C., Torgue, J. J., Grimwade, J. E. & Leonard, A. C. (2006) *Mol Cell* **24**, 581-92.
229. Sutcliffe, J. A. (2005) *Curr Opin Microbiol* **8**, 534-42.
230. Parrish, J. R., Yu, J., Liu, G., Hines, J. A., Chan, J. E., Mangiola, B. A., Zhang, H., Pacifico, S., Fotouhi, F., Dirita, V. J., Ideker, T., Andrews, P. & Finley, R. L., Jr. (2007) *Genome Biol* **8**, R130.
231. Klevens, R. M., Morrison, M. A., Nadle, J., Petit, S., Gershman, K., Ray, S., Harrison, L. H., Lynfield, R., Dumyati, G., Townes, J. M., Craig, A. S., Zell, E. R., Fosheim, G. E., McDougal, L. K., Carey, R. B. & Fridkin, S. K. (2007) *Jama* **298**, 1763-71.
232. Administration, U. S. F. a. D.
233. Charles, P. G. & Grayson, M. L. (2004) *Med J Aust* **181**, 549-53.
234. Silver, L. L. & Bostian, K. A. (1993) *Antimicrob Agents Chemother* **37**, 377-83.
235. Comartin, D. J. & Brown, E. D. (2006) *Curr Opin Pharmacol* **6**, 453-8.
236. Kobayashi, K., Ehrlich, S. D., Albertini, A., Amati, G., Andersen, K. K., Arnaud, M., Asai, K., Ashikaga, S., Aymerich, S., Bessieres, P., Boland, F., Brignell, S. C., Bron, S., Bunai, K., Chapuis, J., Christiansen, L. C., Danchin, A., Debarbouille, M., Dervyn, E., Deuerling, E., Devine, K., Devine, S. K., Dreesen, O., Errington, J., Fillinger, S., Foster, S. J., Fujita, Y., Galizzi, A., Gardan, R.,

- Eschevins, C., Fukushima, T., Haga, K., Harwood, C. R., Hecker, M., Hosoya, D., Hullo, M. F., Kakeshita, H., Karamata, D., Kasahara, Y., Kawamura, F., Koga, K., Koski, P., Kuwana, R., Imamura, D., Ishimaru, M., Ishikawa, S., Ishio, I., Le Coq, D., Masson, A., Mauel, C., Meima, R., Mellado, R. P., Moir, A., Moriya, S., Nagakawa, E., Nanamiya, H., Nakai, S., Nygaard, P., Ogura, M., Ohanan, T., O'Reilly, M., O'Rourke, M., Pragai, Z., Pooley, H. M., Rapoport, G., Rawlins, J. P., Rivas, L. A., Rivolta, C., Sadaie, A., Sadaie, Y., Sarvas, M., Sato, T., Saxild, H. H., Scanlan, E., Schumann, W., Seegers, J. F., Sekiguchi, J., Sekowska, A., Seror, S. J., Simon, M., Stragier, P., Studer, R., Takamatsu, H., Tanaka, T., Takeuchi, M., Thomaidis, H. B., Vagner, V., van Dijl, J. M., Watabe, K., Wipat, A., Yamamoto, H., Yamamoto, M., Yamamoto, Y., Yamane, K., Yata, K., Yoshida, K., Yoshikawa, H., Zuber, U. & Ogasawara, N. (2003) *Proc Natl Acad Sci USA* **100**, 4678-83.
237. Andersson, S. G., Karlberg, O., Canback, B. & Kurland, C. G. (2003) *Philos Trans R Soc Lond B Biol Sci* **358**, 165-77; discussion 177-9.
238. Gardiner, K. & Davison, M. (2000) *Genome Biol* **1**, REVIEWS0002.
239. Rahmani, Z., Blouin, J. L., Creau-Goldberg, N., Watkins, P. C., Mattei, J. F., Poissonnier, M., Prieur, M., Chettouh, Z., Nicole, A., Aurias, A. & et al. (1989) *Proc Natl Acad Sci USA* **86**, 5958-62.
240. Ait Yahya-Graison, E., Aubert, J., Dauphinot, L., Rivals, I., Prieur, M., Golfier, G., Rossier, J., Personnaz, L., Creau, N., Blehaut, H., Robin, S., Delabar, J. M. & Potier, M. C. (2007) *Am J Hum Genet* **81**, 475-91.
241. Eperon, I. C., Anderson, S. & Nierlich, D. P. (1980) *Nature* **286**, 460-7.

242. Arbuzova, S., Hutchin, T. & Cuckle, H. (2002) *Bioessays* **24**, 681-4.
243. Coyle, J. T., Oster-Granite, M. L. & Gearhart, J. D. (1986) *Brain Res Bull* **16**, 773-87.
244. Selkoe, D. J. (2001) *Physiol Rev* **81**, 741-66.